

**DYNAMIC ANALYSIS OF COMPOSITE SANDWICH  
BEAM UNDER THE PASSIVE, SEMI-ACTIVE AND  
ACTIVE VIBRATION CONTROL TECHNIQUES**

Thesis

Submitted in partial fulfillment of the requirement for the degree of

**DOCTOR OF PHILOSOPHY**

by

**NAGIREDLA SURYARAO**



**DEPARTMENT OF MECHANICAL ENGINEERING  
NATIONAL INSTITUTE OF TECHNOLOGY  
KARNATAKA, SURATHKAL, MANGALORE – 575025,  
INDIA**

**AUGUST 2023**



**DYNAMIC ANALYSIS OF COMPOSITE SANDWICH  
BEAM UNDER THE PASSIVE, SEMI-ACTIVE AND  
ACTIVE VIBRATION CONTROL TECHNIQUES**

Thesis

Submitted in partial fulfillment of the requirements for the degree of

**DOCTOR OF PHILOSOPHY**

by

**NAGIREDLA SURYARAO**

Under the guidance of

**Dr. Sharnappa Joladarashi**

Associate Professor

**Dr. Hemantha Kumar**

Associate Professor



**DEPARTMENT OF MECHANICAL ENGINEERING  
NATIONAL INSTITUTE OF TECHNOLOGY  
KARNATAKA, SURATHKAL, MANGALORE - 575025**

**INDIA**

**AUGUST – 2023**



# *Dedication*

*To my Grand Mother*



*To my mother and father,*

*The reason of what I become today.*

*Thanks for your great support and*

*continuous care.*

*To my sister and family members,*

*I am really grateful to all.*



## DECLARATION

I hereby *declare* that the Research Thesis entitled “**DYNAMIC ANALYSIS OF COMPOSITE SANDWICH BEAM UNDER THE PASSIVE, SEMI-ACTIVE AND ACTIVE VIBRATION CONTROL TECHNIQUES**”, which is being submitted to the *National Institute of Technology Karnataka, Surathkal* in partial fulfillment of the requirements for the award of the Degree of *Doctor of Philosophy* is a *bonafide report of the research work carried out by me*. The material contained in this thesis has not been submitted to any University or Institution for the award of any degree.

Register Number: **177155ME030**

Name of the Research Scholar: **NAGIREDLA SURYARAO**

Signature of the Research Scholar: *N. Suryarao*

Department of Mechanical Engineering

Place: NITK, Surathkal

Date: *14/08/2023*

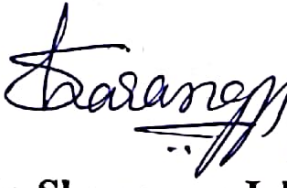




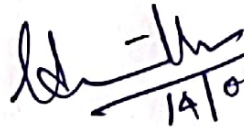
## CERTIFICATE

This is to *certify* that the Research Thesis entitled “**DYNAMIC ANALYSIS OF COMPOSITE SANDWICH BEAM UNDER THE PASSIVE, SEMI-ACTIVE AND ACTIVE VIBRATION CONTROL TECHNIQUES**”, submitted by **NAGIREDLA SURYARAO** (Register Number: 177155ME030) as the record of the research work carried out by him, is *accepted* as the *Research Thesis submission* in partial fulfilment of the requirements for the award of the degree of **Doctor of Philosophy**.


### Research Guide

  
14/08/2023

**Dr. Sharnappa Joladarashi**  
Associate Professor  
Department of Mechanical Engineering

  
14/08/2023

**Dr. Hemantha Kumar**  
Associate Professor  
Department of Mechanical Engineering

  
14.8.2023

**Chairman-DRPC**  
Department of Mechanical Engineering  
National Institute of Technology Karnataka  
Surathkal, Mangalore - 575025



## ACKNOWLEDGEMENT

I wish to express my sincere thanks to my research supervisor **Dr. Sharnappa Joladarashi**, Associate Professor and **Dr. Hemantha Kumar**, Associate Professor, at Department of Mechanical Engineering, National Institute of Technology Karnataka (NITK), Surathkal, for their continuous guidance and support throughout my research work. I extend my sincere gratitude to them for providing me with exceptional academic guidance, inspiration, and motivation. Their constant encouragement, assistance, and comprehensive review throughout my research journey made an invaluable contribution to the successful completion of my thesis. My heartfelt thanks to them.

I am grateful to the Head of the Department, **Dr. Ravikiran Kadoli**, Professor and the former Heads of the Department of Mechanical Engineering, for their support and encouragement. I would also like to express my thanks for their invaluable help, insightful suggestions.

I wish to thank all the members of my Doctoral committee, Professor S. M. Murigendrappa, Department of Mechanical Engineering and Dr. Vadivuchezhian Kaliveeran, Assistant Professor, Department of Water Resources and Ocean Engineering, for their appreciation and valuable suggestions for this research work. I would like to thank Dr. Jeyaraj P., Associate Professor and Dr. Subhaschandra Kattimani, Associate Professor, Department of Mechanical Engineering, for providing their valuable suggestions during my research work. I wish to express my sincere gratitude to all the faculty members of the Department of Mechanical Engineering,

I would like to acknowledge and express my gratitude for the funding support from Department of Science and Technology (DST) file no. ECR/2016/001448 titled “Experimental Investigation of Passive, Semi-active and Active vibration control of Composite Sandwich Structure” under Science and Engineering Research Board, Government of India.

My sincere thanks to all my research mates Rakesh Patil, Ashok Kumar, Hussain, Radhe Saini, Ratnesh, Suhash, Vivek R.S., Rajkumar, Puneeth, Dr. Subash Acharya,

Dr. Rangaraj Desai, Dr. Vipin, Dr. Vinayak, Sohail Bakshi, Atul, Sai Kumar, Kajal Chourasia, Shyamnarayana, Sreekumar and Pradeep for their help and fruitful discussions. I am thankful to everyone who helped and encouraged me during this research work.

Finally, I would like to thank A. Sowndarya Rani, B. Jairam and my family who have been a constant motivation and moral support to me throughout the completion of my research work.

**(SURYARAO NAGIREDLA)**

## ABSTRACT

The present study is aimed at understanding the behavior of sandwich beams and the influence of vibration control methods on the dynamic response. The passive, semi-active, and active vibration control techniques are implemented on the sandwich beams. The present study developed a finite element (FE) formulation for the composite sandwich beam and utilized the Euler-Bernoulli's method for sandwich beam element and Lagrange's approach is considered to obtain the equation of motion (EOM). The FE formulation solution is validated using different case studies available in the literature. The validation process ensures that the developed model is accurate and reliable for predicting the dynamic response of sandwich beams. The study provides insights into the effectiveness of different vibration control methods and the impact of various parameters and boundary conditions on the dynamic response of sandwich beams.

Viscoelastic materials can dissipate the vibrational energy in the form of heat when the structure undergoes cycles of deformation. For the passive vibration control of sandwich beam, two different viscoelastic materials and four different axial gradation configurations of viscoelastic materials are considered. The influence of viscoelastic material and boundary conditions on natural frequency, loss factor, and frequency response are investigated as a part of the initial study. Further, the influence of axial gradation configurations of the viscoelastic materials on the dynamic response is reported. Then, a comparison study of all configurations at different boundary conditions is discussed.

The field-dependent magneto-rheological (MR) fluid is used for the semi-active vibration control of the sandwich beam. MR fluid comes under the category of smart materials, and it can transform its rheological properties when it is exposed to an externally applied magnetic field. This nature of the MR fluid provides additional stiffness and damping for the sandwich beam applications. The effect of combined damping due to composite facings and MR fluid on the dynamic response of composite sandwich beams is discussed. The static, free, and forced vibration analyses of the composite sandwich beam are extracted to understand the influence of various

parameters on the static and dynamic response of the sandwich beam applications. A detailed study is conducted to evaluate the effect of composite laminate angle, magnetic field, and thickness ratio on the static deflection, natural frequency, loss factor, and frequency response. The influence of the magnetic field on the percentage of deviation in natural frequency, loss factor, and static deflection is also discussed. Further, the influence of MR fluid pocket configuration type on the dynamic response of the sandwich beam is presented. The configuration types include 1/4th, 1/2th, 3/4th, and the full length of the MR fluid pockets at different locations. In addition, a detailed study of the influence of each MR fluid pocket configuration type on the natural frequency, loss factor, and frequency response are presented for the clamped-free (CF), clamped-clamped (CC), simply-supported (SS), clamped-simple (CS) and simple-free (SF) boundary conditions.

In addition, two different compositions of in-house MR fluid samples with 24 and 30 percentage of volume fractions of carbonyl iron (CI) particles are prepared. The influence of oscillating driving frequency, strain amplitude, magnetic field, and the percentage of CI particles on the rheological properties of the MR fluid samples are discussed. The properties of MR fluid samples are used in the numerical formulations to explore the influence of the iron particles volume percentage on the dynamic response of the MR sandwich beam.

Further, the active vibration control technique is implemented in combination with passive and semi-active control techniques. The Proportional, Integral, and Derivative (PID) controller is developed to compare the transient response of the sandwich beam with the controller and without the controller.

**Keywords:** *Finite element formulations, Sandwich beam, Magneto-rheological fluid, Viscoelastic material, MR fluid pocket, Active vibration control, Frequency response.*

# TABLE OF CONTENTS

ACKNOWLEDGEMENT .....	i
ABSTRACT.....	iii
TABLE OF CONTENTS.....	v
LIST OF FIGURES .....	ix
LIST OF TABLES.....	xv
NOMENCLATURE .....	xvii
ABBREVIATIONS & NOTATIONS .....	xix
1. INTRODUCTION .....	1
1.1 SANDWICH STRUCTURES AND APPLICATIONS.....	1
1.2 VISCOELASTIC MATERIALS.....	3
1.3 MAGNETORHEOLOGICAL FLUID.....	4
1.4 ACTIVE VIBRATION CONTROL .....	7
1.5 ORGANIZATION OF THESIS.....	8
2. LITERATURE REVIEW .....	11
2.1 INTRODUCTION.....	11
2.2 DYNAMIC STUDIES ON SANDWICH STRUCTURES WITH VISCOELASTIC CORE MATERIAL .....	11
2.3 MAGNETO-RHEOLOGICAL FLUIDS, CHARACTERIZATION AND APPLICATIONS .....	14
2.4 DYNAMIC STUDIES ON THE SEMI-ACTIVE CONTROL OF SANDWICH STRUCTURES .....	17
2.5 ACTIVE VIBRATION CONTROL OF SANDWICH STRUCTURES .....	22
2.6 MOTIVATION .....	24
2.7 OBJECTIVES .....	25
2.8 SCOPE OF RESEARCH WORK .....	25

2.9 SUMMARY .....	26
3. METHODOLOGY .....	27
3.1 INTRODUCTION.....	27
3.2 THE MATHEMATICAL MODEL OF THE COMPOSITE SANDWICH BEAM .....	27
3.3 ELEMENTAL STIFFNESS MATRIX.....	32
3.4 ELEMENTAL MASS MATRIX .....	35
3.5 FINITE ELEMENT FORMULATION .....	37
3.6 SOLUTION PROCEDURE .....	39
3.7 VALIDATION .....	42
3.7.1 Convergence .....	42
3.7.2 Validation for viscoelastic sandwich beam .....	42
3.7.3 Validation for MR fluid sandwich beam .....	45
3.8 SUMMARY .....	47
4. DYNAMIC RESPONSE OF SANDWICH BEAM WITH VISCOELASTIC CORE MATERIAL.....	49
4.1. INTRODUCTION.....	49
4.2. INFLUENCE OF VISCOELASTIC MATERIAL .....	49
4.3. INFLUENCE OF BOUNDARY CONDITION.....	52
4.4. INFLUENCE OF AXIAL GRADATION OF VEM .....	57
4.5 SUMMARY .....	61
5. STATIC AND DYNAMIC RESPONSE OF THE COMPOSITE MR FLUID SANDWICH BEAM .....	63
5.1 INTRODUCTION.....	63
5.2 INFLUENCE OF LAMINATE ANGLE .....	63
5.3 INFLUENCE OF MAGNETIC FIELD .....	68



5.4 INFLUENCE OF THICKNESS RATIO .....	71
5.5 INFLUENCE OF BOUNDARY CONDITION.....	75
5.6 INFLUENCE OF MR FLUID POCKET CONFIGURATION .....	81
5.6.1 Configuration type-I.....	82
5.6.2 Configuration type-II.....	85
5.6.3 Configuration type-III.....	88
5.6.4 Configuration type-IV .....	88
5.7 INFLUENCE OF LOCATION OF MR FLUID POCKET .....	91
5.8 PREPARATION AND CHARACTERIZATION OF AN IN-HOUSE MAGNETORHEOLOGICAL FLUID.....	95
5.8.1 Materials and equipment used for the preparation of MR fluid samples ...	95
5.8.2 MR fluid preparation procedure .....	96
5.8.3 The microstructure of CI particles.....	97
5.8.4 Rheological experimental setup.....	98
5.8.5 Rheological results of MR fluid .....	99
5.8.6 Frequency-dependent rheological properties.....	101
5.8.7 Amplitude Strain dependent rheological properties .....	101
5.8.8 Magnetic field dependent rheological properties .....	102
5.8.9 Volume fraction dependent rheological properties .....	103
5.9 ESTIMATION OF STORAGE MODULUS AND LOSS FACTOR EQUATIONS FROM RHEOLOGICAL STUDIES.....	104
5.10 INFLUENCE OF VOLUME FRACTION OF MR FLUID ON THE DYNAMIC RESPONSE OF THE SANDWICH BEAM.....	104
5.11 SUMMARY .....	106
6. ACTIVE VIBRATION CONTROL OF COMPOSITE SANDWICH BEAM .....	107
6.1 INTRODUCTION.....	107

6.2 MODELLING AND ANALYSIS OF SANDWICH BEAMS USING PID CONTROLLER .....	107
6.2.1 Combined effect of Passive and Active vibration control on sandwich beam response .....	111
6.2.2 Combined effect of Semi-active and Active vibration control on sandwich beam response.....	113
6.3 SUMMARY .....	114
7. SUMMARY AND CONCLUSIONS .....	115
7.1 SUMMARY .....	115
7.2 CONCLUSIONS.....	116
7.2.1 Passive vibration control of sandwich beam with viscoelastic material ...	116
7.2.2 Semi-active vibration control of sandwich beam with MR fluid .....	117
7.2.3 Combined effect of passive, semi-active and active vibration control for the sandwich beam .....	118
7.3 SCOPE OF FUTURE WORK.....	118
APPENDIX-I.....	121
REFERENCES .....	127
LIST OF PUBLICATIONS .....	143
CURRICULUM VITAE.....	145

## LIST OF FIGURES

Figure 1.1 Sandwich beam configuration .....	2
Figure 1.2 Cyclic Stress and Strain curves vs. time for Viscoelastic materials.....	4
Figure 1.3 MR fluid (a) Without Magnetic field and (b) With Magnetic field .....	5
Figure 1.4 Stress vs strain curve for the MR fluids .....	6
Figure 1.5 Basic control loop.....	7
Figure 3.1 Flowchart of the present research work.....	28
Figure 3.2 Configuration of (a) sandwich beam element and (b) deformation diagram .....	29
Figure 3.3 Composite sandwich beam with laminate angle configuration ( $\phi$ ) .....	31
Figure 3.4 The flow chart of the FE formulations implementation .....	40
Figure 3.5 convergence study for the (a) 1 <sup>st</sup> mode and (b) 2 <sup>nd</sup> mode.....	42
Figure 4.1 Effect of viscoelastic material on natural frequency for (a) CF (b) CC (c) SS and (d) CS boundary conditions .....	50
Figure 4.2 Effect of viscoelastic material on loss factor for (a) CF (b) CC (c) SS and (d) CS boundary conditions .....	51
Figure 4.3 Effect of viscoelastic material on frequency response for (a) CF (b) CC (c) SS and (d) CS boundary conditions .....	52
Figure 4.4 Effect of boundary condition on natural frequency for (a) Mode-1 (b) Mode-2 (c) Mode-3 (d) Mode-4 (e) Mode-5 .....	53
Figure 4.5 Effect of boundary condition on loss factor for (a) mode-1 (b) mode-2 (c) mode-3 (d) mode-4 (e) mode-5.....	54

Figure 4.6 The percentage (%) of change in loss factor of the VEM-1 compared to the VEM-2 .....	55
Figure 4.7 The normalized fundamental five modes (a, b, c and d) real part of the transverse deflection of CF, CC, SS and CS boundary conditions.....	56
Figure 4.8 Axial gradation configurations of viscoelastic material (a) Configuration-I (b) Configuration-II (c) Configuration-III and (d) Configuration-IV .....	57
Figure 4.9 Influence of viscoelastic material configuration on natural frequency for (a) CF (b) CC (c) SS (d) CS conditions.....	58
Figure 4.10 Influence of viscoelastic material configuration on loss factor for (a) CF (b) CC (c) SS (d) CS conditions .....	59
Figure 4.11 Influence of viscoelastic material configuration on frequency response for (a) CF (b) CC (c) SS (d) CS conditions .....	60
Figure 5.1 Effect of laminate angle on static deflection .....	65
Figure 5.2 Variation in (a) Natural frequency and (b) Loss factor with laminate angle .....	65
Figure 5.3 Influence of combined damping on vibration amplitude at different laminate angles of face layer (a) $0^0$ (b) $30^0$ (c) $60^0$ and (d) $90^0$ degrees.....	66
Figure 5.4 The forced vibration response of the sandwich beam at different laminate angles .....	67
Figure 5.5 The combined damping effect on loss factor value with respect to the laminate angle .....	68
Figure 5.6 Effect of magnetic field on static deflection.....	68
Figure 5.7 Variation in (a) natural frequency and (b) loss factor with the applied magnetic field.....	69

Figure 5.8 Influence of combined damping on vibration amplitude at different magnetic fields (a) 0G (b) 500G (c) 1000G and (d) 2000G for the sandwich beam laminate angle 30/Core/30 configuration .....	70
Figure 5.9 The forced vibration response of the sandwich beam at different magnetic fields.....	71
Figure 5.10 Effect of thickness ratio on static deflection .....	71
Figure 5.11 Variation in (a) natural frequency and (b) loss factor with the thickness ratio .....	72
Figure 5.12 Influence of combined damping on vibration amplitude response at different thickness ratios (a) 0.5 (b) 2 (c) 4 and (d) 6 .....	73
Figure 5.13 The forced vibration response of the sandwich beam at thickness ratios.	74
Figure 5.14 The percentage (%) of deviation in (a) natural frequency and (b) loss factor with the applied magnetic field.....	75
Figure 5.15 The percentage (%) of reduction in static deflection of the sandwich beam with the applied magnetic field.....	75
Figure 5.16 Variation in Natural frequency under (a) CF (b) CC (c) SS (d) CS and (e) SF boundary conditions at different magnetic fields .....	79
Figure 5.17 Variation in loss factor under (a) CF (b) CC (c) SS (d) CS and (e) SF boundary conditions at different magnetic fields.....	80
Figure 5.18 Configuration Type - I.....	81
Figure 5.19 Configuration Type - II .....	82
Figure 5.20 Configuration Type - III .....	82
Figure 5.21 Configuration Type - IV .....	82

Figure 5.22 Variation in Natural frequency under (a) CF (b) CC (c) SS (d) CS and (e) SF boundary conditions for type-I configuration.....	83
Figure 5.23 Variation in Loss factor under (a) CF (b) CC (c) SS (d) CS and (e) SF boundary conditions for type-I configuration.....	84
Figure 5.24 Variation in Natural frequency under (a) CF (b) CC (c) SS (d) CS and (e) SF boundary conditions for type-II configuration.....	86
Figure 5.25 Variation in Loss factor under (a) CF (b) CC (c) SS (d) CS and (e) SF boundary conditions for type-II configuration.....	87
Figure 5.26 Variation in Natural frequency under (a) CF (b) CC (c) SS (d) CS and (e) SF boundary conditions for type-III configuration.....	89
Figure 5.27 Variation in Loss factor under (a) CF (b) CC (c) SS (d) CS and (e) SF boundary conditions for type-III configuration.....	90
Figure 5.28 Variation in (a) Natural frequency and (b) Loss factor under different boundary conditions for type-IV configuration.....	91
Figure 5.29 Influence of location of MR fluid pocket type on the natural frequency for (a) CF, (b) CC, (c) SS, (d) CS and (e) CF boundary conditions.....	92
Figure 5.30 Influence of location of MR fluid pocket type on loss factor for (a) CF, (b) CC, (c) SS, (d) CS and (e) CF boundary conditions.....	93
Figure 5.31 The influence of location of MR fluid pocket on the forced vibration response of the MR composite sandwich beam.....	94
Figure 5.32 (a) Line diagram of the stirrer (b) MR fluid preparation using a mechanical stirrer.....	97
Figure 5.33 Particle size distribution curve of the CI particles.....	97
Figure 5.34 CI particles microstructure magnified view at (a) 4000x and (b) 25000x.....	98

Figure 5.35 Magnetization curve of CI particles using VSM Testing.....	98
Figure 5.36 Rheometry setup.....	99
Figure 5.37 Variation in (a) Magnetic flux density, and (b) Viscosity with the applied current .....	100
Figure 5.38 Shear stress-strain curve to find the yield strain.....	100
Figure 5.39 Frequency dependency of (a) Storage Modulus and (b) loss factor at different currents.....	101
Figure 5.40 Strain amplitude dependency of (a) Storage modulus, (b) Loss factor at 2A current .....	102
Figure 5.41 Magnetic field dependency of (a) Storage modulus (b) Loss factor at different driving frequencies.....	103
Figure 5.42 Volume fraction dependency of (a) Storage modulus, (b) Loss factor for S-I and S-II samples with frequency .....	103
Figure 5.43 Variation in natural frequency for (a) S-I sample (b) S-II sample with respect to the magnetic field (c) Natural frequency (d) Frequency response for S-I and S-II samples .....	105
Figure 5.44 Variation in (a) Natural frequency (b) Frequency response of the sandwich beam for S-I and S-II samples .....	105
Figure 6.1 Procedure to implement the PID control on sandwich beam .....	107
Figure 6.2 Composite sandwich beam with the core material.....	108
Figure 6.3 System identification procedure flowchart to get the transfer function ...	109
Figure 6.4 PID Controller Block Diagram.....	110
Figure 6.5 Input signals (a) Impulse and (b) Sine signal .....	111

Figure 6.6 Combined effect of active and passive control on (a) Free vibration and (b) Forced vibration response ..... 112

Figure 6.7 Combined effect of active and Semi-active control on (a) Free vibration and (b) Forced vibration response ..... 114



## LIST OF TABLES

Table 3.1 Boundary conditions considered for the present study.....	41
Table 3.2 Fundamental five natural frequencies.....	43
Table 3.3 Fundamental five Natural frequencies.....	43
Table 3.4 Geometrical and Material properties of composite face layers and viscoelastic material with Length = 1000mm, and width = 25mm (Arvin et al., 2010) .....	44
Table 3.5 Natural frequency and Loss factor values for Case-2.....	44
Table 3.6 Fundamental five Natural frequencies (rad/s) .....	45
Table 3.7 Geometrical and Material properties of different layers with Length = 300mm, and width = 30mm (Rajamohan et al., 2010b)).....	45
Table 3.8 Natural frequencies for Case-1 .....	46
Table 3.9 Natural frequencies.....	46
Table 3.10 Properties of MR fluid sandwich beam with L = 400 mm, and b = 25 mm .....	47
Table 3.11 Natural frequency and Loss factor.....	47
Table 4.1 Material properties of face layers and viscoelastic materials .....	49
Table 5.1 Material properties of the Graphite/Epoxy composite face material and MR fluid.....	64
Table 5.2 Length and location of the MR fluid pocket and silicone rubber for different configurations of sandwich beam .....	76
Table 5.3 Natural frequency of C4 (fully filled) configuration at different magnetic field value for CF, CC, SS, CS and SF boundary conditions.....	77

Table 5.4 Loss factor of C4 (fully filled) configuration at different magnetic field value for CF, CC, SS, CS and SF boundary conditions .....	78
Table 5.5 MR fluid samples composition .....	95
Table 5.6 Storage modulus and loss factor equations of MR fluid samples.....	104

## NOMENCLATURE

$\Phi$  : Phase angle

$E'$  : Elastic storage modulus (MPa)

$E''$  : Elastic loss modulus (MPa)

$E^*$  : Complex elastic modulus (MPa)

$\eta$  : Loss factor

$u$  : Longitudinal displacement (mm)

$w$  : Transverse displacement (mm)

$\theta$  : Rotational displacement

$h_1$  : Thickness of top face layer (mm)

$h_2$  : Thickness of the core layer (mm)

$h_3$  : Thickness of the bottom face layer (mm)

$z$  : The coordinate in the thickness direction

$G^*$  : Complex shear modulus (MPa)

$G'$  : Shear storage modulus (MPa)

$G''$  : Shear loss modulus (MPa)

$B$  : Magnetic field

$\sigma$  : Axial stress (MPa)

$\varepsilon$  : Axial strain (mm/mm)

$\tau$  : Shear stress (MPa)

$\gamma$  : Shear strain

$l_e$  : Elemental length

$l$  : Length of the beam (mm)

$b$  : Width of the beam (mm)

$V$  : Strain energy

$T$  : Kinetic energy

$\bar{Q}_{ij}$  : Reduced stiffness matrix

$A$  : Cross-sectional area

$I$  : Moment of inertia

$\rho$  : Density ( $\text{kg/m}^3$ )

$q^e$  : Elemental displacement vector

$N_i(x)$  : Polynomial shape functions

$k^e$  : Elemental stiffness matrix

$m^e$  : Elemental mass matrix

$f^e$  : Elemental force vector

$M$  : Global mass matrix

$K$  : Global stiffness matrix

$F$  : Global force vector

$\omega$  - Radial frequency (rad/s)

$\nu$  - Poisson's ratio

$f$  : Natural frequency (Hz)

$\mu$  : Viscosity (Cst)

## ABBREVIATIONS & NOTATIONS

ER : Electro-rheological

MR : Magneto-rheological

CLD : Constrained Layer Damping

NGV : Nozzle Guide Vanes

CI : Carbonyl Iron

PID : Proportional, Integral, and Derivative

FE : Finite Element

DOF : Degree of Freedom

EOM : Equations of Motion

MATLAB : Matrix Laboratory

LQR : Linear Quadratic Regulator

c/s : Cross-section

MOI : Moment of Inertia

SE : Strain Energy

KE : Kinetic Energy

Imag : Imaginary

CF : Clamped-Free

CC : Clamped-Clamped

SS : Simply-Supported

CS : Clamped-Simple

SF : Simple-Free

VEM : Viscoelastic Material

VEM-1 : Viscoelastic Material – 1

VEM-2 : Viscoelastic Material – 2

MRF : Magneto-rheological Fluid

NFD : Natural Frequency Deviation

LFD : Loss Factor Deviation

BCs : Boundary Conditions

S – I : MR fluid Sample – I

S – II : MR fluid Sample – II

Vol% : Volume Percentage

SEM : Scanning Electron Microscopy

VSM : Vibratory Sample Magnetometer

MCR : Modular Compact Rheometer

MRD : Magneto-rheology Device

TF : Transfer Function







# **CHAPTER – 1**

## **INTRODUCTION**

Vibration in structural components is an important aspect because it can cause a severe problem, including fatigue, stress, and failure of components. The excessive vibration amplitudes lead to structural damage and compromise the safety and integrity of the structural component. Therefore, it is important to understand and control vibrations in structural components. Resonance is the most common phenomenon in the structural components, where the natural frequency of the component matches the frequency of the external excitation, and leads to large amplitude of vibration (Balamurugan and Narayanan, 2002). The resonance can be prevented by designing components with adequate stiffness and damping. The sandwich beams are one of the most widely used structural components in engineering applications due to their high strength-to-weight ratio and damping capabilities. The amplitude of structural vibrations can be controlled or reduced to some extent with the help of viscoelastic damping materials, smart materials such as Electro-rheological (ER) fluids, Magento-rheological fluids and active elements like piezoelectric materials in structural applications.

### **1.1 SANDWICH STRUCTURES AND APPLICATIONS**

The use of viscoelastic-based sandwich structures in aeronautical, automotive, defence vehicles, and civil engineering applications is increased due to their high stiffness-to-weight and strength-to-weight ratios (Trindade et al., 2000). Viscoelastic materials can dissipate the vibrational energy in the form of heat when the structure undergoes cycles of deformation (Shakouri et al., 2021). For the first time, Oberst conducted a dynamic study on base beam structures with the viscoelastic material bonded to the base beam on one side (Oberst, H.; Becker, G. W.; Frankenfeld, 1952). Even though the technique of applying damping material on one side of the base structure is provided a little damping to the structure, this technique fails to utilize the full damping capabilities of the viscoelastic material. This leads to constrained layer damping (CLD), in which viscoelastic material is placed between the two stiff elastic face layers. In CLD, the viscoelastic material tends to dissipate energy due to shear deformation when the

structure is vibrating (DiTaranto and Blasingame, 1967; Kerwin, 1959; Mahmoudkhani and Laghaie, 2022; Mead, 2013; Mead and Markus, 1969, 1970). Sandwich structures can be used for damping applications due to their ability to dissipate energy through viscoelastic materials as a core of the sandwich. The most commonly used viscoelastic core material, such as rubber or foam, has the ability to absorb and dissipate energy in response to mechanical stress and deformation (Afshin et al., 2011; Sun et al., 2022). The sandwich structures can be designed to have high damping capacity by optimizing the properties of the viscoelastic core material, such as its density, stiffness, and damping coefficient (Hao and Rao, 2005).

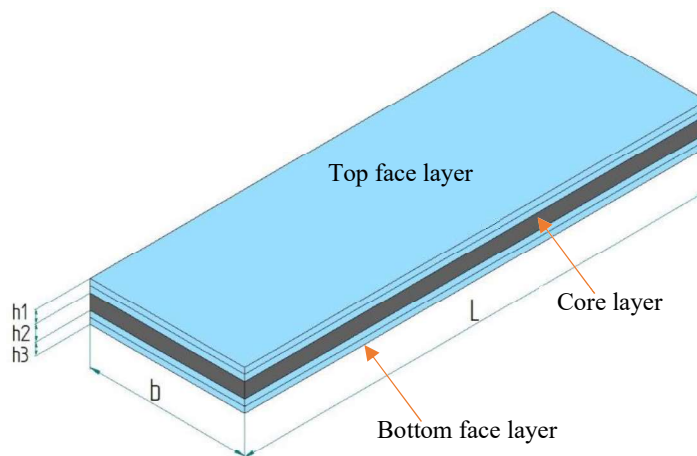


Figure 1.1 Sandwich beam configuration

The thickness of the core material can also be adjusted to achieve the desired level of damping. Sandwich structures can be used in a variety of damping applications, such as in buildings and bridges to reduce vibrations caused by wind or earthquakes, in automotive and aerospace applications to reduce noise and vibration, and in sporting equipment to reduce shock and impact. They can also be used in electronic devices to protect against shock and vibration. Sandwich structures are commonly used in aircraft wings, tail surfaces, and aircraft fuselage due to their high strength and stiffness. The core materials are sandwiched between two face sheets made of composite materials to create a lightweight yet strong and durable structure (Huang et al., 2016b; Zhou et al., 2016).

## 1.2 VISCOELASTIC MATERIALS

Viscoelasticity is the property of a material that exhibits both viscous and elastic characteristics when undergoing deformation. Viscous materials, such as liquids, resist shear flow and strain linearly with the time when force is applied. The elastic materials strain when stretched and immediately return to their original state once the stress is removed (Lakes, 2009).

A purely elastic material is one in which all the energy stored in the sample during loading is returned when the load is removed. As a result, the stress and strain curves for elastic materials move completely in phase. The Hooke's Law applies to elastic materials, where the stress is proportional to the strain, and the modulus is defined as the ratio of stress to strain. The complete opposite of an elastic material is a purely viscous material. This material does not return any energy stored during stress at a loading frequency and is out-of-phase with the strain by some phase angle and it varies between 0 and 90 degrees. The larger the angle, the greater the damping in the material (Chakraborty and Ratna, 2020).

For a viscoelastic material, the modulus is a complex quantity. The real part of this complex term (Storage modulus ( $E'$ )) relates to the elastic behaviour of the material and defines the elastic nature of the material. The imaginary component (Loss modulus ( $E''$ )) relates to the material's viscous behaviour, and defines the dissipative energy ability of the material (Gould et al., 2019).

$$\text{Complex Modulus}(E^*) = E' + iE'' \quad (1.1)$$

The tangent " $\delta$ " is called as the loss factor of the material, and the loss factor can be written in terms of storage and modulus.

$$\text{Loss factor}(\eta) = \tan \delta = \frac{E''}{E'} \quad (1.2)$$

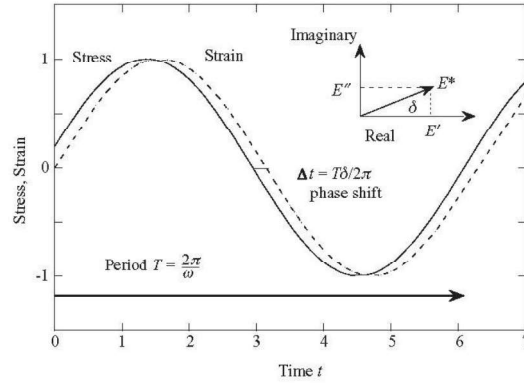


Figure 1.2 Cyclic Stress and Strain curves vs. time for Viscoelastic materials

(Courtesy: Lakes, 2009)

Researchers have implemented passive control methods to prevent this problem in the initial stage. Even though passive materials reduce vibration amplitude to some extent, they cannot change their properties according to the application requirements. These limitations of passive materials provide a way to think of smart and intelligent materials. Smart materials can change their properties upon application of external fields. The usage of smart materials along with composite materials is increased because of their lightweight and directional properties advantage. Some practical applications of smart sandwich beams are in turbine stator and rotor blades, nozzle guide vanes (NGVs), airplane propellers, and instrument devices (Ghorbanpour Arani and Soleymani, 2019a). The composite sandwich structures are finding more applications in aeronautical, automotive, defence technology, and civil engineering due to their high strength to weight and stiffness to weight ratios.

### 1.3 MAGNETORHEOLOGICAL FLUID

MR fluids are one of the categories of smart materials. MR fluid changes its rheological properties more quickly and reversibly when introducing an external field. Rabinow presented the magneto-rheological effect of MR fluid for the first time (Rabinow, 1948). MR fluid varies its yield stress and viscosity values very quickly in the presence of an externally applied field and displays field-dependent rheological properties (Iglesias et al., 2012; Kumar Kariganaur et al., 2022b; Lopez-Lopez et al.,

2021). When an external magnetic field is applied, magnetic dipole makes the particles form strong interactions. This causes the iron particles to form a chain-like structure in the externally applied magnetic field direction. Because of this, the liquid state of the MR fluid will be changed to a semi-solid state and reversibly on the removal of external field. MR fluids response is in the range of few milliseconds in the presence of external stimuli. MR fluids can produce a higher yield stresses based on the iron particles volume percentage concentration and external field applied (S Genç.; PP Phulé, 2007s). Response time of MR fluids has great importance in most applications. MR fluids found importance in many potential applications such as in seat dampers, shock absorbers, brakes, clutches, engine mounts, dampers for vibration control and sandwich structures applications for vibration control due to quick response time (Kciuk, M.; Turczyn, 2012; Kumar Kariganaur et al., 2022a; Olabi and Grunwald, 2007).

In the absence of a magnetic field, the iron particles in the MR fluid are randomly distributed as illustrated in figure 1.3 (a). When an external magnetic field is applied, the iron particles become polarized and form a chain-like structure, as shown in figure 1.3 (b). This chain formation increases the stiffness of the MR fluid, which can be adjusted instantaneously and continuously by changing the magnitude of the applied magnetic field. This characteristic enables devices that use MR fluid to exhibit rapidly responsive and adjustable properties.

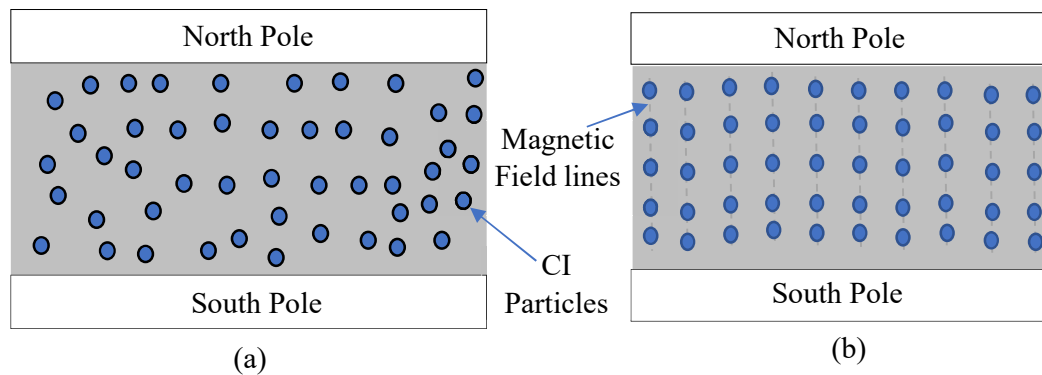


Figure 1.3 MR fluid (a) Without Magnetic field and (b) With Magnetic field

MR fluids caught more attention among the researchers for sandwich structure applications due to its adjustable nature of rheological properties like storage modulus and loss modulus in the presence of an external magnetic field. In sandwich structures, MR fluids can be used as the core material, allowing for the creation of smart sandwich

structures that can adjust their mechanical properties in response to an external magnetic field. When a magnetic field is applied to the MR fluid, it has the ability to increase its stiffness, thereby causing the sandwich structure to become stiffer as well. This property of the MR fluid can be utilized for damping purposes, where precise control over the damping effect is desired. This enables the creation of smart and adaptive structures that can respond to changing environmental conditions in real time.

The rheological behavior of MR fluid is dependent on the presence or absence of a magnetic field. In the absence of a magnetic field, the behavior of the MR fluid can be explained using Newtonian fluid mechanics. However, when a magnetic field is present, the MR fluid exhibits distinct non-Newtonian behavior, specifically Bingham plastic behavior. The rheology of MR fluid is commonly divided into two regimes: pre-yield and post-yield conditions. Each regime has a unique constitutive equation that describes the flow behavior of the MR fluid (Jolly et al., 1999; Li et al., 1999) as given below:

$$\tau = G^* \dot{\gamma} \quad \tau < \tau_y \quad (1.3)$$

$$\tau = \tau(B) + \mu \dot{\gamma} \quad \tau > \tau_y \quad (1.4)$$

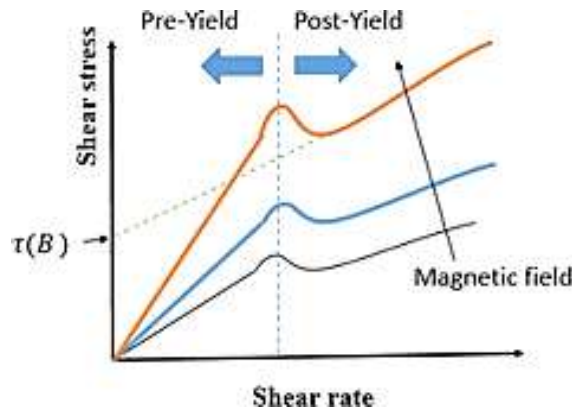


Figure 1.4 Stress vs strain curve for the MR fluids

(Courtesy: Choi and Han, 2005; Li et al., 1999)

where,  $\gamma$  is shear strain,  $\dot{\gamma}$  is shear rate,  $\tau(B)$  is field dependent shear stress,  $\mu$  is post-yield viscosity,  $B$  is magnetic flux density,  $G^*$  is complex shear modulus and  $\tau$  and  $\tau_y$  is shear stress of MR fluid.

## 1.4 ACTIVE VIBRATION CONTROL

Active vibration control is a technique used to reduce or eliminate unwanted vibrations in a system by using feedback control. The technique involves measuring the vibration of the system and generating an equal and opposite force to cancel out the vibration. The feedback control system can be implemented using a variety of sensors, actuators, and control algorithms. The active vibration control is commonly used in engineering applications such as aerospace, automotive, and manufacturing (Welsh, 2018). In aerospace structures, the active vibration control can be used to reduce the noise and vibration caused by the engines or air turbulence. In automobile applications, the active suspension systems can be used to provide a smoother ride by reducing the vibrations caused by uneven road surfaces (Elliott, 2010).

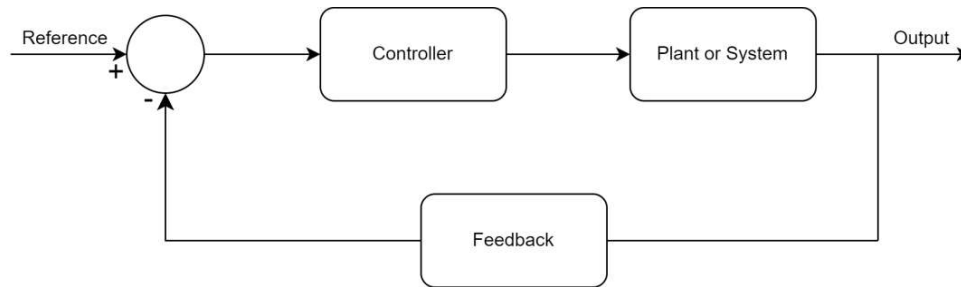


Figure 1.5 Basic control loop

PID controller is one of popular control techniques used in engineering applications to reduce the amplitude of vibration (Khot et al., 2011; Toulson and Wilmshurst, 2012). This controller is a type of control system used in engineering and automation applications to regulate the behavior of a system. The proportional component of the controller produces an output that is proportional to the error between the desired setpoint and the measured process variable. The integral component sums up the error over time and produces an output that is proportional to the integral of the error. The derivative component produces an output that is proportional to the rate of change of the error. The combination of these three components, the PID controller can generate an output that is able to correct any deviation between the setpoint and the actual process variable, as well as any trends or changes in the process variable over time (Qin and Sun, 2020s). The PID controller is widely used in engineering applications where precise control is required.

## 1.5 ORGANIZATION OF THESIS

This thesis helps to understand the influence of various vibration control techniques on the dynamic response of the sandwich beam applications. The passive, semi-active and active vibration control methods are developed and investigated the influence of different parameters and boundary conditions on the dynamic response of the sandwich beam. For the present study, the finite element (FE) formulations are developed for the composite sandwich beam. The developed FE formulation considered a Euler-Bernoulli's method with a twelve degree of freedom (DOF) sandwich beam element and the Lagrange's approach is utilized to obtain the equations of motion (EOM). Further, the developed FE formulations solution is validated with the available literature by taking different case studies. Matrix Laboratory (MATLAB) code snippets are developed to obtain the static, free and forced vibration response of the sandwich beam.

The whole thesis is aligned into seven chapters, and the contents of each chapter are summarized as follows:

**Chapter-1:** This chapter gives the brief introduction to composite materials, viscoelastic materials and Magneto-rheological fluids. Additionally, the applications of constrained layer damping with the passive, semi-active and active materials for vibration control of sandwich structures is discussed.

**Chapter-2:** This chapter thoroughly explains the literature review carried out for the present work. Further, the motivation, objectives, and scope of research work are also discussed.

**Chapter-3:** This chapter includes the FE formulations for the composite sandwich beam is discussed in this chapter. The current developed FE formulation considered Euler-Bernoulli's method for the sandwich beam element and the Lagrange's approach is utilized to obtain the EOM. The implementation of MATLAB code for the FE formulations to get the static deflection, free vibration, and forced vibration response of sandwich beams under different boundary conditions is discussed throughout the chapter. Further, the developed FE formulations solution is validated with the available literature by taking different case studies.



**Chapter-4:** This chapter presents the influence of type of viscoelastic material and boundary conditions on natural frequency, loss factor and frequency response of sandwich beam as a part of the initial study. Further, the influence of four different axial gradation configurations of the viscoelastic materials on the dynamic response of the sandwich beam is investigated.

**Chapter-5:** The effect of combined damping due to composite facings and MR fluid on the static and dynamic response of composite sandwich beam is discussed in this chapter. The present study helps to understand the effect of various parameters on the static and dynamic response of the sandwich beam applications. The static, free, and forced vibration analyses on composite sandwich beam are extracted. A detailed study is discussed to evaluate the impact of laminate angle, magnetic field, and thickness ratio on static deflection, natural frequency, loss factor, and frequency response. The influence of magnetic field on the percentage of deviation in natural frequency, loss factor, and static deflection is also explained. The Influence of MR fluid pocket configuration type on natural frequency, loss factor and frequency response are presented to address the influence of location and length of the MR fluid pocket. Further, the rheological studies of an in-house prepared MR fluid samples are discussed. Two different compositions of MR fluid samples with 24 and 30 percent (%) volume fractions of carbonyl iron (CI) particles are prepared. The influence of oscillating driving frequency, strain amplitude, magnetic field, and the percentage of CI particle on the rheological properties of the MR fluid samples are discussed. Further, the properties of MR fluid samples are used in the numerical formulation to explore the influence of the Iron particles percentage in the MR fluid on the dynamic response of the MR sandwich beam.

**Chapter-6:** This chapter discusses the active vibration control of sandwich beam with the combination of passive and semi-active control. Proportional, Integral and Derivative (PID) controller is implemented to compare the transient response of the sandwich beam with controller and without controller.

**Chapter-7:** In this chapter, a comprehensive overview of the research work is included. The most significant results and conclusions are presented, and the scope for future work is also discussed in this chapter.



## **CHAPTER – 2**

### **LITERATURE REVIEW**

#### **2.1 INTRODUCTION**

The dynamic studies on sandwich structures with viscoelastic material, characterization of magnetorheological fluid, applications of MR fluid in various engineering applications, and active vibration control methods have been discussed in this chapter.

#### **2.2 DYNAMIC STUDIES ON SANDWICH STRUCTURES WITH VISCOELASTIC CORE MATERIAL**

In the earlier stage, researchers have conducted analytical and numerical studies on the sandwich beams to find the natural frequency and loss factors and to explore the potential capabilities of the sandwich structures in real world applications. The following literature summarizes the important aspects on viscoelastic materials in sandwich beam applications.

Kerwin (1959) presented the influence of a damping material for flexural waves in structures. The proposed damping material is a viscoelastic layer that is constrained between two stiff layers, which is capable of absorbing and dissipating energy during flexural wave propagation. A theoretical model was developed to analyze the damping performance of the constrained viscoelastic layer. The developed model was validated using the experimental studies on beam specimens with different configurations.

DiTaranto and Blasingame (1967) conducted an experimental study to evaluate the damping performance of the material in various configurations of sandwich beams. The results showed that the composite damping material was effective in reducing the vibration amplitudes of the sandwich beams. The damping performance was found to be influenced by various factors such as the thickness and properties of the viscoelastic layer.

Mead and Markus (1970) presented the damping performance of sandwich beams with an encasté damping treatment. A thin layer of a viscoelastic material at the clamped or fixed end of a sandwich beam is used, which is capable of absorbing and dissipating

energy during vibration. A theoretical model is developed to analyze the damping performance of the encastré damping treatment. The results showed that the encastré damping treatment was effective in reducing the vibration amplitudes and noise levels of the sandwich beams.

Rao (1978) discussed the dynamic behavior of sandwich beams under different boundary conditions. The natural frequencies and loss factors of sandwich beams under different boundary conditions were determined. The model considers the effects of the geometry, material properties, and boundary conditions on the dynamic behavior of the sandwich beams.

Lifshitz and Leibowitz (1987) proposed a theoretical model to optimize the design of sandwich beams for maximum viscoelastic damping. The proposed design focuses on maximizing the damping capacity of sandwich beams by optimizing the thickness and properties of the viscoelastic layer. The results showed that the optimal design of sandwich beams for maximum viscoelastic damping involves selecting a viscoelastic layer with high loss factor and optimizing the thickness of the viscoelastic layer.

Sakiyama et al. (1996) presented the discrete Green function method for the free vibration analysis of sandwich beams with an elastic or viscoelastic core. The proposed method aims to accurately predict the natural frequencies and mode shapes of sandwich beams with different core materials and configurations. The study found that the natural frequencies of sandwich beams with a viscoelastic core are lower than those of sandwich beams with an elastic core, indicating a higher damping capacity.

Baber et al. (1998) presented a finite element method for analyzing the dynamic behavior of viscoelastic sandwich beams under harmonic excitation. The proposed model focuses on accurately predicting the vibration and damping behavior of sandwich beams with a viscoelastic core under harmonic loading. The study concluded that the damping behavior of sandwich beams is influenced by the frequency and amplitude of the harmonic excitation.

Kung and Singh (1998) discussed the use of CLD patches to reduce the vibration amplitude of beams. The CLD patches consist of a viscoelastic layer sandwiched between two metal layers and are attached to the beam at specific locations. The study

focuses on beams with multiple patches that are constrained to move in the axial direction. The results show that increasing the number of CLD patches and locating them at the antinodes of the vibration mode leads to better vibration reduction.

The theoretical study of the vibration and damping characteristics of a sandwich beam structure containing a viscoelastic constraining layer is investigated. The EOM for the sandwich beam were derived using the Hamilton's principle. The results show that the presence of the viscoelastic layer can significantly increase the damping of the sandwich beam and reduce the amplitude of vibration. (Barbosa and Farage, 2008; Hao and Rao, 2005).

Arikoglu and Ozkol (2010) discussed the use of differential transform method (DTM) for analyzing the vibration behavior of composite sandwich beams with a viscoelastic core. The viscoelastic core of the sandwich beam is modeled using the Kelvin-Voigt model, which considers both elastic and viscous behavior of the material. The governing equation for the vibration analysis is derived using the principle of virtual work. The results show that the DTM is an effective method for analyzing the vibration behavior of composite sandwich beams with a viscoelastic core.

Arvin et al. (2010) developed a FE formulation to study the vibration behavior of a composite sandwich beam with a viscoelastic core under free and forced vibration conditions.

Bilasse et al. (2010) presented a study on the vibration behavior of viscoelastic sandwich beams using both linear and nonlinear analysis techniques. The study considers a sandwich beam composed of two identical face sheets and a viscoelastic core, and investigates the effects of material damping, core thickness, and boundary conditions on the vibration response of the beam. The study shows that the material damping and core thickness have a considerable influence on the vibration response of the sandwich beam.

Grewal et al. (2013) performed the parametric study to address the effect of viscoelastic material thickness on damping and developed an optimization problem to find the suitable number of viscoelastic patches to obtain the maximum damping for the structure.

Huang et al. (2016a) presented a study on the damping mechanism of sandwich structures composed of elastic face sheets and a viscoelastic core. The study shows that the damping mechanism in elastic–viscoelastic–elastic sandwich structures is a combination of several factors, including material damping in the viscoelastic core, frictional damping at the interface between the core and face sheets, and radiation damping due to the energy dissipation in the surrounding medium.

Patil et al. (2020) conducted the studies on the vibration behavior of a disc brake system. The free and forced vibration analysis of the back plate and brake insulator of a disc brake system was discussed.

Lewandowski et al. (2021) presented a study on the dynamic behavior of multi-layered viscoelastic beams using the refined zig-zag theory. The analysis of the natural frequencies and mode shapes of multi-layered viscoelastic beams with different material and geometrical properties was discussed. The refined zig-zag theory takes the shear deformation effects into account for each layer of the beam. The study concluded that the refined zig-zag theory provides more accurate results compared to the classical beam theory, particularly for beams with a large number of layers and/or high damping ratios.

The effectiveness of graphite particulates inclusion in the core material on loss factor is discussed and also performed a parametric study to find the optimal parameters for maximum damping in the sandwich structure (Gupta et al., 2020; Gupta and Panda, 2021).

However, to achieve the optimal or higher damping for the sandwich beam or plate applications, some studies reported the effectiveness of partial and full treatment of viscoelastic patches on loss factors (Gao et al., 2022; Garg et al., 2022; Khalfi and Ross, 2016; Zhang et al., 2021).

### **2.3 MAGNETO-RHEOLOGICAL FLUIDS, CHARACTERIZATION AND APPLICATIONS**

Magnetorheological (MR) fluids come under the category of smart materials, which shows a significant change in their rheology under the influence of external magnetic field. Smart materials change their properties in a significant way when they are

exposed to externally applied fields. Rainbow reported MR fluids for the first time in 1948 and demonstrated the application of these fluids in clutches (Rabinow, 1948).

Gamota and Filisko (1991) conducted the rheological studies to find the rheological properties like storage modulus, loss modulus and loss factor value of ER fluids using a sinusoidally oscillating shear strain of frequency. The results of their measurements, which include the complex shear modulus and loss factor of the ER material over a range of frequencies and electric field strengths are presented. The storage and loss modulus increased with the externally applied magnetic field and decrement in loss factor.

Weiss et al. (1994) discussed the various factors that can influence the viscoelastic properties of ER/MR fluids, such as the concentration and size of the magnetic or electrically polarizable particles, the strength and frequency of the applied field, and the temperature and shear rate of the material. The oscillatory rheometer test method was used to find the rheological properties of the ER and MR fluids. The yield strain obtained for the MR fluid using this method is 0.5 to 0.8%. Finally, the author also discussed some of the potential applications of MR fluids and ER Fluids in areas such as vibration damping, shock absorption, and energy harvesting.

Ashour et al. (1996) provided a comprehensive overview of magnetorheological fluids, including their materials, characterization, and devices. MR fluids are smart fluids that can change their rheological properties in response to an external magnetic field, making them useful in various industrial applications. The applications of MR fluids in various devices, such as vibration damping, shock absorption, and haptic actuators were examined.

Li et al. (1999) conducted the rheological studies on MR fluids to understand the complex viscoelastic behavior and its relationship with the applied magnetic field. The study concluded that the viscoelastic behavior of MR fluids is highly dependent on the applied magnetic field strength, frequency, and the type and concentration of magnetic particles in the fluid. The results suggest that MR fluids exhibit both viscous and elastic behaviors, which can be controlled by adjusting the magnetic field strength and frequency. The study also highlighted the importance of considering the viscoelastic

behavior of MR fluids in the design of MR-based devices and systems, such as dampers and vibration isolators.

An overview of the properties and applications of commercial MR fluids are presented. The properties of various commercial MR fluids, including their yield strength, viscosity, and sedimentation stability is discussed. The potential applications of MR fluids, such as in vibration damping, clutches, brakes devices and adaptive shock absorbers also explored (Abdel-Wahab et al., 2018; Jolly et al., 1999; López-López et al., 2006; Olabi and Grunwald 2007).

The wide range of applications of MR fluids in fields such as robotics, aerospace, and automotive engineering is presented. The magnetic dipole makes the iron particles in the MR fluid to form strong interactions, when an external magnetic field is applied. This causes the iron particles to form a chain-like structure in the direction of externally applied magnetic field. Because of this, the liquid state of the MR fluid will be changed to a semi-solid state and reversibly on the removal of external field. MR fluids response is in the range of few milliseconds in the presence of an external stimuli. MR fluids can produce a higher yield stresses based on the iron particles volume percentage concentration and external field applied (S Genç.; PP Phulé, 2007).

Elizabeth Premalatha et al. (2012) prepared several iron-based MR fluids using carbonyl iron particles and silicone oil as the carrier fluid. Several experimental studies were conducted to investigate the influence of the magnetic field strength and particle concentration on the magneto-mechanical properties of the MR fluids, including the yield stress, viscosity, and shear modulus. The influence of particle concentration and surface modification on the magneto-rheological response was also discussed.

Ashtiani et al. (2015) conducted a comprehensive overview of the preparation and stabilization procedures of MR fluids. The different approaches used for the preparation of MR fluids, including the dispersion of magnetic particles in a carrier fluid, the use of surfactants and dispersants to stabilize the suspension, and the addition of rheological modifiers to improve the performance of the fluid is discussed. The effects of particle size, shape, and concentration on the rheological properties of MR fluids also presented. MR fluid typically contains of CI particles (20-40 volume %), carrier fluid (60-80



volume %) and an anti-settling agent (additive). The CI particles size vary in the range of 1-10  $\mu\text{m}$  which are spherical shape.

The yield stress and apparent viscosity of the MR fluids can be varied very quickly under the influence of an external field. MR fluids show magnetic field dependent rheological properties (Genc, 2022; Iglesias et al., 2012; Muddebihal and Patil, 2020; Zhu et al., 2019).

The response time of MR fluids has great importance in most applications. Because of the quick, controllable rheological properties and reversible quality of the MR fluids, they found many potential applications in the field of vibration control devices, dampers, brakes and clutch applications. MR fluid potential applications and basic characteristic properties are presented (Daniel et al., 2019; HE and HUANG, 2005; Olabi and Grunwald, 2007; Seid et al., 2019; Vishwakarma et al., 2022).

MR fluid devices operate under the dynamic conditions in different applications. The dynamic characterization studies are conducted on the MR fluids to meet the appropriate application design specifications (Kamble et al., 2021; Kumbhar et al., 2015; Muhammad et al., 2006).

The strain-controlled rheometer was used to analyse the viscoelastic parameters of the MR fluids. The influence of particle size distribution, volume fraction percentage and applied field on the rheological parameters are reported (Acharya et al., 2021; Allien et al., 2020; Chiriac and Stoian, 2010; Guo et al., 2018; Jolly et al., 1999; Kumar Kariganaur et al., 2022a; b; Kumar et al., 2021; Li et al., 1999; Ramkumar et al., 2022)

## **2.4 DYNAMIC STUDIES ON THE SEMI-ACTIVE CONTROL OF SANDWICH STRUCTURES**

Since the passive materials offer limited advantages over the damping and stiffness capabilities, the usage of field dependent materials such as ER/MR fluids is increased in sandwich structural applications (Aldemir, 2003; Berg et al., 1996; Dyke et al., 1998; Makris et al., 1996; Rahn and Joshi, 1998; Stanway et al., 1996; Zhang and Roschke, 1999). MR fluids can have their rheological properties, such as viscosity and shear modulus, rapidly and reversibly adjusted by applying a magnetic field. This allows for greater control over the damping and stiffness of the material, making it suitable for a

wider range of applications (Mazlan et al., 2007; Nguyen and Choi, 2009; Occhiuzzi et al., 2003; Oh and Onoda, 2002). The use of magnetic fields to control the rheological properties of MR fluids requires low power consumption, making them energy-efficient and cost-effective to use.

The potential of electro-rheological (ER) fluids in composite materials is discussed. The ER fluids exhibit a reversible change in viscosity when an electric field is applied, which can be useful in creating materials with controllable mechanical properties. The experiments are conducted by embedding ER fluids into different types of composite materials, including fiber-reinforced composites and laminates, and testing their mechanical properties under various conditions. The results of the experiments showed that the addition of ER fluids to composite materials can significantly improve their mechanical properties, especially under dynamic loading conditions (Choi et al., 1990; Gandhi et al., 1989).

Choi et al. (1992) explored the behavior of laminate composites filled with ER fluid under forced vibration. The study investigated the effect of the ER fluid on the mechanical properties of the composite under different electric fields.

Haiqing et al. (1993) studied the influence of an ER fluid layer on the vibration amplitude of a cantilever beam. The study uses a theoretical model to investigate the damping effect of the ER fluid layer on the beam vibration. The mathematical model is discussed for the cantilever beam with the ER fluid layer. The study concluded that the ER fluid layer can effectively suppress the vibration of the cantilever beam, particularly at its resonance frequency. The damping effect depends on various factors such as the thickness of the fluid layer, the strength of the applied electric field, and the amplitude of vibration.

The usage of ER materials in adaptive beams is investigated. An adaptive beam model subjected to simply supported boundary conditions was developed. Further, the potential applications of ER materials in the design of adaptive structures, such as bridges, buildings, and aerospace structures was presented (Yalcintas et al., 1995; Yalcintas and Coulter, 1995a; b, 1998).

The amplitude-dependent dynamic characteristics of the ER sandwich beam is investigated. The simulation results showed that the ER fluid can significantly reduce the dynamic response of the sandwich beam. The influence of different parameters, such as the applied electric field and the thickness of the ER fluid layer, on the dynamic response of the sandwich beam was presented (Haiqing and King, 1997; Lee, 1995; Oyadiji, 1996).

Yalcintas and Dai (1999) investigated the performance of MR and ER materials and their applications in adaptive structures. The various applications of these materials in adaptive structures such as vibration control systems, shock absorbers, and clutches was explored. The performance of both materials was compared in terms of their response time, stability, and energy consumption. The article concluded that both MR and ER materials have their strengths and weaknesses and that the choice of material depends on the specific application. However, magnetorheological materials shown better response time and energy efficiency, while electrorheological materials have higher stability.

Harland et al. (2001) investigated the use of ER/MR filled inserts to control vibration transmission in beams. The inserts are designed to be placed inside the beam and can be adjusted in real-time to provide both passive and adaptive control of vibrations. The effectiveness of the inserts in reducing vibration transmission is demonstrated through simulations and experiments. The results showed that the ER/MR inserts can significantly reduce vibration transmission and that the level of reduction can be controlled by adjusting the applied voltage.

Choi et al. (2001) studied the effectiveness of ER fluid plate for reducing noise in a cabin. The ER fluid-based plate is a device that uses an electric field to alter the viscosity and stiffness of the fluid, thereby changing its damping properties and ability to absorb sound. The experimental tests were conducted using a vibration shaker and an acoustic test chamber. The results showed that the ER fluid-based plate was effective in reducing vibration and noise transmission in the low-frequency range. The study also concluded that the ER fluid-based plate was more effective than traditional passive damping materials in reducing noise transmission.

The dynamic response of MR materials in the adaptive beams were studied under different magnetic fields. The study showed that the adaptive beam model accurately predicts the dynamic behavior of MR materials under different magnetic fields and can be used to design and optimize MR-based devices (Sun et al., 2003; Yalcintas and Dai, 2004).

Tzou et al. (2004) provided an overview of the field of structronics, which is the integration of smart materials, sensors, actuators, and electronics in structural systems. The potential benefits of structronic systems, including increased performance, energy efficiency, and safety. The characteristics of smart materials, including piezoelectric materials, shape memory alloys, and magnetostrictive materials was explained and also discussed the principles of precision sensors and actuators, such as fiber-optic sensors and electroactive polymers.

Yeh and Shih (2006) discussed the dynamic behavior and instability of MR fluids in the adaptive beams. The experimental setup was developed to study the dynamic behavior of a cantilever beam with an attached MR damper. Several excitation methods, including impulse and harmonic excitations were given, to study the natural frequencies and damping characteristics of the beam. The study concluded that the dynamic instability occurs when the damping capacity of the MR damper is not sufficient to control the vibrations of the beam.

Lara-Prieto et al. (2010) investigated the vibration characteristics of MR sandwich beams in a cantilever configuration. The experimental studies were conducted with and without an applied magnetic field to determine the changes in the natural frequencies and damping ratios of the beam. The obtained results showed that the MR sandwich beam exhibited a high level of damping control and could adjust its natural frequencies in response to changes in the magnetic field. The damping ratio of the beam increased significantly with an applied magnetic field, indicating that MR materials could be effective for vibration control applications.

The vibration characteristics of a multi-layer beam structure containing MR fluid for fully and partially filled sandwich beam is explored. The study utilized an analytical approach and FE method to analyze the frequency response of the beam and to predict

its vibration behavior. The Galerkin method was used to obtain the natural frequencies and mode shapes of the beam. The effect of various parameters such as the thickness of the MR fluid layer, magnetic field strength, and the number of layers on the vibration behavior of the beam is also investigated. The results showed that the presence of the MR fluid layer significantly affects the vibration characteristics of the beam (Arumugam et al., 2017; Rajamohan et al., 2010b; a, 2011).

Eshaghi et al. (2015) developed an FE model to study the dynamic response of the sandwich structure using classical plate theory. The frequency and field-dependent complex shear moduli of the two MR fluids were identified from both the experimental data and the FE model results. The study also investigated the effect of different parameters, such as magnetic field strength and fluid concentration, on the pre-yield properties of MR fluids. The results show that these parameters can significantly affect the fluid's rheological properties and should be considered when designing and using MR fluids in engineering applications.

The vibration behavior of laminated composite beams that are integrated with a magnetorheological (MR) fluid layer is discussed. The study aimed to investigate the effect of the MR fluid layer on the natural frequencies and mode shapes of the composite beams under different boundary conditions. The FE method is utilized to model the laminated composite beams and simulate their vibration behavior (Naji, 2017; Naji et al., 2016, 2018; Zabihollah et al., 2020).

Eshaghi et al. (2017) discussed the influence of partial treatment of MR fluid on sandwich beam response for the applied magnetic field and location of MR fluid pocket is presented. It is concluded that the considerable change in shear strain location provides significant damping properties.

The numerical and experimental dynamic analysis of composite sandwich beams with a magnetorheological elastomer honeycomb core is discussed. The FE analysis simulations were performed to determine the natural frequencies, mode shapes, and dynamic response of the beams with different core configurations. The results show that the magnetorheological elastomer honeycomb core improves the dynamic behavior of the sandwich beams. The experimental results were compared with the numerical

simulations, and a good agreement was found between them. The results show that the magnetorheological elastomer honeycomb core improves the dynamic behavior of the sandwich beams (de Souza Eloy et al., 2018, 2019).

The genetic algorithm based optimization technique is used to find the effective number of MR fluid pockets and determined the optimal location of MR fluid pockets to suppress the supersonic flutter in the sandwich structure (Nezami and Gholami, 2019).

The vibrational analysis of a rotating sandwich beam with MR core and varying cross-section in supersonic airflow is explored. The study aimed to investigate the impact of the beam's size on its vibration characteristics under various operational conditions. To obtain the governing equations, the Hamilton's principal in conjunction with modified first strain gradient theory (MFSGT) is applied. The size-dependent differential equations of motion are solved based on the Galerkin method. The study concluded that the beam's size has a significant impact on its vibration characteristics, with smaller beams exhibiting higher natural frequencies and more localized mode shapes. Additionally, the study show that the magnetic field has a considerable effect on the beam's natural frequencies, with increasing magnetic field strength leading to an increase in natural frequencies and a shift in mode shapes towards the beam's edges (Ghorbanpour Arani and Soleymani, 2019a; b).

The experimental and numerical studies are conducted on the sandwich beams with MR fluid/elastomer for the free and forced vibration response at different magnetic field values (Acharya et al., 2021; Allien et al., 2020; Kolekar and Venkatesh, 2019; Rokn-Abadi et al., 2020b; a; Selvaraj et al., 2021; Selvaraj and Ramamoorthy, 2020).

The theoretical modelling and vibration characteristics of a blade-disk rotor assembly, spinning double-blade beam assembly and pre-twisted blade-shaft assembly are implemented based on the Euler- Bernoulli beam theory (Zhao et al., 2021d; c, 2022b)).

## **2.5 ACTIVE VIBRATION CONTROL OF SANDWICH STRUCTURES**

Lam et al. (1997) discussed the application of two methods for controlling vibrations in structures: passive constrained layer damping (PCLD) and active control. The different types of active control techniques, including open-loop and closed-loop control were discussed. Further, a combined approach in which PCLD and active

control are used together. The PCLD reduces the amplitude of the vibration, and the active control further reduces it by applying a force to counteract the remaining vibration.

The use of a Linear Quadratic Regulator (LQR) controller to achieve the active vibration control of flexible structures is discussed. The LQR controller is used to calculate the control input required to reduce the vibration of the structure. The simulation results showed that the LQR controller is able to achieve a significant reduction in vibration compared to an uncontrolled system (Rajamohan et al., 2011; Zhang et al., 2008).

Khot et al. (2012, 2013) presented a study on the use of a PID based output feedback controller for active vibration control of a cantilever beam. The study aimed to suppress the vibration of the beam caused by external disturbances and to enhance the stability of the system. The simulation results indicate that the PID-based output feedback controller effectively suppresses the vibration of the cantilever beam and enhances the stability of the system. The study also shows that the performance of the controller is affected by the choice of PID controller parameters, and tuning these parameters is crucial to achieve optimal performance.

The use of piezoelectric patches to control the vibration of smart structures is studied. The results of the experiments showed that the piezoelectric patches are effective in reducing the vibration of the beam (Heganna and Joglekar, 2016; Kusagur et al., 2020).

Rimašauskienė et al. (2019) investigated the effectiveness of active-passive vibration control methods on a thin-walled composite beam. The study involved the fabrication of a composite beam and the implementation of two types of vibration control methods: active and passive. The active control method used piezoelectric actuators and sensors to generate vibrations that counteracted the natural frequency of the beam, while the passive control method utilized CLD to absorb vibrations. The active control method was found to be more effective in reducing the vibration amplitudes and improving the damping ratio compared to the passive control method.

Tian et al. (2020) discussed the use of a laminated piezoelectric beam element for the dynamic analysis of piezo-laminated smart beams and a genetic algorithm (GA)-based LQR active vibration control.

Reddy et al. (2021) investigated the nonlinear dynamics and active control of smart beams using piezoelectric actuators. The study involved the development of a mathematical model for a smart beam with piezoelectric actuators, which is subjected to external loading. The model took into account the nonlinearities of the beam, such as geometric and material nonlinearities, and the coupling between the shear and extensional modes of the piezoelectric actuators. The results of the study showed that the nonlinear dynamics of the smart beam can be controlled using piezoelectric actuators. The study found that the shear mode of the piezoelectric actuator is more effective in controlling the beam than the extensional mode.

The bending vibration control of a smart beam embedded with magnetorheological (MR) fluid subjected to wind-induced galloping effects is investigated. The study involved the fabrication of a smart beam with MR fluid embedded within it and subjected to external wind-induced galloping effects. The beam was equipped with sensors and actuators for active control of its bending vibration. The results of the study showed that the use of MR fluid embedded in the smart beam can effectively reduce the bending vibration of the beam under wind-induced galloping effects. The active control system was able to adaptively adjust the damping properties of the MR fluid to achieve optimal vibration control (Bolat and Sivrioglu, 2020; Sivrioglu and Bolat, 2020).

## **2.6 MOTIVATION**

Sandwich beams are widely used in engineering applications due to their high strength-to-weight ratio, but they can be susceptible to vibration and noise problems under the dynamic environment. The higher amplitudes of vibration are one of the severe and considerable problems when it comes to structural applications. Vibration control of these structures is always a potential area for the researchers. From the available literature it is found that there exist very few literatures on the semi-active vibration control of sandwich structures with the MR fluids and also combination of active



control with the passive and semi-active vibration control for the composite sandwich structure. The motivation of this work is to study the dynamic response of the sandwich structures using passive, semi-active and active vibration control and combination of these strategies.

## **2.7 OBJECTIVES**

1. To investigate the vibrational response of composite sandwich beams with the passive damping using viscoelastic material.
2. To prepare and investigate the rheological properties of different compositions of In-house MR fluid samples for the sandwich beam applications.
3. To evaluate the static and dynamic behaviour of composite sandwich beams with MR fluid core material.
4. To study the dynamic response of a composite sandwich beam with the combination effect of passive and active control damping technique, semi-active and active control damping technique.

## **2.8 SCOPE OF RESEARCH WORK**

- To study the dynamic response of the sandwich beam, the FE formulations are developed. The FE formulation considered a Euler-Bernoulli's method and the Lagrange's approach is utilized to obtain the EOM. Further, the developed FE formulations solution is validated with the available literature by taking different case studies. The FE code snippets are developed to obtain the static, free and forced vibration response of the sandwich beam.
- To study the influence of type of viscoelastic material and boundary conditions on natural frequency, loss factor and frequency response of sandwich beam with the developed finite element formulation.
- To investigate the effect of combined damping due to composite facings and MR fluid on the static and dynamic response of composite sandwich beam. The static, free, and forced vibration analyses on composite sandwich beam are explored. A detailed study is discussed to evaluate the impact of laminate angle, magnetic field, and thickness ratio on static deflection, natural frequency, loss factor, and frequency response. The influence of magnetic field on the percentage of

deviation in natural frequency, loss factor, and static deflection is also explained. Further, Influence of MR fluid pocket configuration type on natural frequency, loss factor and frequency response are discussed to address the influence of location and length of the MR fluid pocket. Finally, influence of the in-house prepared MR fluid on the dynamic response of the sandwich beam is presented.

- To study the active vibration control of sandwich beam with the combination of passive and semi-active. The PID controller is implemented to compare the transient response of the sandwich beam with controller and without controller.

## **2.9 SUMMARY**

This chapter provides a comprehensive overview of the literature review conducted for the current research. The literature review encompasses a thorough analysis of the existing research works in the field to establish the research gap, and research objectives. Moreover, the chapter also discusses the motivation behind the research work, which highlights the significance, relevance and scope of the study.

# **CHAPTER – 3**

## **METHODOLOGY**

### **3.1 INTRODUCTION**

The developed FE formulations for the composite sandwich beam are discussed. The FE formulation considered the Euler-Bernoulli's method for sandwich beam element and the Lagrange's approach is utilized to obtain the equation of motion (EOM). Further, the developed FE formulations solution is validated with the available literature by taking different case studies. The present study is divided into three categories named as passive, semi-active and active vibration control of composite sandwich beams. The overall methodology of the present study is illustrated in the flowchart figure 3.1.

### **3.2 THE MATHEMATICAL MODEL OF THE COMPOSITE SANDWICH BEAM**

The sandwich beam configuration consists of three layers, in which the core material is sandwiched between two composite facings as shown in figure 3.2 and 3.3. The FE method is used to formulate the sandwich beam equations. The subsequent assumptions are utilized for the present problem.

- The transverse and shear strain in the composite facings is ignored.
- There is no slippage in the interface of all the layers.

A sandwich beam element with twelve degrees of freedom (DOF) in the top and bottom composite face layers is considered for the present formulation.

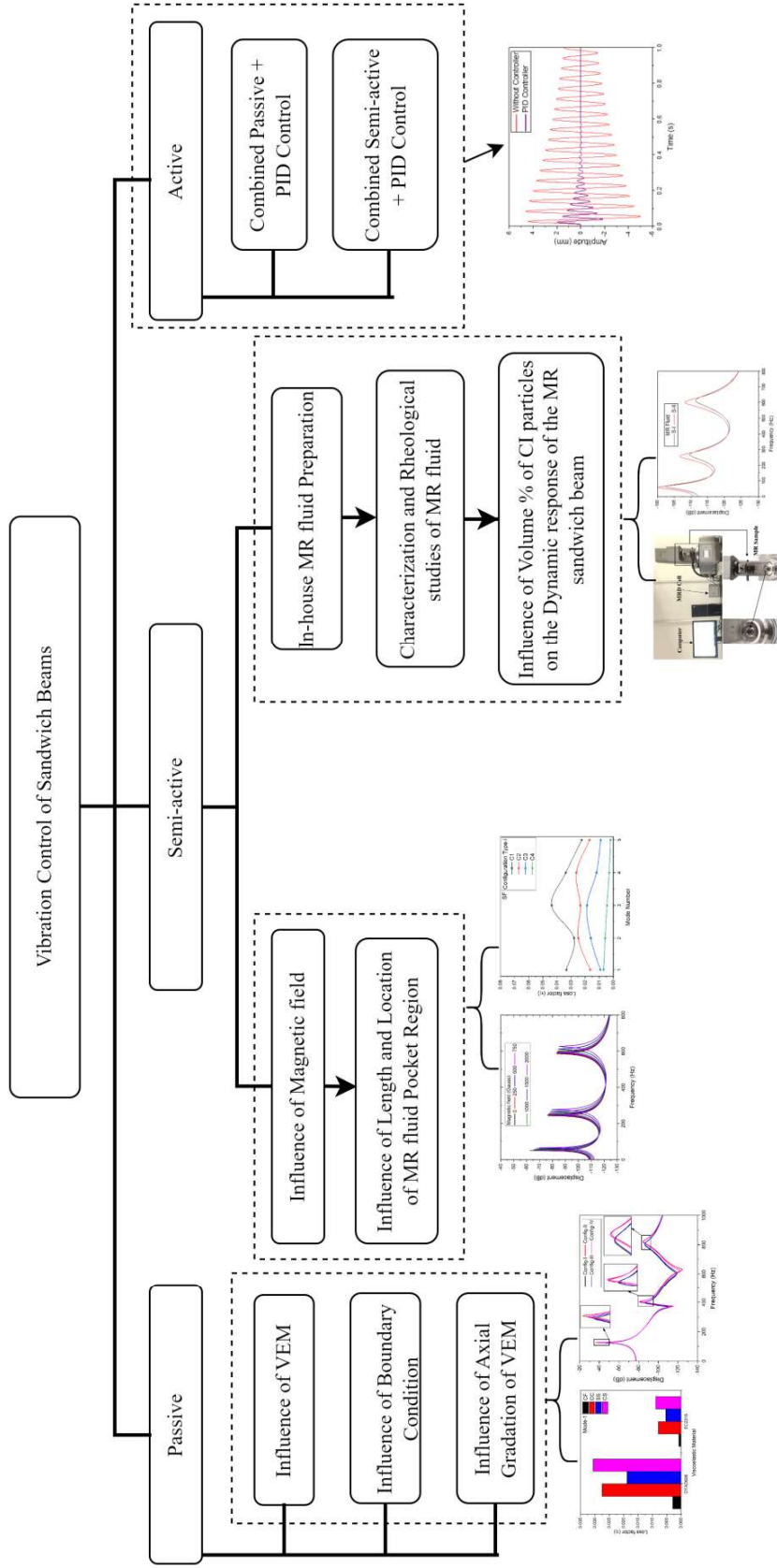


Figure 3.1 Flowchart of the present research work

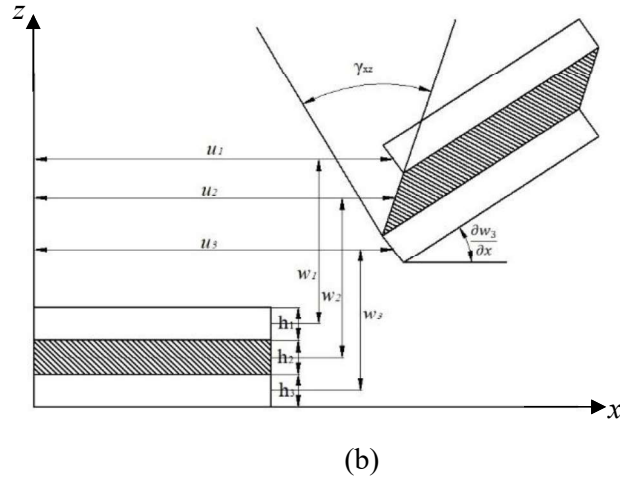
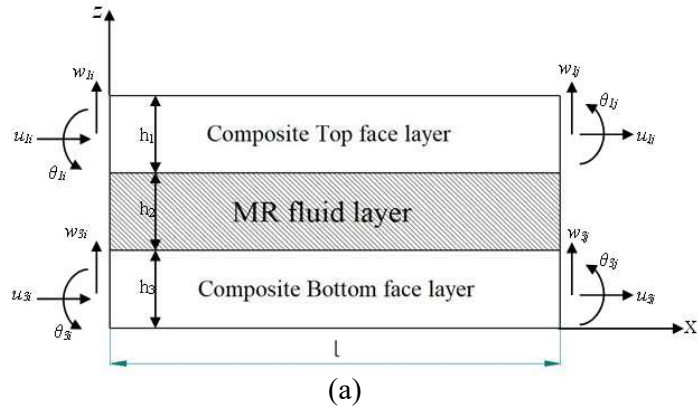


Figure 3.2 Configuration of (a) sandwich beam element and (b) deformation diagram

Three DOF in the top and bottom facings are taken at each side. Namely, longitudinal displacement ( $u$ ), transverse displacement ( $w$ ), and rotation ( $\theta$ ). Figure 3.2 (a) and (b) illustrate the DOF considered for the sandwich beam element and deformation diagram, respectively. Based on the assumptions made, the displacements can be written as (Arvin et al., 2010)

$$\begin{cases} u'_1 = u_1 - (z - e_1)\theta_1 & \frac{h_2}{2} \leq z \leq \frac{h_2}{2} + h_1 & e_1 = \frac{h_1 + h_2}{2} \\ u'_3 = u_3 - (z + e_3)\theta_3 & -h_3 - \frac{h_2}{2} \leq z \leq -\frac{h_2}{2} & e_3 = \frac{h_3 + h_2}{2} \end{cases} \quad (3.1)$$

where  $u'_1$  and  $u'_3$  are the general longitudinal displacements in the top and bottom face layers.  $u_i$  and  $\theta_i$  are the longitudinal displacement and rotation of the neutral axis of the top and bottom composite facings, respectively, where  $i=1,3$ .  $z$  is the sandwich beam

element's coordinate in the thickness direction.  $h_1$ ,  $h_2$ , and  $h_3$  are the thicknesses of the top, core, and bottom face layers.

Further, the longitudinal and transverse displacements in the core layer are assumed as linearly dependent on the coordinate  $z$ .

$$u'_2 = a + bz; \quad w'_2 = a' + b'z \quad (3.2)$$

$a$ ,  $b$ ,  $a'$  and  $b'$  Eq. 3.2 are the constants that need to be found using the following considerations.

$$\begin{cases} w'_2 \Big|_{\frac{h_2}{2}} = w_1; & w'_2 \Big|_{-\frac{h_2}{2}} = w_3; \\ u'_2 \Big|_{\frac{h_2}{2}} = u'_1 \Big|_{\frac{h_2}{2}}; & u'_2 \Big|_{-\frac{h_2}{2}} = u'_3 \Big|_{-\frac{h_2}{2}} \end{cases} \quad (3.3)$$

Based on the above assumption and using Eq. 3.1 and 3.2, the longitudinal and transverse displacements in the core can be rewritten as,

$$u'_2 = \left[ \frac{u_1 + u_3}{2} + \frac{h_1 \theta_1 - h_3 \theta_3}{4} \right] + \left[ \frac{u_1 - u_3}{h_2} + \frac{h_1 \theta_1 + h_3 \theta_3}{2h_2} \right] z \quad (3.4)$$

$$w'_2 = \left[ \frac{w_1 + w_3}{2} \right] + \left[ \frac{w_1 - w_3}{h_2} \right] z \quad (3.5)$$

$w_1$  and  $w_3$  in Eq. 3.5 are the transverse displacements of the top and bottom composite facings, respectively and  $\theta_1 = \frac{\partial w_1}{\partial x}$ , and  $\theta_3 = \frac{\partial w_3}{\partial x}$ .

Further, based on the classical theory of the beam/Euler Bernoulli beam theory (Arvin et al., 2010; Ghorbanpour Arani and Soleymani, 2019b) for the face layers, the strain-displacement relationship equations are derived for each layer as follows,

**Top face layer:**

$$\left\{ \begin{array}{l} \varepsilon_{x1} = \frac{\partial u'_1}{\partial x} = \frac{\partial u_1}{\partial x} - (z - e_1) \frac{\partial^2 w_1}{\partial x^2}, \quad \varepsilon_{z1} = \frac{\partial w_1}{\partial z} = 0 \\ \gamma_{xz1} = 2\varepsilon_{xz1} = \frac{\partial w_1}{\partial x} + \frac{\partial u'_1}{\partial z} = 0 \end{array} \right. \quad (3.6)$$

**Bottom face layer:**

$$\left\{ \begin{array}{l} \varepsilon_{x3} = \frac{\partial u'_3}{\partial x} = \frac{\partial u_3}{\partial x} - (z + e_3) \frac{\partial^2 w_3}{\partial x^2}, \quad \varepsilon_{z3} = \frac{\partial w_3}{\partial z} = 0 \\ \gamma_{xz3} = 2\varepsilon_{xz3} = \frac{\partial w_3}{\partial x} + \frac{\partial u'_3}{\partial z} = 0 \end{array} \right. \quad (3.7)$$

**MR fluid core layer:**

$$\left\{ \begin{array}{l} \varepsilon_{x2} = \frac{\partial u'_2}{\partial x} = \left[ \frac{\partial u_1}{\partial x} + \frac{\partial u_3}{\partial x} + \frac{h_1}{2} \frac{\partial^2 w_1}{\partial x^2} - \frac{h_3}{2} \frac{\partial^2 w_3}{\partial x^2} \right] + \left[ \frac{\partial u_1}{\partial x} - \frac{\partial u_3}{\partial x} + \frac{h_1}{2h_2} \frac{\partial^2 w_1}{\partial x^2} + \frac{h_3}{2h_2} \frac{\partial^2 w_3}{\partial x^2} \right] z \\ \varepsilon_{z2} = \frac{\partial w'_2}{\partial z} = \left[ \frac{w_1 - w_3}{h_2} \right] \\ \gamma_{xz2} = 2\varepsilon_{xz2} = \frac{\partial w'_2}{\partial x} + \frac{\partial u'_2}{\partial z} = \left[ \frac{u_1 - u_3}{h_2} + \frac{(h_1 + h_2)\theta_1 + (h_3 + h_2)\theta_3}{2h_2} \right] + \left[ \frac{\theta_1 - \theta_3}{h_2} \right] z \end{array} \right. \quad (3.8)$$

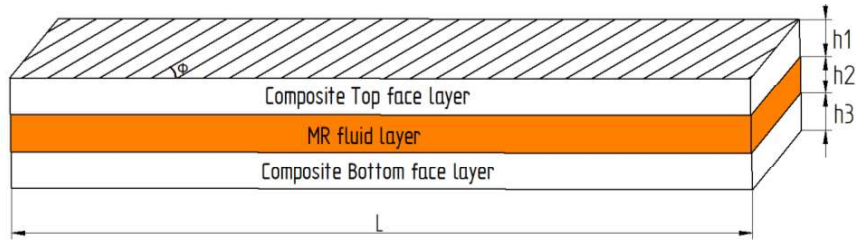


Figure 3.3 Composite sandwich beam with laminate angle configuration ( $\phi$ )

The complex shear modulus of the MR fluid is given as

$$G_{MRF}^*(B) = G'_{MRF}(B) + iG''_{MRF}(B) \quad (3.9)$$

Where  $G'_{MRF}(B)$  represents the real part (storage modulus) that gives the amount of energy stored and  $G''_{MRF}(B)$  represents the imaginary part (loss modulus) that gives

the amount of energy dissipated while undergoing one deformation cycle in terms of the magnetic field. B is the magnetic field in gauss (G).

### 3.3 ELEMENTAL STIFFNESS MATRIX

Lagrange's energy method is utilized to get EOM for the present sandwich beam problem. It is necessary to obtain the sandwich beam's total strain and kinetic energy equations to do so. The total strain energy (SE) expressed as (Lee, 1995) follows

$$V = \frac{1}{2} \iiint_v (\sigma_{ij} \varepsilon_{ij}) dV \quad (3.10)$$

$\sigma_{ij}$  and  $\varepsilon_{ij}$  in Eq. 3.10 are the stress and the strain in each layer. Further, the stresses in the y-direction are neglected, i.e.,

$$\sigma_{xy} = 0; \sigma_{yy} = 0; \text{ and } \sigma_{zy} = 0 \quad (3.11)$$

#### Top face layer:

From Eq. 10, strain energy in the top face layer is written as

$$V_1^e = \frac{b}{2} \int_{\frac{h_2}{2}}^{\frac{h_2}{2}+h_1} \int_0^l (\sigma_{x1} \varepsilon_{x1} + \sigma_{z1} \varepsilon_{z1} + 2\sigma_{xz1} \varepsilon_{xz1}) dx dz \quad (3.12)$$

The stress-strain relationship matrix for the top face layer is given (Jack R. and Sierakowski, 2008; Robert M., 1999) as

$$\begin{Bmatrix} \sigma_{x1} \\ \sigma_{z1} \\ \sigma_{xz1} \end{Bmatrix} = \begin{bmatrix} \bar{Q}_{11} \\ \bar{Q}_{13} \\ \bar{Q}_{14} \end{bmatrix}_1 \begin{bmatrix} \bar{Q}_{13} \\ \bar{Q}_{33} \\ \bar{Q}_{35} \end{bmatrix}_1 \begin{bmatrix} 2\bar{Q}_{15} \\ 2\bar{Q}_{35} \\ 2\bar{Q}_{55} \end{bmatrix}_1 \begin{Bmatrix} \varepsilon_{x1} \\ \varepsilon_{z1} \\ \varepsilon_{xz1} \end{Bmatrix} \quad (3.13)$$

Since the transverse and shear strain in the top face layer is zero, Eq. 3.12 is simplified to

$$V_1^e = \frac{b}{2} \int_{\frac{h_2}{2}}^{\frac{h_2}{2}+h_1} \int_0^l (\{\varepsilon_{x1}\} \bar{Q}_{ij} \{\varepsilon_{x1}\}^T) dx dz \quad (3.14)$$

After substituting the strain-displacement Eq. (3.6) into Eq. 3.14, the strain energy in the top face layer is



$$V_1^e = \frac{b}{2} \int_{\frac{h_2}{2}}^{\frac{h_2+h_1}{2}} \int_0^l \left( \left\{ \frac{\partial u_1}{\partial x} - (z-e_1) \frac{\partial^2 w_1}{\partial x^2} \right\} \bar{Q}_{ij} \right)_1 \left\{ \frac{\partial u_1}{\partial x} - (z-e_1) \frac{\partial^2 w_1}{\partial x^2} \right\}^T dx dz \quad (3.15)$$

$$V_1^e = \frac{\bar{Q}_{11}}{2} \int_0^l \left( A_1 \left( \left\{ \frac{\partial u_1}{\partial x} \right\} \left\{ \frac{\partial u_1}{\partial x} \right\}^T \right) + I_1 \left( \left\{ \frac{\partial^2 w_1}{\partial x^2} \right\} \left\{ \frac{\partial^2 w_1}{\partial x^2} \right\}^T \right) \right) dx \quad (3.16)$$

$A_1 = b \times h_1$  and  $I_1 = \frac{bh_1^3}{12}$  in Eq. 3.16 are the cross-sectional (c/s) area and moment of inertia (MOI) of the stop face layer.  $\bar{Q}_{11}$  is the reduced stiffness matrix constant and it is given as (Jack R. and Sierakowski, 2008)

$$\bar{Q}_{11} = Q_{11} \cos^4 \phi + Q_{22} \sin^4 \phi + 2(Q_{12} + 2Q_{66}) \sin^2 \phi \cos^2 \phi \quad (3.17)$$

$$\text{In which, } \begin{cases} Q_{11} = \frac{E_1(1+i\eta_1)}{1-\nu_{12}\nu_{21}}; & Q_{12} = \frac{\nu_{12}E_2(1+i\eta_2)}{1-\nu_{12}\nu_{21}}; \\ Q_{22} = \frac{E_2(1+i\eta_2)}{1-\nu_{12}\nu_{21}}; & \bar{Q}_{66} = G_{12}(1+i\eta_{12}) \end{cases} \quad (3.18)$$

### Bottom face layer:

Similar procedure is followed for the bottom face layer, and the strain energy in the bottom face layer can be obtained as

$$V_3^e = \frac{b}{2} \int_{-\frac{h_3}{2}}^{\frac{h_2}{2}} \int_0^l \left( \left\{ \frac{\partial u_3}{\partial x} - (z-e_3) \frac{\partial^2 w_3}{\partial x^2} \right\} \bar{Q}_{ij} \right)_3 \left\{ \frac{\partial u_3}{\partial x} - (z-e_3) \frac{\partial^2 w_3}{\partial x^2} \right\}^T dx dz \quad (3.19)$$

$$V_3^e = \frac{\bar{Q}_{11}}{2} \int_0^l \left( A_3 \left( \left\{ \frac{\partial u_3}{\partial x} \right\} \left\{ \frac{\partial u_3}{\partial x} \right\}^T \right) + I_3 \left( \left\{ \frac{\partial^2 w_3}{\partial x^2} \right\} \left\{ \frac{\partial^2 w_3}{\partial x^2} \right\}^T \right) \right) dx \quad (3.20)$$

$A_3 = b \times h_3$  and  $I_3 = \frac{bh_3^3}{12}$  in Eq. 3.20 are the c/s area and area MOI of the bottom face layer and  $\bar{Q}_{11}$  is the reduced stiffness matrix constant.

**Core layer:**

The stress-strain relationship matrix for the core layer is given (Jack R. and Sierakowski, 2008) as

$$\begin{Bmatrix} \sigma_{x2} \\ \sigma_{z2} \\ \sigma_{xz2} \end{Bmatrix} = \begin{bmatrix} Q_{11})_2 & Q_{13})_2 & 0 \\ Q_{13})_2 & Q_{33})_2 & 0 \\ 0 & 0 & 2Q_{55})_2 \end{bmatrix} \begin{Bmatrix} \epsilon_{x2} \\ \epsilon_{z2} \\ \epsilon_{xz2} \end{Bmatrix} \quad (3.21)$$

$$\text{In which, } \begin{cases} Q_{11})_2 = \frac{E_{MRF}^*}{1-\nu_{MRF}^2}; & Q_{13})_2 = \frac{\nu_{MRF} E_{MRF}^*}{1-\nu_{MRF}^2}; \\ Q_{33})_2 = \frac{E_{MRF}^*}{1-\nu_{MRF}^2}; & \bar{Q}_{55})_2 = G_{MRF}^* \end{cases} \quad (3.22)$$

Where  $Q_{ij})_2$  is the stiffness matrix constants for core the layer.

After substituting the strain-displacement Eq. 3.8 into 3.13 and the strain energy is written as follows

$$V_2^e = \frac{b}{2} \int_{-\frac{h_2}{2}}^{\frac{h_2}{2}} \int_0^l \left( \left( \left\{ \frac{\partial u_2'}{\partial x} \right\} Q_{ij})_2 \left\{ \frac{\partial u_2'}{\partial x} \right\}^T \right) + \left( \left\{ \frac{\partial w_2'}{\partial z} \right\} Q_{ij})_2 \left\{ \frac{\partial w_2'}{\partial z} \right\}^T \right) + \left( \left\{ \frac{\partial w_2'}{\partial x} + \frac{\partial u_2'}{\partial z} \right\} Q_{ij})_2 \left\{ \frac{\partial w_2'}{\partial x} + \frac{\partial u_2'}{\partial z} \right\}^T \right) dx dz \quad (3.23)$$

$$V_2^e = \frac{1}{2} \int_0^l \left( (Q_{11})_2 \left( (A_2 \{B_1\} \{B_1\}^T) + (I_2 \{B_2\} \{B_2\}^T) \right) + (Q_{33})_2 (A_2 \{B_3\} \{B_3\}^T) + 2(Q_{13})_2 (A_2 \{B_1\} \{B_3\}^T) + (Q_{55})_2 (A_2 (\{B_4\} \{B_4\}^T) + I_2 (\{B_5\} \{B_5\}^T)) \right) dx \quad (3.24)$$

$A_2 = b \times h_2$  and  $I_2 = \frac{bh_2^3}{12}$  in Eq. 3.24 are the c/s area and area MOI of the MR fluid core layer and

$$\left\{ \begin{array}{l} B_1 = \left[ \frac{\frac{\partial u_1}{\partial x} + \frac{\partial u_3}{\partial x}}{2} + \frac{h_1 \frac{\partial^2 w_1}{\partial x^2} - h_3 \frac{\partial^2 w_3}{\partial x^2}}{4} \right]; \quad B_2 = \left[ \frac{\frac{\partial u_1}{\partial x} - \frac{\partial u_3}{\partial x}}{h_2} + \frac{h_1 \frac{\partial^2 w_1}{\partial x^2} + h_3 \frac{\partial^2 w_3}{\partial x^2}}{2h_2} \right]; \\ B_3 = \left[ \frac{w_1 - w_3}{h_2} \right]; \quad B_4 = \left[ \frac{u_1 - u_3}{h_2} + \frac{(h_1 + h_2)\theta_1 + (h_3 + h_2)\theta_3}{2h_2} \right]; \quad B_5 = \left[ \frac{\theta_1 - \theta_3}{h_2} \right] \end{array} \right. \quad (3.25)$$

Total strain energy ( $V^e$ ) associated with the sandwich beam is the summation of strain energies of all the layers. Hence,

$$V^e = V_1^e + V_2^e + V_3^e \quad (3.26)$$

### 3.4 ELEMENTAL MASS MATRIX

To obtain the elemental mass matrix, the total kinetic energy (KE) of the sandwich beam is needed. The basic form of the KE is given as follows

$$T = \frac{1}{2} \iiint_{dV} \rho_i (\dot{x})^2 dV \quad (3.27)$$

The displacements considered in the top, core layer, and bottom face layer are substituted into Eq. 3.27 to get the total kinetic energy of the sandwich beam and expressed as

$$T^e = \frac{1}{2} \iiint_{dV} \left( \begin{array}{l} \left( \rho_1 \left( \frac{\partial u_1'}{\partial t} \right)^2 \right) + \left( \rho_2 \left( \frac{\partial u_2'}{\partial t} \right)^2 \right) + \left( \rho_3 \left( \frac{\partial u_3'}{\partial t} \right)^2 \right) \\ + \left( \rho_1 \left( \frac{\partial w_1'}{\partial t} \right)^2 \right) + \left( \rho_2 \left( \frac{\partial w_2'}{\partial t} \right)^2 \right) + \left( \rho_3 \left( \frac{\partial w_3'}{\partial t} \right)^2 \right) \end{array} \right) dV \quad (3.28)$$

$$T^e = \frac{1}{2} \iiint_{dV} \left( \left( \rho_1 \left( \frac{\partial u'_1}{\partial t} \right)^2 \right) + \left( \rho_2 \left( \frac{\partial u'_2}{\partial t} \right)^2 \right) + \left( \rho_3 \left( \frac{\partial u'_3}{\partial t} \right)^2 \right) \right. \\ \left. + \left( \rho_1 \left( \frac{\partial w'_1}{\partial t} \right)^2 \right) + \left( \rho_2 \left( \frac{\partial w'_2}{\partial t} \right)^2 \right) + \left( \rho_3 \left( \frac{\partial w'_3}{\partial t} \right)^2 \right) \right) dV \quad (3.29)$$

$$T^e = \frac{1}{2} \iiint_{dV} \left( \left( \rho_1 \left( \frac{\partial u'_1}{\partial t} \right) \left( \frac{\partial u'_1}{\partial t} \right)^T \right) + \left( \rho_2 \left( \frac{\partial u'_2}{\partial t} \right) \left( \frac{\partial u'_2}{\partial t} \right)^T \right) + \left( \rho_3 \left( \frac{\partial u'_3}{\partial t} \right) \left( \frac{\partial u'_3}{\partial t} \right)^T \right) \right. \\ \left. + \left( \rho_1 \left( \frac{\partial w'_1}{\partial t} \right) \left( \frac{\partial w'_1}{\partial t} \right)^T \right) + \left( \rho_2 \left( \frac{\partial w'_2}{\partial t} \right) \left( \frac{\partial w'_2}{\partial t} \right)^T \right) + \left( \rho_3 \left( \frac{\partial w'_3}{\partial t} \right) \left( \frac{\partial w'_3}{\partial t} \right)^T \right) \right) dV \quad (3.30)$$

Where,  $\frac{\partial}{\partial t}$  is the partial derivative of time. After rearranging the displacements of all the layers and integration, Eq. 3.29 can be rewritten as

$$T^e = \frac{1}{2} \int_0^l (\rho_1 A_1 D_1 + (\rho_2 A_2 + \rho_r A_r) D_2 + \rho_3 A_3 D_3 + \rho_1 I_1 D_4 + (\rho_2 I_2 + \rho_r I_r) D_5 + \rho_3 I_3 D_6) dx \quad (3.31)$$

$\rho_1$ ,  $\rho_2$ ,  $\rho_r$  and  $\rho_3$  in Eq. 3.30 are the density of the face layer, core layer/MR fluid, rubber sealant, and bottom face layer, respectively.  $A_r = b_r \times h_2$ ,  $I_r = b_2 \times h_2^3$  are c/s area and area MOI of the rubber sealant material and

$$\left\{ \begin{array}{l} D_1 = \left( (\dot{u}_1)^2 + (\dot{w}_1)^2 \right); D_2 = \left( \left( \left( \frac{\dot{u}_1 + \dot{u}_3}{2} \right) + \left( \frac{h_1 \dot{\theta}_1 - h_3 \dot{\theta}_3}{4} \right) \right)^2 + \left( \frac{\dot{w}_1 + \dot{w}_3}{2} \right)^2 \right); \\ D_3 = \left( (\dot{u}_3)^2 + (\dot{w}_3)^2 \right); D_4 = \left( (\dot{\theta}_1)^2 \right); D_5 = \left( \left( \frac{\dot{u}_1 - \dot{u}_3}{h_2} + \frac{h_1 \dot{\theta}_1 + h_3 \dot{\theta}_3}{2h_2} \right)^2 + \left( \frac{\dot{w}_1 - \dot{w}_3}{h_2} \right)^2 \right); \\ D_6 = \left( (\dot{\theta}_3)^2 \right) \end{array} \right. \quad (3.32)$$

Where  $\dot{u}_1 = N_{u_1}(x)\{\dot{q}^e(t)\}$ ;  $\dot{u}_3 = N_{u_3}(x)\{\dot{q}^e(t)\}$ ;  $\dot{w}_1 = N_{w_1}(x)\{\dot{q}^e(t)\}$ ;  $\dot{w}_3 = N_{w_3}(x)\{\dot{q}^e(t)\}$ ;

$$\dot{\theta}_1 = \frac{\partial \dot{w}_1}{\partial x}; \quad \dot{\theta}_3 = \frac{\partial \dot{w}_3}{\partial x}$$

### 3.5 FINITE ELEMENT FORMULATION

In this present study, a sandwich beam element with six DOF on each side is taken. Each side of the sandwich beam element is associated with three DOF in the top and three in the bottom face layer. Namely, Axial displacement ( $u$ ), Transverse displacement ( $w$ ), and rotational displacement ( $\theta$ ). Left side DOF of the sandwich beam is represented with  $q_i$  and the right side with  $q_j$ . The displacements associated with axial, transverse and rotational displacement can be written as a combination of nodal displacement vector and shape functions:

$$\begin{aligned} \{q^e\} &= \begin{Bmatrix} q_i \\ q_j \end{Bmatrix} \\ &= \{w_{i1} \quad \theta_{i1} \quad u_{i1} \quad w_{i3} \quad \theta_{i3} \quad u_{i3} \quad w_{j1} \quad \theta_{j1} \quad u_{j1} \quad w_{j3} \quad \theta_{j3} \quad u_{j3}\}^T \end{aligned} \quad (3.33)$$

The elemental displacements are given as

$$\begin{cases} u_1(x,t) = N_{u_1}(x)\{q^e(t)\} \\ w_1(x,t) = N_{w_1}(x)\{q^e(t)\} \\ u_3(x,t) = N_{u_3}(x)\{q^e(t)\} \\ w_3(x,t) = N_{w_3}(x)\{q^e(t)\} \end{cases} \quad (3.34)$$

$$\begin{cases} N_{u_1}(x) = \{(0 \quad 0 \quad N_1(x) \quad 0 \quad 0 \quad 0 \quad 0 \quad 0 \quad N_4(x) \quad 0 \quad 0 \quad 0)\} \\ N_{u_3}(x) = \{(0 \quad 0 \quad 0 \quad 0 \quad 0 \quad N_1(x) \quad 0 \quad 0 \quad 0 \quad 0 \quad 0 \quad N_4(x))\} \\ N_{w_1}(x) = \{(N_2(x) \quad N_3(x) \quad 0 \quad 0 \quad 0 \quad 0 \quad N_5(x) \quad N_6(x) \quad 0 \quad 0 \quad 0 \quad 0)\} \\ N_{w_3}(x) = \{(0 \quad 0 \quad 0 \quad N_2(x) \quad N_3(x) \quad 0 \quad 0 \quad 0 \quad 0 \quad N_5(x) \quad N_6(x) \quad 0)\} \end{cases} \quad (3.35)$$

$N_{u_1}(x)$ ,  $N_{u_3}(x)$ ,  $N_{w_1}(x)$  and  $N_{w_3}(x)$  in Eq. 3.35 are polynomial shape functions.

$$\text{In which, } \begin{cases} N_1(x) = 1 - \frac{x}{l_e}; & N_2(x) = 1 - \frac{3x^2}{l_e^2} + \frac{2x^3}{l_e^3}; & N_3(x) = x - \frac{2x^2}{l_e} + \frac{x^3}{l_e^2} \\ N_4(x) = \frac{x}{l_e}; & N_5(x) = \frac{3x^2}{l_e^2} - \frac{2x^3}{l_e^3}; & N_6(x) = -\frac{x^2}{l_e} + \frac{x^3}{l_e^2} \end{cases} \quad (3.36)$$

The elemental stiffness matrix is obtained by substituting the elemental displacements shown in Eq. 3.34 into Eq. 3.26, and elemental strain energy can be written as

$$V^e = \frac{1}{2} \{q^e\}^T \left( [k_1^e] + [k_2^e] + [k_3^e] \right) \{q^e\} \quad (3.37)$$

$$V^e = \frac{1}{2} \{q^e\}^T ([k^e]) \{q^e\} \quad (3.38)$$

Where elemental stiffness matrix  $[k^e] = [k_1^e] + [k_2^e] + [k_3^e]$ .

$[k_1^e]$ ,  $[k_2^e]$  and  $[k_3^e]$  are elemental stiffness matrices of the top, core layer and bottom composite face layers, respectively.

The elemental mass matrix is obtained by substituting the elemental displacements shown in Eq. 3.34 into Eq. 3.30, and the elemental KE of the sandwich beam is written as

$$T^e = \frac{1}{2} \{\dot{q}^e\}^T ([m^e]) \{\dot{q}^e\} \quad (3.39)$$

Lagrange's energy method is adopted to obtain the EOM for the present study from (Zhao et al., 2022a, 2021b; a, 2022c). Generally, Lagrange's equation is in the form of

$$\frac{d}{dt} \left( \frac{\partial T^e}{\partial \dot{q}_i} \right) - \frac{\partial T^e}{\partial q_i} + \frac{\partial V^e}{\partial q_i} = R_i, \quad i = 1, \dots, n \quad (3.40)$$

Where  $n$  is the total DOF assumed and  $R_i$  is the force vector associated with the  $i^{th}$  DOF of the system. The elemental EOM (Eq. 3.41) is obtained by substituting the elemental strain and kinetic energies in Eq. 3.38 and 3.39 into Eq. 3.40.

$$[m^e] \{\ddot{q}^e\} + [k^e] \{q^e\} = \{f^e\} \quad (3.41)$$

In which  $[m^e]$  and  $[k^e]$  are elemental mass and stiffness matrix and  $\{f^e\}$  is the load column vector.

Global mass, stiffness, and force vector matrices are obtained by assembling the elemental matrices. The final form of EOM for the sandwich beam is written as

$$[M]\{\ddot{q}\} + [K]\{q\} = \{F\} \quad (3.42)$$

$$\text{Where, } \{F\} = \begin{pmatrix} 0 \\ \vdots \\ \int_0^L f(x,t)[N_{w_1}(x)]dx \\ 0 \\ 0 \\ 0 \\ 0 \\ 0 \end{pmatrix} \quad (3.43)$$

$M$ ,  $K$  and  $F$  in Eq. 3.42 are the global mass, stiffness and force matrices, respectively. For the static problem, taking  $\{\ddot{q}\} = 0$ , the governing equation becomes,

$$[K]\{q\} = \{F\} \quad (3.44)$$

The external force applied is zero for the free vibration analysis, and the equation of motion (Eq. 3.42) becomes

$$[M]\{\ddot{q}\} + [K]\{q\} = 0 \quad (3.45)$$

Solving Eq. 3.45, natural frequency of sandwich beam is obtained as

$$[[K] - \omega^2[M]] = 0 \quad (3.46)$$

Since the complex shear modulus approach is used for the MR fluid core, the eigen values obtained are complex. The loss factor is obtained by taking the ratio of the imaginary part of the eigen value to the real part of the eigen value (Arvin et al., 2010; Patil et al., 2020).

$$\text{Loss factor } (\eta) = \frac{\text{Imag}(\omega_n^2)}{\text{real}(\omega_n^2)} \quad (3.47)$$

### 3.6 SOLUTION PROCEDURE

The FE formulations established for the sandwich beam in the current study are numerically programmed using the MATLAB platform. The procedure followed for

the implementation of FE formulations is presented in the flowchart figure 3.4. The solution technique begins with the geometrical and material parameters of individual layers of the sandwich beam.

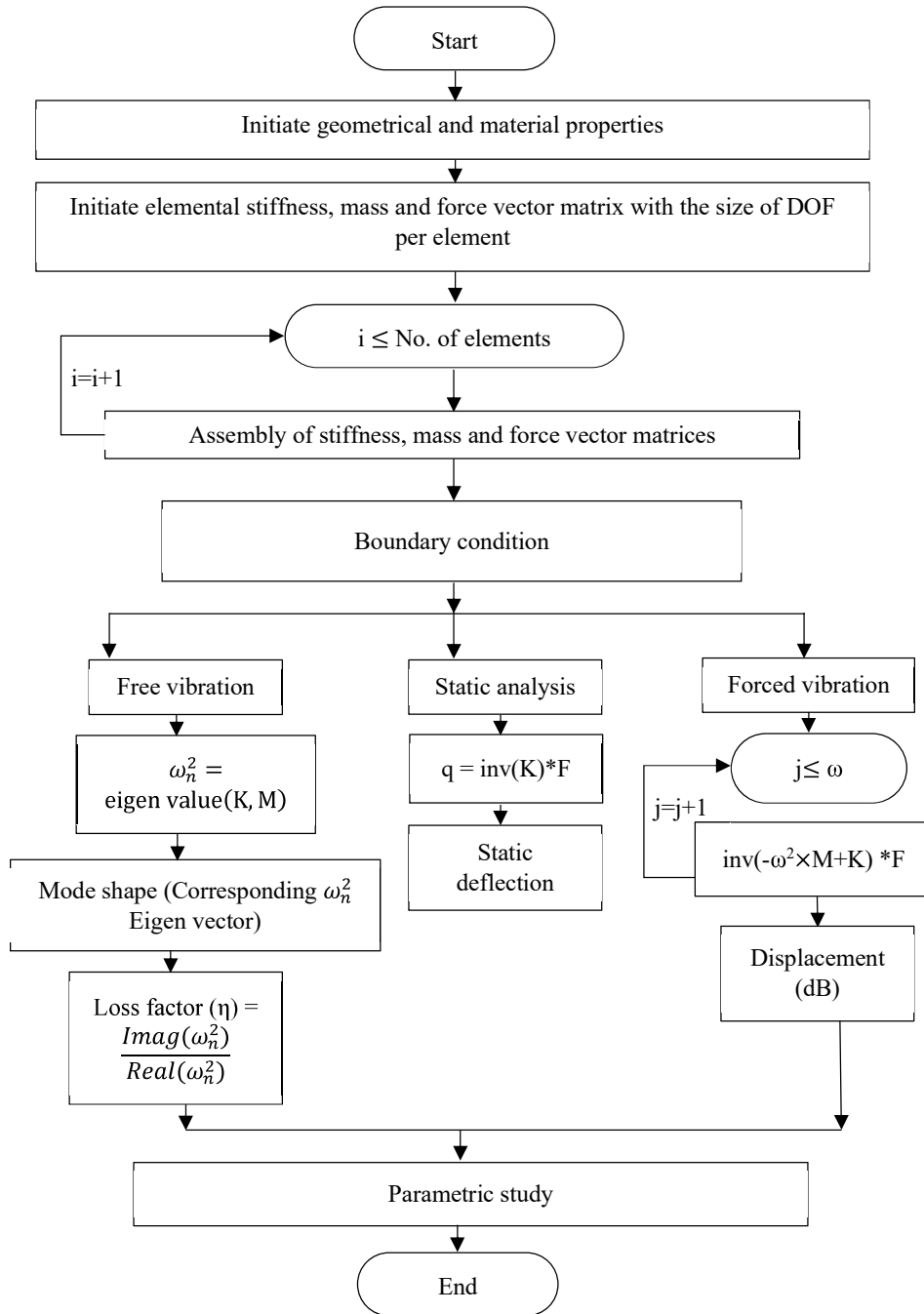


Figure 3.4 The flow chart of the FE formulations implementation



After that, elemental mass, stiffness, and force vector matrices are initiated with the size of DOF per element. Further, the global mass and stiffness matrices are assembled up to number of elements to obtain the convergent solution. Then, the boundary conditions are imposed on the assembled global stiffness, mass, and force vector matrices as shown in procedure flowchart figure 3.4. The DOF arrested at each end of the sandwich beam element is presented in the table 3.1. The static, free, and forced vibration responses of the composite sandwich beam can be taken using the procedure flowchart shown in figure 3.4. For static analysis, the transverse displacement data of the top face layer will be stored by solving the Eq. 3.44. The natural frequency is obtained by solving the eigenvalue problem in Eq. 3.46, and loss factor is determined by taking the ratio of imaginary part to the real part of the corresponding eigen value (natural frequency). Further, mode shapes can be extracted using the eigenvectors corresponding to the particular eigen value. The forced vibration response can also be taken in the frequency domain with respect to the transverse deflection.

Table 3.1 Boundary conditions considered for the present study

Boundary Condition	At $x = 0$	At $x = L$
Clamped-Free (CF)	$u_{0_1} = 0, w_{0_1} = 0 \quad w'_{0_1} = 0$ $u_{0_3} = 0, w_{0_3} = 0 \quad w'_{0_3} = 0$	--
Clamped-Clamped (CC)	$u_{0_1} = 0, w_{0_1} = 0 \quad w'_{0_1} = 0$ $u_{0_3} = 0, w_{0_3} = 0 \quad w'_{0_3} = 0$	$u_{l_1} = 0, w_{l_1} = 0 \quad w'_{l_1} = 0$ $u_{l_3} = 0, w_{l_3} = 0 \quad w'_{l_3} = 0$
Simply-Supported (SS)	$u_{0_1} = 0, w_{0_1} = 0$ $u_{0_3} = 0, w_{0_3} = 0$	$u_{l_1} = 0, w_{l_1} = 0$ $u_{l_3} = 0, w_{l_3} = 0$
Clamped-Simple (CS)	$u_{0_1} = 0, w_{0_1} = 0 \quad w'_{0_1} = 0$ $u_{0_3} = 0, w_{0_3} = 0 \quad w'_{0_3} = 0$	$u_{l_1} = 0, w_{l_1} = 0$ $u_{l_3} = 0, w_{l_3} = 0$
Simple-Free (SF)	$u_{0_1} = 0, w_{0_1} = 0$ $u_{0_3} = 0, w_{0_3} = 0$	--

### 3.7 VALIDATION

#### 3.7.1 Convergence

The convergence of the solution and validation study for the present FE formulation is discussed in this section. A convergence study is done for two fundamental modes, as shown in figure 3.5 (a) and (b), respectively. For this, material and geometrical properties are taken from ref. (Arikoglu and Ozkol, 2010).

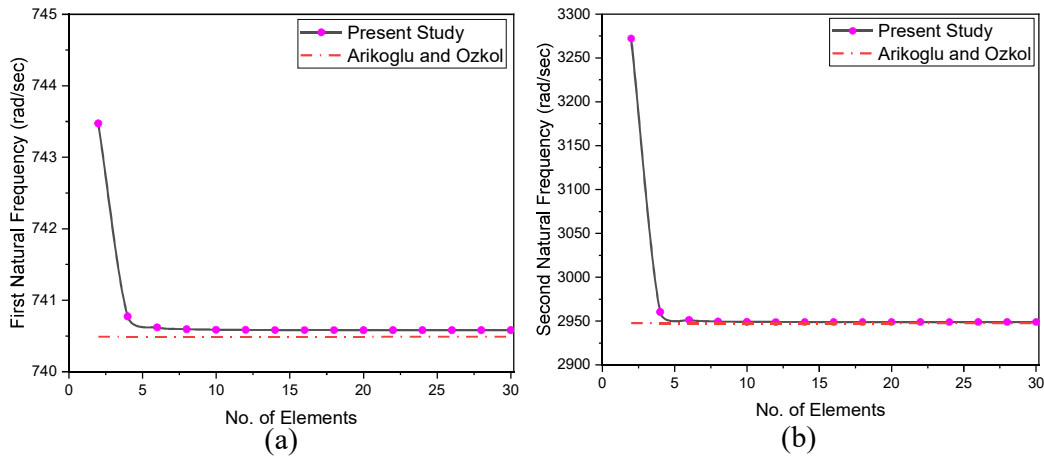


Figure 3.5 convergence study for the (a) 1<sup>st</sup> mode and (b) 2<sup>nd</sup> mode

For the convergence confirmation, up to thirty elements are taken. For the cantilever condition, the decent convergence is appeared at around 20 elements for the first and second modes, respectively.

The results obtained from the present FE formulation are compared with the available literature for free vibration analysis in order to validate the current formulation and solution technique. For this, different validation case studies from the literature are considered. The case studies are presented as follows,

#### 3.7.2 Validation for viscoelastic sandwich beam

The developed FE formulation procedure is validated for the sandwich beams with the viscoelastic core material and the validation study covers the different case studies including different boundary conditions.

##### 3.7.2.1 Case – 1

The properties of each layer are taken from the ref. (Howson and Zare, 2005). The results of the present formulation are validated, as illustrated in table 3.2. The fixed end

boundary condition is considered in this case. The obtained outcomes are very near and accurate to both the theoretical and experimental results.

Table 3.2 Fundamental five natural frequencies

<b>Mode</b>	<b>Present study</b>	<b>Howson and Zare, (2005)</b>	<b>Marur and Kant, (1996)</b>	<b>Raville et al., (1960) (Experimental)</b>
1	34.626	34.5965	33.563	--
2	93.272	93.1	90.364	--
3	177.694	177.155	172.07	185.5
4	284.022	282.784	274.91	280.3
5	408.672	406.325	395.42	399.4s

### 3.7.2.2 Case – 2

The properties of different layers are taken from the Ref. (Howson and Zare, 2005). The results of the present formulation are validated for the cantilever condition as presented in table 3.3. The extracted results are well agreed with the literature.

Table 3.3 Fundamental five Natural frequencies

<b>Mode</b>	<b>Present study</b>	<b>Howson and Zare, (2005)</b>	<b>Marur and Kant, (1996)</b>	<b>Ahmed, (1971)</b>
1	33.74923	33.7513	33.7	33.97
2	198.9427	198.992	197.5	200.5
3	512.1983	512.307	505.5	517
4	907.3198	907.299	890.5	918
5	1350.145	1349.65	1321	1368

### 3.7.2.3 Case-3

Table 3.4 Geometrical and Material properties of composite face layers and viscoelastic material with Length = 1000mm, and width = 25mm (Arvin et al., 2010)

Layers	Thickness (mm)	Elastic Moduli (GPa)		Shear Moduli (G <sub>12</sub> ) (MPa)	Density (ρ) (kg/m <sup>3</sup> )	Poisson's ratio (ν)
		E <sub>11</sub>	E <sub>22</sub>			
Top face layer (h <sub>1</sub> )	4	141.2	9.72	5530	1536	0.28
Viscoelastic layer (h <sub>2</sub> )	20	$E^* = 2G^*(1+\nu)$		$7.039 \times 10^{-1} + 2.1117 \times 10^{-1}i$	970	0.49
Bottom face layer (h <sub>3</sub> )	4	141.2	9.72	5530	1536	0.28

Properties of the different layers considered for this case are shown in table 3.4. The comparison of natural frequency and loss factor values are presented in table 3.5. The results obtained with this current formulation are found to be in close agreement with the referred literature (Arvin et al., 2010).

Table 3.5 Natural frequency and Loss factor values for Case-2

Mode	Natural Frequency		Loss Factor	
	Present study	Arvin et al., (2010)	Present study	Arvin et al., (2010)
s1	6.61290	6.70358	0.21310	0.21464
2	21.95129	22.31863	0.19795	0.19635
3	42.89322	43.80716	0.17361	0.16836
4	69.46200	71.45456	0.13166	0.12535
5	103.52788	107.08980	0.09899	0.09291

### 3.7.2.4 Case – 4

The properties of different layers are taken from the ref. (Patil et al., 2020). The results of the present formulation are validated as presented in table 3.6. The results are in well agreed with the literature available.

Table 3.6 Fundamental five Natural frequencies (rad/s)

Mode	Present study	Patil et al., (2020)
1	740.825	740.500
2	2948.853	2947.900
3	6628.896	6624.075
4	11780.159	11765.055

### 3.7.3 Validation for MR fluid sandwich beam

Further, the validation study is extended for the sandwich beams with the MR fluid by taking different cases from the available literature.

#### 3.7.3.1 Case - 1

The results obtained from current formulation and solution technique are validated with the existing literature for free vibration analysis. Ref. (Rajamohan et al., 2010b) presented the theoretical natural frequency values for the clamped-clamped boundary condition.

Table 3.7 Geometrical and Material properties of different layers with Length = 300mm, and width = 30mm (Rajamohan et al., 2010b))

Layers	Thickness (mm)	Elastic Moduli (E) (GPa)	Shear Moduli ( $G^*$ )	Density ( $\rho$ ) ( $\text{kg/m}^3$ )
Top face layer ( $h_1$ )	1	68	--	2700
MR fluid layer ( $h_2$ )	1.15	--	$G'(B) + iG''(B)$	3500
Bottom face layer ( $h_3$ )	1	68	--	2700

$$\text{Storage Modulus } G'(B) = -3.3691B^2 + 4.9975 \times 10^3 B + 0.873 \times 10^6$$

$$\text{Loss Modulus } G''(B) = -0.9B^2 + 0.8124 \times 10^3 B + 0.1855 \times 10^6$$

Storage and loss modulus are considered in terms of magnetic field (B). Properties of the different layers taken are shown in table 3.7. The comparison of natural frequency values is presented in table 3.8. The results obtained with this current formulation are found to be in good agreement with the ref. (Rajamohan et al., 2010b).

Table 3.8 Natural frequencies for Case-1

Field intensity (G)	Natural Frequency (Hz)			
		Mode-I	Mode-II	Mode-III
0	Rajamohan et al., (2010b)	57.66	139.66	255.93
	Present study	55.68	137.60	255.27
250	Rajamohan et al., (2010b)	66.52	154.74	275.59
	Present study	66.25	154.97	277.27

### 3.7.3.2 Case - 2

Further, the FE model is validated with an adaptive sandwich structure with a simply supported boundary condition at zero (0) Oe. The properties of the three layers of sandwich beam are taken from ref. (Yalcintas and Dai, 2004). The obtained results with the current formulation are very close and in good agreement with the ref. (Yalcintas and Dai, 2004) as shown in table 3.9.

Table 3.9 Natural frequencies

Mode	Natural Frequency	
	Yalcintas and Dai, (2004)	Present study
1	24.11	23.1133
2	66.18	61.1418
3	126.28	120.7505
4	207.34	202.6328
5	310.39	307.4029

### 3.7.3.3 Case - 3

Further, the results obtained with the current model are validated with the published literature of ref. (Yeh and Shih, 2006). The properties of each layer are tabulated in table 3.10. The validation of natural frequency and loss factor at a magnetic field of 900 Oe are presented in table 3.11. The findings obtained with this formulation are quite similar to those reported by ref. (Yeh and Shih, 2006).

Table 3.10 Properties of MR fluid sandwich beam with  $L = 400$  mm, and  $b = 25$  mm

Layers	Thickness (mm)	Elastic Moduli (E) (GPa)	Shear Moduli ( $G^*$ ) (MPa)	Density ( $\rho$ ) (kg/m <sup>3</sup> )
Top face layer (h <sub>1</sub> )	1.0	70	--	2700
MR fluid layer (h <sub>2</sub> )	1.0	--	$G'(B) + iG''(B)$	3500
Bottom face layer (h <sub>3</sub> )	1.0	70	--	2700

Storage Modulus  $G'(B) = 3.11 \times 10^{-7} B^2 + 3.56 \times 10^{-4} B + 0.578$

Loss Modulus  $G''(B) = 3.47 \times 10^{-9} B^2 + 3.85 \times 10^{-6} B + 6.31 \times 10^{-3}$

Table 3.11 Natural frequency and Loss factor

Mode	Natural Frequency		Loss Factor	
	Present study	Yeh and Shih, (2006)	Present study	Yeh and Shih, (2006)
1	29.347	25.561	0.006502	0.005757
2	70.262	69.807	0.005930	0.005650
3	130.946	130.759	0.004204	0.004147
4	211.822	211.784	0.002965	0.002953
5	314.234	314.228	0.002150	0.002145

### 3.8 SUMMARY

The developed FE formulations for the composite sandwich beam is discussed in this chapter. The current developed FE formulation considered the Euler-Bernoulli's method for the sandwich beam element and the Lagrange's approach is utilized to obtain the EOM. The implementation of MATLAB code for the FE formulations to get the static deflection, free vibration, and forced vibration response of sandwich beams under different boundary conditions is discussed throughout the chapter. Further, the

developed FE formulations solution is validated with the available literature by taking different case studies.



## CHAPTER – 4

# DYNAMIC RESPONSE OF SANDWICH BEAM WITH VISCOELASTIC CORE MATERIAL

### 4.1. INTRODUCTION

Even the literature suggests the numerous studies on the dynamic response of the sandwich beam with the viscoelastic core material, the influence of axial gradation of the viscoelastic material on the dynamic response of the sandwich beam is not explored much in the available literature. The present study has conducted the extensive studies on the influence of axial gradation on the dynamic response of the sandwich beam with viscoelastic material. There are two types of viscoelastic core material are considered for the study, namely DYAD 606 (VEM-1) and EC2216 (VEM-2). Further, the influence of viscoelastic material, boundary condition and configuration of the viscoelastic material on natural frequency, loss factor and frequency response are discussed.

Table 4.1 Material properties of face layers and viscoelastic materials

---

**Top and Bottom face layer** (Arikoglu and Ozkol, 2010)

$$E_1 = E_3 = 69 \text{ GPa}, \rho_1 = \rho_3 = 2800 \text{ kg/m}^3$$

**Viscoelastic Material** (Sharnappa et al., 2007)

**1. DYAD 606 (VEM-1)**

$$G'_{VEM-1} = 0.187 \text{ GPa}, G''_{VEM-1} = 0.388 \times G'_{VEM-1}, \rho_{VEM-1} = 1200 \text{ kg/m}^3$$

**2. EC2216 (VEM-2)**

$$G'_{VEM-2} = 0.575 \text{ GPa}, G''_{VEM-2} = 0.3 \times G'_{VEM-2}, \rho_{VEM-2} = 1250 \text{ kg/m}^3$$

---

### 4.2. INFLUENCE OF VISCOELASTIC MATERIAL

The influence of viscoelastic material on dynamic behavior of the sandwich beam for various boundary conditions is discussed in this section. The material properties utilized for the current study are illustrated in table 4.1. The length of 300mm and width of 25mm is considered for all the results presented. In addition, thickness of 1mm is taken for both the face layers and viscoelastic material. VEM-1 and VEM-2 are considered

as the viscoelastic materials. The boundary conditions considered are CF, CC, SS and CS. Free vibration study is conducted to get the natural frequency and loss factor. Figure 4.1 (a), (b), (c) and (d) illustrates the variation in natural frequency for VEM-1 and VEM-2 viscoelastic sandwich beam for various boundary conditions, respectively. The natural frequency obtained for the sandwich beam with VEM-2 material is more compared to the VEM-1 for all the boundary constraints (Pradeep and Ganesan, 2006). This is because the storage modulus of the VEM-2 material is relatively more than VEM-1. This leads to higher stiffness of the overall sandwich beam.

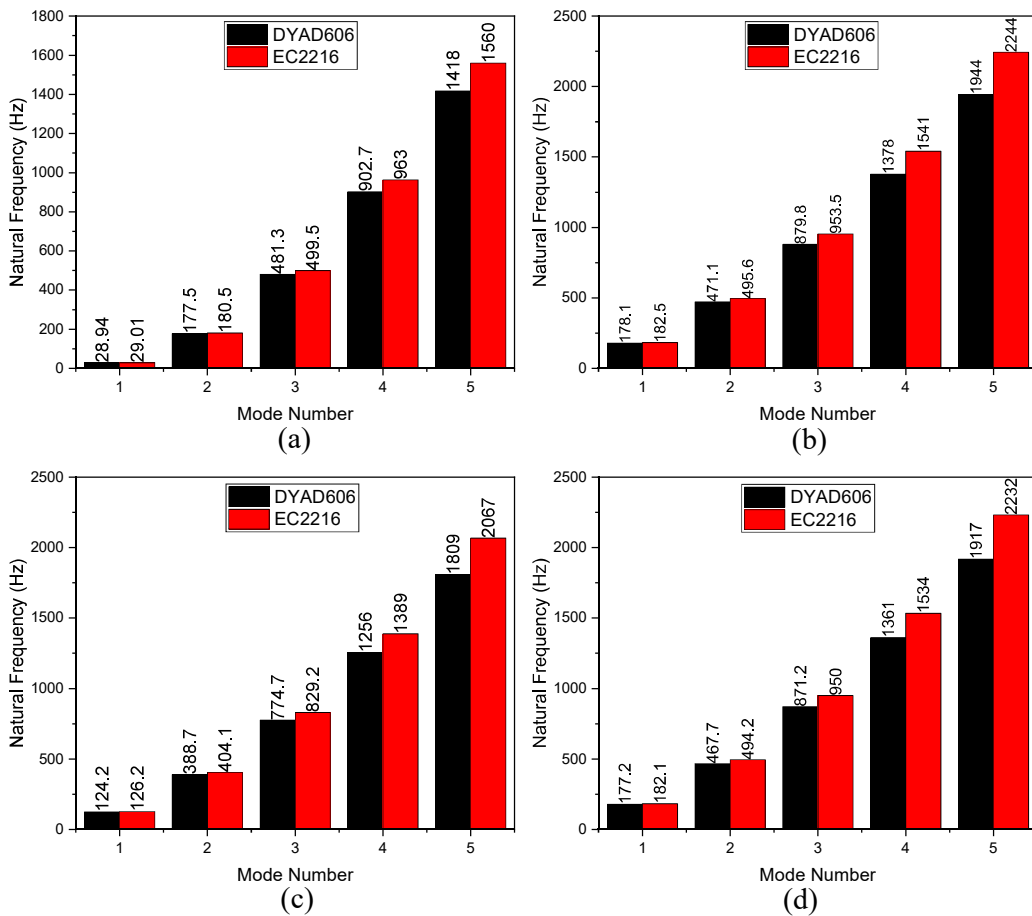


Figure 4.1 Effect of viscoelastic material on natural frequency for (a) CF (b) CC (c) SS and (d) CS boundary conditions

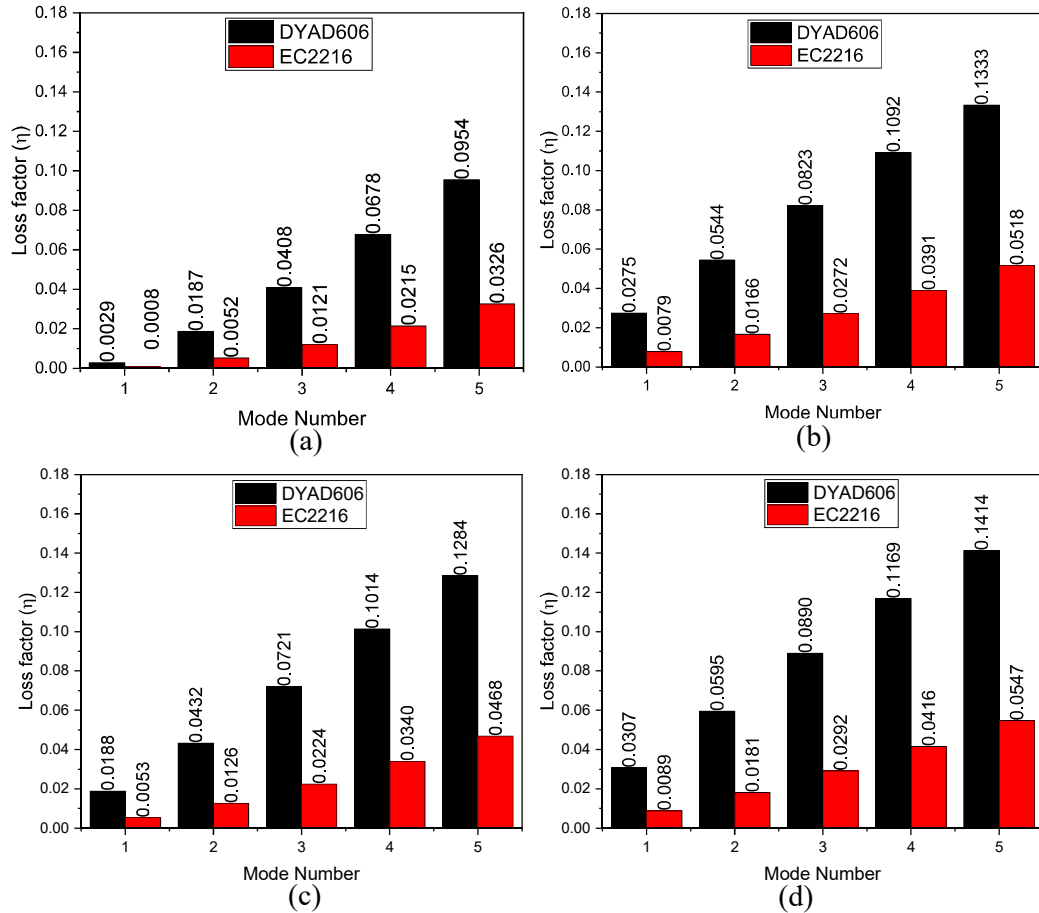


Figure 4.2 Effect of viscoelastic material on loss factor for (a) CF (b) CC (c) SS and (d) CS boundary conditions

The influence of viscoelastic material on loss factor for the various boundary conditions are illustrated in figure 4.2 (a), (b), (c) and (d) respectively. For all boundary conditions, the sandwich beam with VEM-1 material has a higher loss factor compared to that of VEM-2 material. This is due to VEM-1 material's ability to dissipate more shear strain energy during deformation, resulting in higher loss factor values (Pradeep and Ganesan, 2006; Sharnappa et al., 2007). Additionally, the higher modes exhibit higher loss factor values for all the boundary conditions.

Forced vibration study is conducted to obtain the frequency response of the sandwich beam. For this, harmonic load with constant force of 2N is applied. The load is applied in the transverse direction for all the boundary conditions. The frequency response of the sandwich beam for different boundary conditions is illustrated in figure 4.3 (a), (b),

(c) and (d) respectively. The relative reduction in the peak amplitude of the sandwich beam with VEM-1 material is higher than the VEM-2 (Pradeep and Ganesan, 2006). The reduction in peak vibration amplitude is clearly illustrated in figure 4.3 for all the boundary conditions. This reduction is due to more dissipation of mechanical vibration amplitude energy into heat of the sandwich beam with VEM-1 material. This behavior is more helpful for structural applications where higher amplitudes of vibration are needed to controlled.

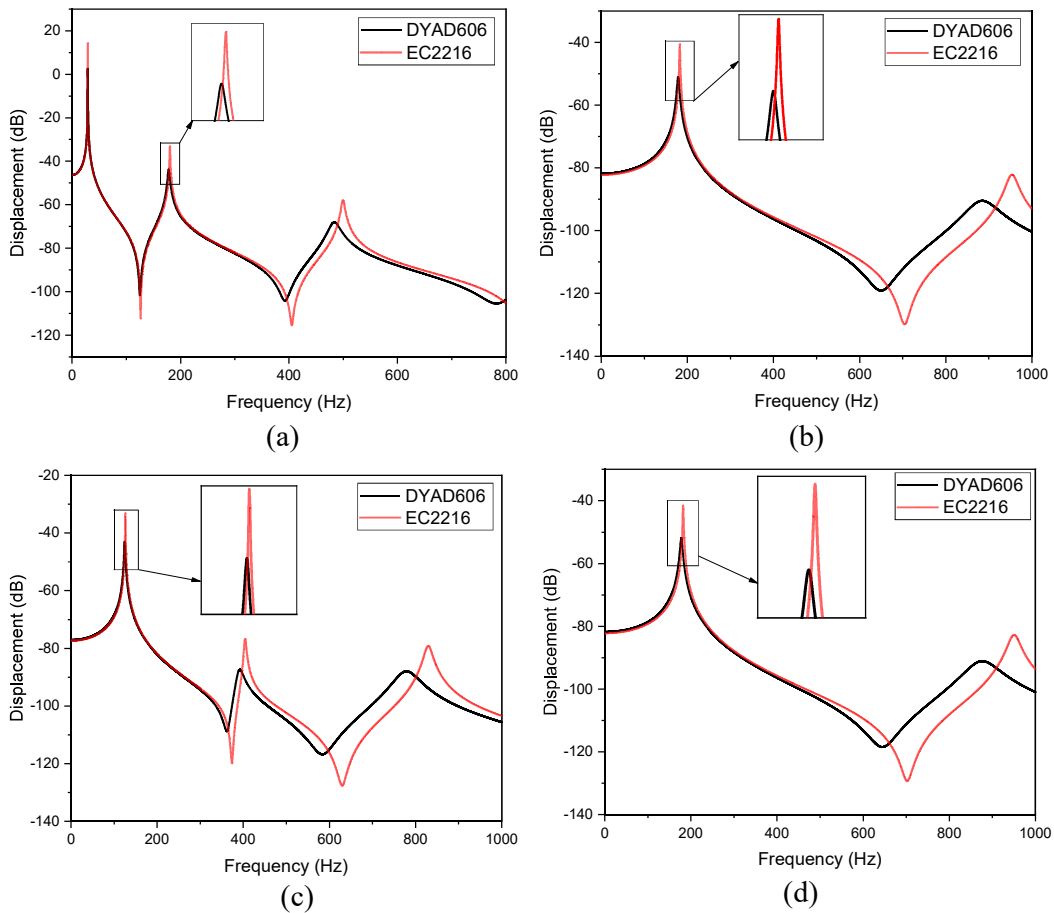


Figure 4.3 Effect of viscoelastic material on frequency response for (a) CF (b) CC (c) SS and (d) CS boundary conditions

### 4.3. INFLUENCE OF BOUNDARY CONDITION

The impact of boundary condition on sandwich beam’s dynamic response is presented in this section. The boundary conditions considered are CF, CC, SS and CS. The natural

frequency of the sandwich beam with VEM-1 and VEM-2 material for the five fundamental modes are illustrated in figure 4.4.

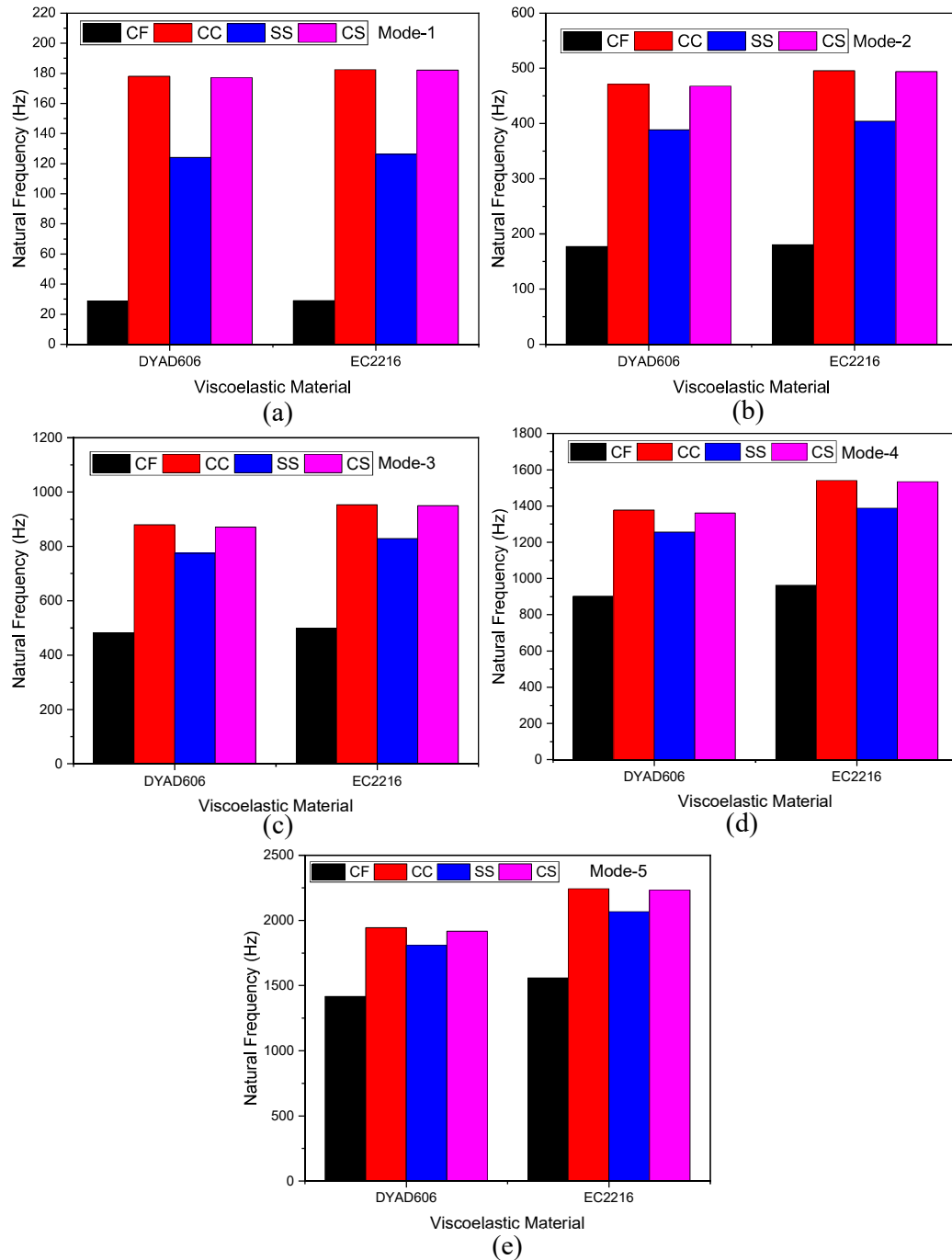


Figure 4.4 Effect of boundary condition on natural frequency for (a) Mode-1 (b) Mode-2 (c) Mode-3 (d) Mode-4 (e) Mode-5

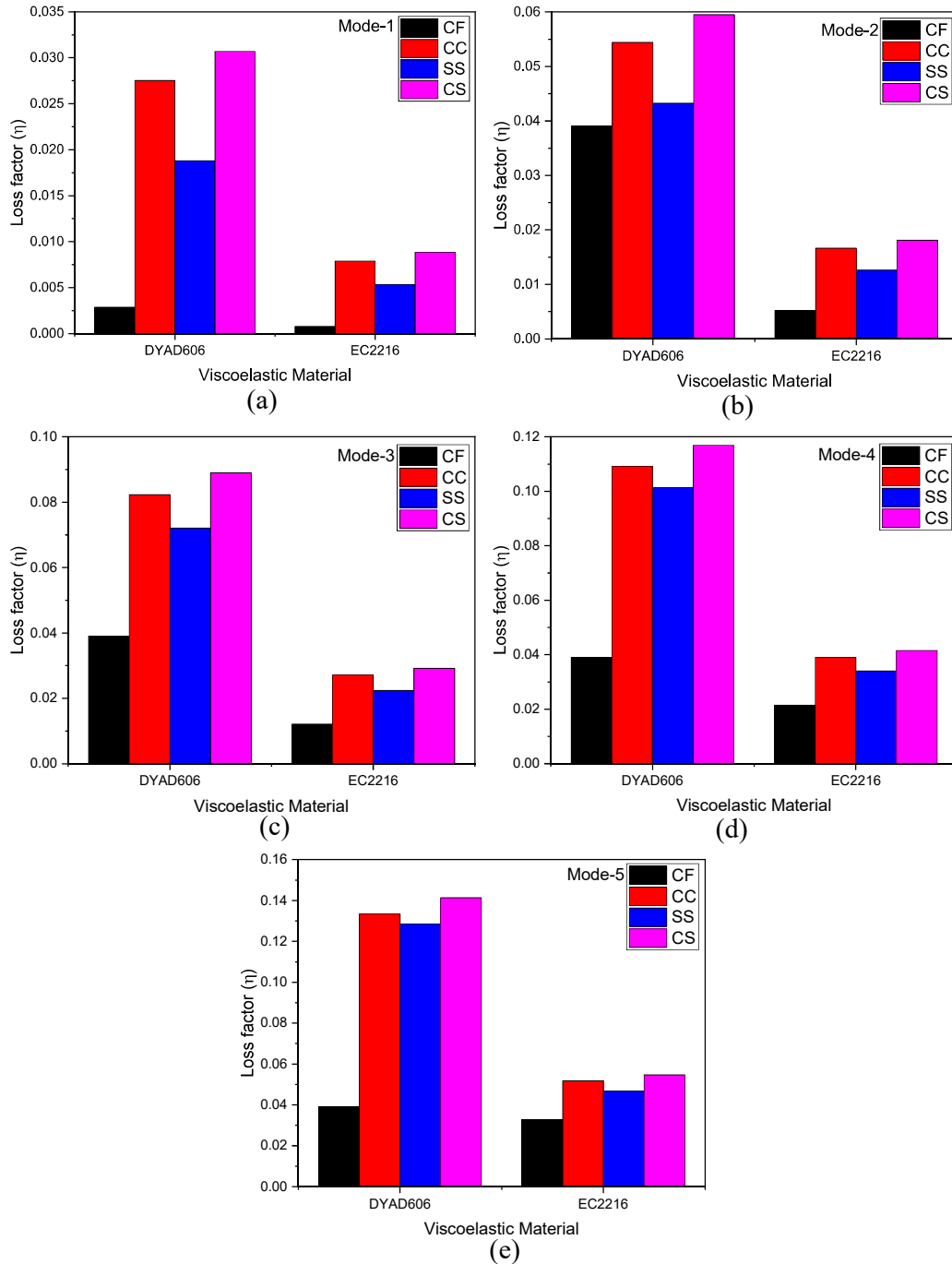


Figure 4.5 Effect of boundary condition on loss factor for (a) mode-1 (b) mode-2 (c) mode-3 (d) mode-4 (e) mode-5

The natural frequency is less for CF condition at all the modes as the CF condition is more flexible and less stiff relatively compared to the other boundary conditions. The CC boundary condition stiffness is higher due to degrees of freedom fixed on both sides

of the sandwich beam compared to CF, CS and SS boundary conditions (Rajamohan et al., 2010b). This leads to higher natural frequency values for the CC boundary condition at all modes.

The variation in loss factor for the sandwich beam with different viscoelastic materials for CF, CC, SS and CS boundary conditions is illustrated in figure 4.5 for the fundamental five modes respectively. From the results obtained, it is observed that the loss factor for the CS condition is relatively more compared to other boundary conditions. The CS condition effectively dissipates more mechanical strain energy into the form of heat due to shear action of the core material while deforming than the other boundary conditions. This leads to higher loss factor values for the CS boundary condition at all five fundamental modes. Further, the percentage (%) of change in loss factor of the VEM-1 compared to the VEM-2 is calculate as follows

$$\text{The percentage (\%) of change in loss factor} = \frac{\eta_{VEM-1} - \eta_{VEM-2}}{\eta_{VEM-1}} \times 100 \quad (4.1)$$

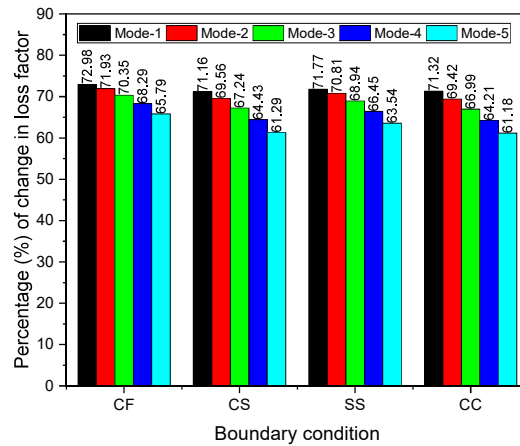


Figure 4.6 The percentage (%) of change in loss factor of the VEM-1 compared to the VEM-2

The percentage of change in loss factor with respect to the boundary condition is illustrated in the figure 4.6. The loss factor of the VEM-1 is increased by 72.98%, 71.16%, 71.77%, and 71.32% when compared to the VEM-2 at the first fundamental

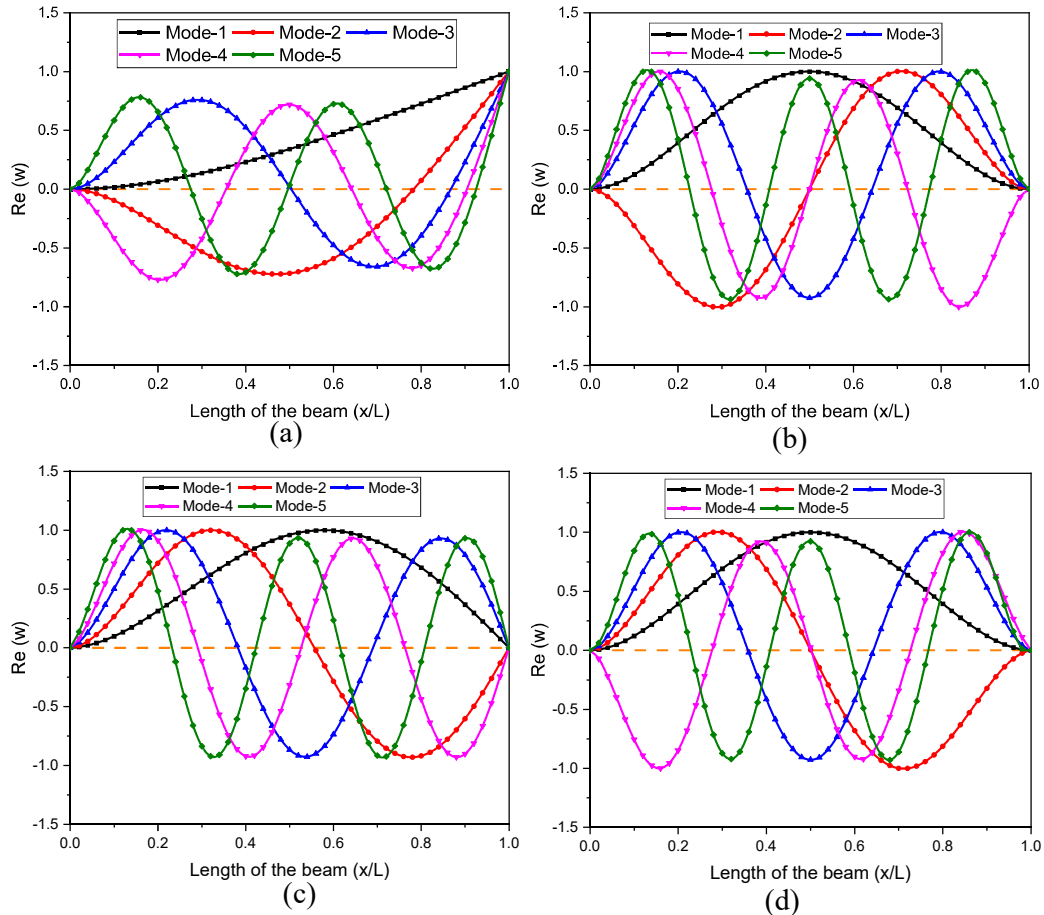


Figure 4.7 The normalized fundamental five modes (a, b, c and d) real part of the transverse deflection of CF, CC, SS and CS boundary conditions

mode for the CF, CS, SS, and CC boundary conditions, respectively. The maximum percentage of change in loss factor is observed for the CF boundary condition.

The mode shapes of five fundamental modes are extracted for all the boundary conditions. The mode shapes are drawn using eigen vectors corresponding to the eigen values (natural frequencies). The normalised real and imaginary parts are presented since viscoelastic material is modelled using complex modulus approach. All the five modes with real and imaginary parts of transverse displacement are drawn for CF, CC, SS and CS boundary conditions are shown in figure 4.7, respectively.



#### 4.4. INFLUENCE OF AXIAL GRADATION OF VEM

In this section, the influence of different axial gradation configurations of DYAD 606 (VEM-1) and EC2216 (VEM-2) viscoelastic materials on the dynamic behavior of the sandwich beam is discussed. Four different types of axial gradation configurations of viscoelastic materials are considered. Configuration-1 consists of two portions of the viscoelastic material with the beam's first half-length containing VEM-1 and the second half-length consisting of VEM-2, as shown in figure 4.8 (a). Configuration-2 also consists of two portions of viscoelastic material, in which first half length of the beam contains VEM-2 and the second half length contains VEM-1 as shown in figure 4.8 (b). Configuration-3 and 4 comprise four portions of alternative layers of VEM-1 and VEM-2, as illustrated in figure 4.8 (c) and (d), respectively.

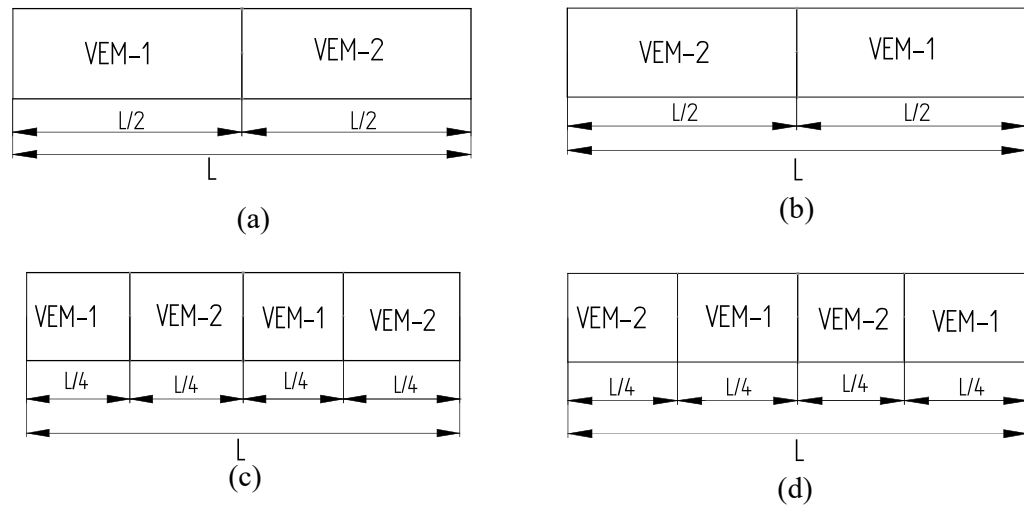


Figure 4.8 Axial gradation configurations of viscoelastic material (a) Configuration-I (b)

Configuration-II (c) Configuration-III and (d) Configuration-IV

The influence of different axial gradation configurations of viscoelastic material on natural frequency for the five fundamental modes under CF, CC, SS and CS boundary conditions are illustrated in figure 4.9 (a), (b), (c) and (d) respectively. There is a considerable and minimal variation in natural frequency for all boundary conditions. There is very minimal change in natural frequency is observed for the CC and CS boundary condition. The relative change in mass and stiffness of all the four configurations almost have no impact on the natural frequency of the sandwich.

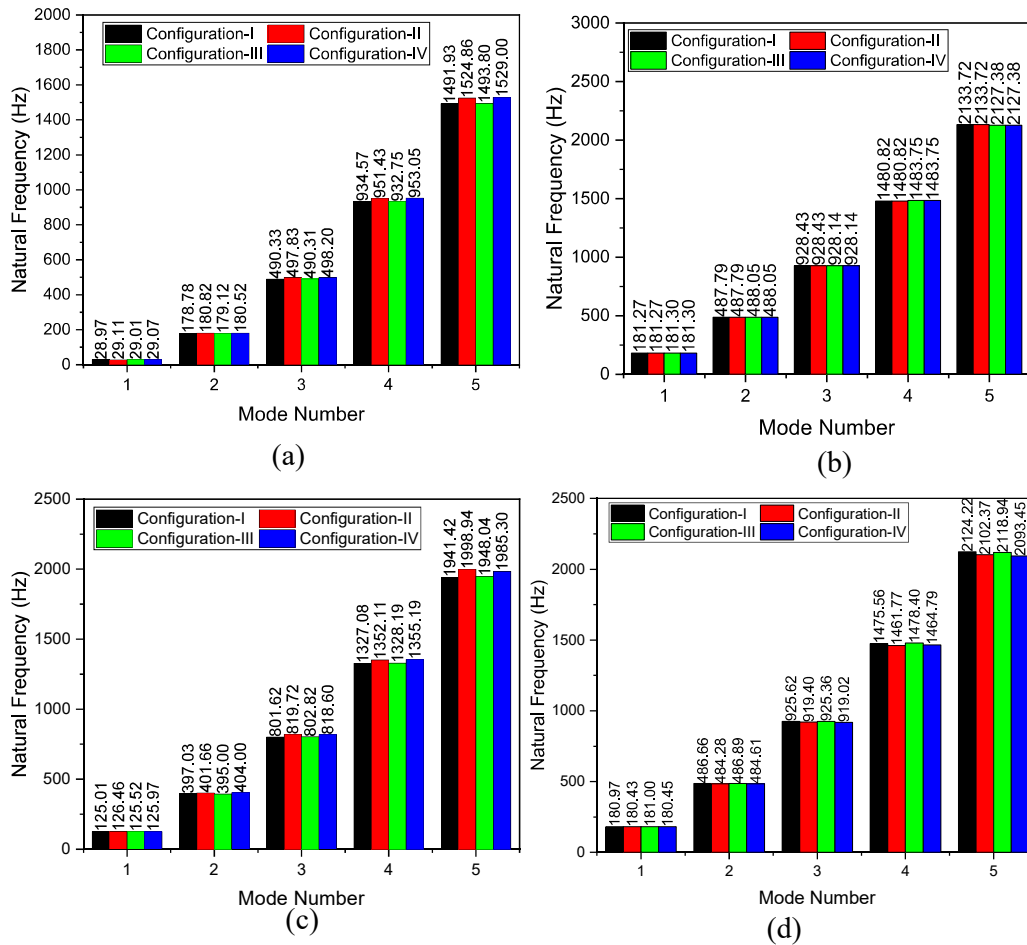


Figure 4.9 Influence of viscoelastic material configuration on natural frequency for (a) CF (b) CC (c) SS (d) CS conditions

For CC and CS boundary conditions, the natural frequency of configuration I and II are same and the natural frequency of configuration III and IV are also same at all the modes as illustrated in figure 4.9 (b) and (d). The configuration-II is able to produce slightly higher stiffness values at all the five modes for CF and SS conditions. The variation in natural frequency is very less at lower modes and there is considerable variation in natural frequency at higher modes as shown in figure 4.9 (a) and (c).

Further, the influence of viscoelastic material configuration on loss factor is explored. There is a very significant variation is observed as illustrated in figure 4.10 (a), (b), (c) and (d) for CF, CC, SS and CS boundary conditions respectively. Configuration-I is able to provide the higher loss factor values for the CF, CC and SS boundary conditions at the fundamental mode as shown in figure 4.10 (a), (b) and (c). The minimal change

is observed in the loss factor for CC condition at all the modes. The influence of viscoelastic material configuration is very less on CC condition, as shown in figure 4.10 (b). For CF condition, configuration-I is more effective at the first three fundamental modes and fifth mode and configuration-III is effective at 4th mode. For CC condition, configuration-I and II behaved in a similar manner at all the modes and they produced more loss factor values compared to the configuration-III and IV. This may be due to less variation in the ratio of total energy dissipated to total energy stored in the sandwich beam for the CC condition. For SS condition, configuration-I is more effective at the first fundamental mode whereas configuration-III is good at higher modes as shown in figure 4.10 (c).

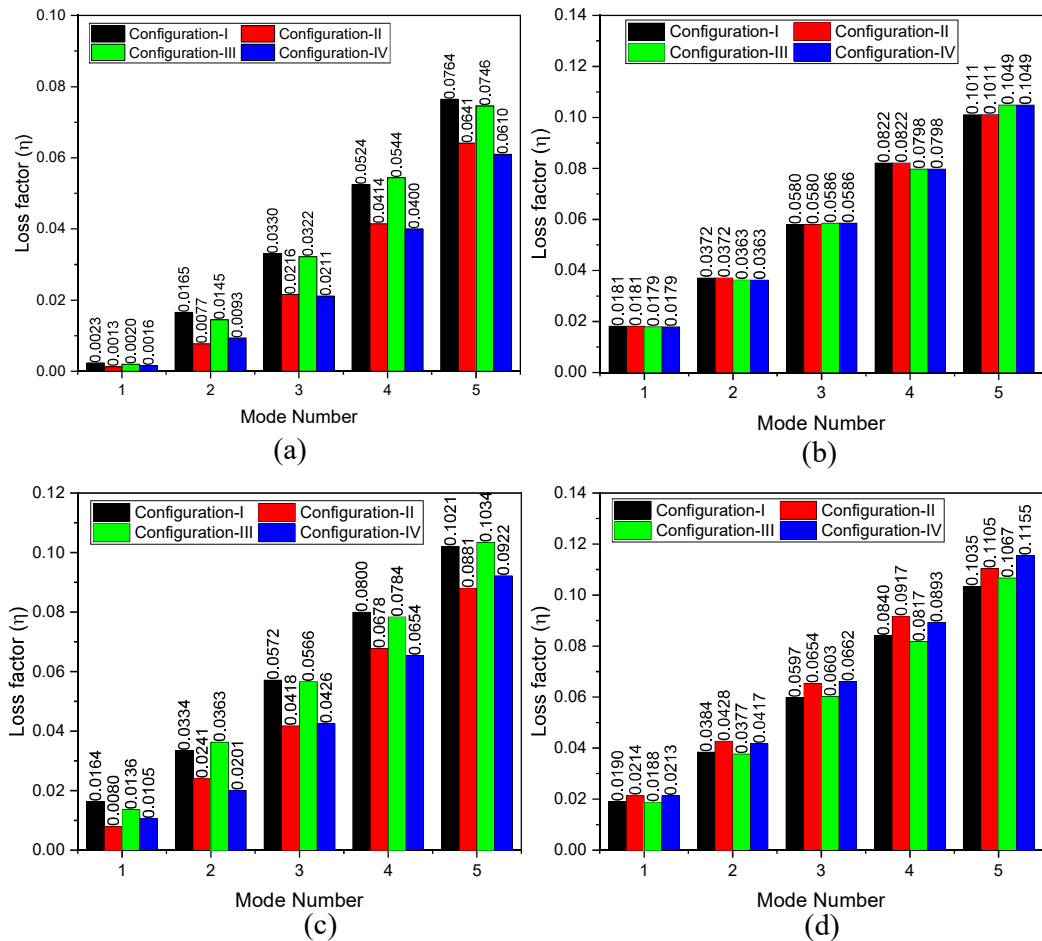


Figure 4.10 Influence of viscoelastic material configuration on loss factor for (a) CF (b) CC (c) SS (d) CS conditions

For CS condition, configuration-II is produced the higher loss factor values at the lower modes whereas the configuration-IV has provided good damping at higher modes as shown in figure 4.10 (d). CS condition is produced higher loss factor values compared to other boundary conditions at all the modes.

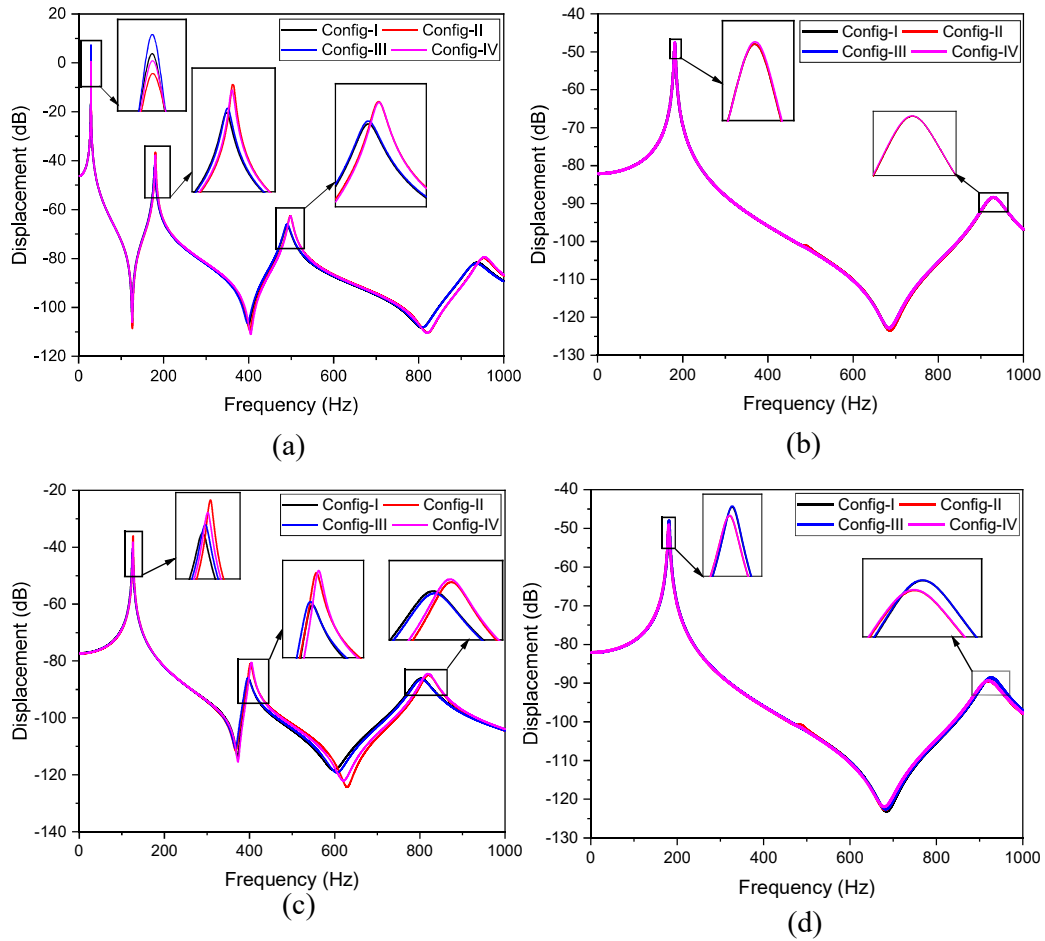


Figure 4.11 Influence of viscoelastic material configuration on frequency response for (a) CF (b) CC (c) SS (d) CS conditions

The sandwich beam's frequency response with viscoelastic material configurations for various boundary conditions is illustrated in figure 4.11 (a), (b), (c), and (d), respectively. As discussed above, the configuration of viscoelastic material for CC condition has minimal effect on the peak amplitude of vibration, as shown in figure 4.11 (b). The results show a significant reduction in peak amplitude of vibration for the CF, SS, and CS conditions. The type of viscoelastic material configuration techniques

helpful in avoiding the higher amplitudes vibrations for structural applications at particular modes for a particular boundary condition.

#### **4.5 SUMMARY**

In this chapter, the influence of the type of viscoelastic materials and axial gradation configurations of viscoelastic materials on the dynamic response of sandwich beam are discussed. Two different viscoelastic materials and four different axial gradation of the viscoelastic material is considered. The comparison of percentage of change in loss factor for the viscoelastic materials is discussed. In addition, the detailed study of influence of these parameters on the natural frequency, loss factor and frequency response along with the mode shapes are presented.



## **CHAPTER – 5**

# **STATIC AND DYNAMIC RESPONSE OF THE COMPOSITE MR FLUID SANDWICH BEAM**

### **5.1 INTRODUCTION**

The usage of smart materials along with composite materials is increased because of their lightweight and directional properties advantage. Even passive materials suppress vibration amplitude to some extent, they cannot change their properties according to the application requirements. MR fluids are one of the categories of smart materials, they can change their rheological properties more quickly upon application of an external field. The usage of smart materials along with composite materials is increased because of their lightweight and directional properties advantage. In actual engineering, the change in rheological properties of MR fluids provides an additional stiffness and damping for the sandwich beam applications. Some of the practical applications of smart sandwich beams are in the stator and rotor blades of turbine, NGVs, airplane propellers, and instrument devices (Ghorbanpour Arani and Soleymani, 2019c). Smart materials like MR fluids in the sandwich structures is an emerging area. From the available literature, it is observed that there is a lack of extensive study on the influence of different parameters on the static and dynamic response of the composite MR sandwich beam. In this chapter, a detailed study is conducted to evaluate the influence of laminate angle, magnetic field, and thickness ratio on the static deflection, natural frequency, loss factor, and frequency response. Further, the study is extended to explore the influence of MR fluid pocket configuration on the dynamic response of the composite sandwich beam.

### **5.2 INFLUENCE OF LAMINATE ANGLE**

The graphite-epoxy composite material is considered as the face layers for the sandwich beam. The length of 400mm and width of 25mm are taken for all the results presented in this section. The material properties utilized for composite facings and MR fluid are shown in table 5.1. Further, a thickness of 1mm is taken for the composite face layers. The laminate angle of the composite face layer is considered as one of the parameters

to study the influence on the static deflection, natural frequency, loss factor, and frequency response. The laminate angle of  $0^0$ ,  $15^0$ ,  $30^0$ ,  $45^0$ ,  $60^0$ ,  $75^0$ , and  $90^0$  degrees are considered. For static analysis, a load of 2N is applied transversely in the middle of the sandwich beam's top face layer. For this study, a constant of 1mm thickness is maintained for both the composite facings and MR fluid. A magnetic field of 500G is considered for all the results presented in this section.

Table 5.1 Material properties of the Graphite/Epoxy composite face material and MR fluid

<b>Graphite/Epoxy</b> (Pradeep et al., 2007)	
Youngs Modulus (GPa)	$E_1 = 137; E_2 = 8.96$
Shear Modulus (GPa)	$G_{12} = 7.1$
Poisson's ratio	$\nu_{12} = 0.3$
Density ( $\text{kg/m}^3$ )	$\rho_{comp} = 1600$
Loss factor	$\eta_1 = 0.0045; \eta_2 = 0.0422; \eta_{12} = 0.075$
<b>MR fluid</b> (Yeh and Shih, 2006)	
Shear Modulus (MPa):	
$\left. \begin{aligned} \text{Storage Modulus } G'_{MRF}(B) &= 3.11 \times 10^{-7} B^2 + 3.56 \times 10^{-4} B + 0.578 \\ \text{Loss Modulus } G''_{MRF}(B) &= 3.47 \times 10^{-9} B^2 + 3.85 \times 10^{-6} B + 6.31 \times 10^{-3} \end{aligned} \right\} 0 \leq B \leq 2000$	
$\text{lossfactor } (\eta) = \frac{G''_{MRF}(B)}{G'_{MRF}(B)}$	
Youngs Modulus (MPa):	
$E_{MRF}^* = 2G_{MRF}^* (1 + \nu_{MRF}) = 2((G'_{MRF}(B))(1 + i\eta))(1 + \nu_{MRF})$	
Density ( $\text{kg/m}^3$ )	$\rho_{MRF} = 3500 \text{ kg/m}^3$
Poisson's ratio	$\nu_{MRF} = 0.3$

Figure 5.1 shows the static deflection of the MR fluid composite sandwich beam with respect to the laminate angle. Minimum deflection is observed for the laminate angle of zero ( $0^0$ ) degrees than other laminate angles. The value of the transverse deflection is attaining higher values as the laminate angle of the composite facings is increasing. This is due to the higher stiffness value of the composite face layer at zero laminate



angle. This concludes that the laminate angle has a substantial influence on the overall stiffness of the composite sandwich beam. For free vibration analysis, damping in both the composite facings and MR fluid layer is considered. The natural frequency and loss factor for the five fundamental modes with respect to the composite face layer laminate angle are presented in this section.

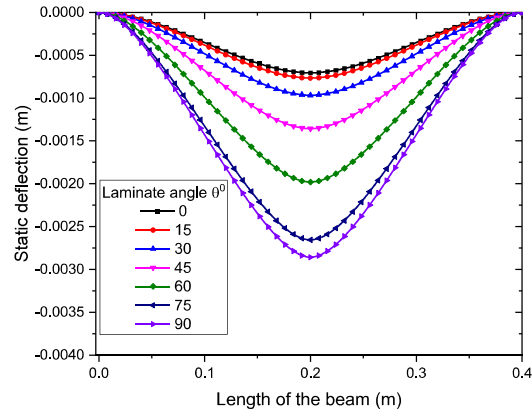


Figure 5.1 Effect of laminate angle on static deflection

Figure 5.2 (a) illustrates the natural frequency of the composite sandwich beam with laminate angle. The value of the natural frequency is decreased as the laminate angle increases (Arvin et al., 2010; Pradeep et al., 2007). Higher values of natural frequency are observed at the laminate angle of zero degrees for all the modes. This is due to the fact that the stiffness is more at zero degrees laminate angle. The decrease in natural frequency value is more rapid from zero ( $0^0$ ) to  $75^0$  degrees of the laminate angle.

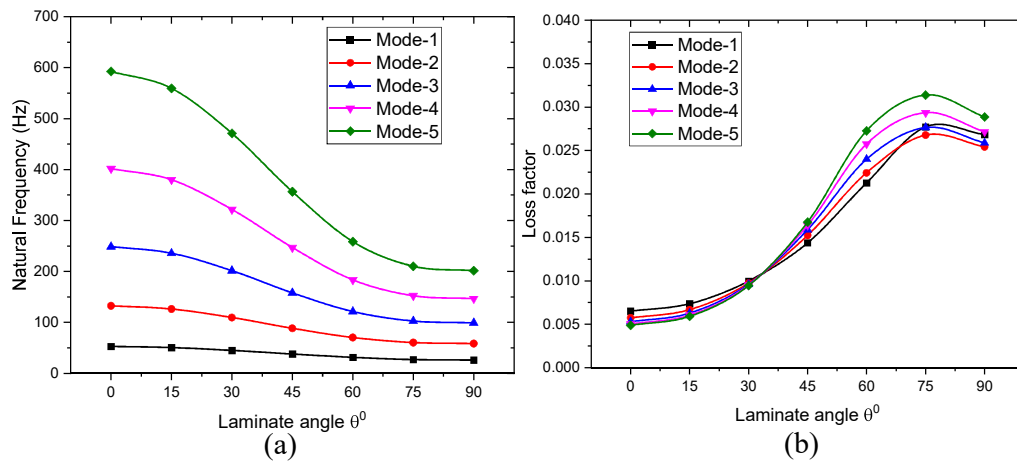


Figure 5.2 Variation in (a) Natural frequency and (b) Loss factor with laminate angle

Figure 5.2 (b) shows the change in loss factor values for the fundamental five modes with the laminate angle. The loss factor value is displayed a similar trend for all the laminate angles irrespective of the mode. At zero degrees laminate angle, the loss factor value of the first fundamental mode is higher compared to other modes. At higher laminate angles, the loss factor value of higher modes dominated the first fundamental mode.

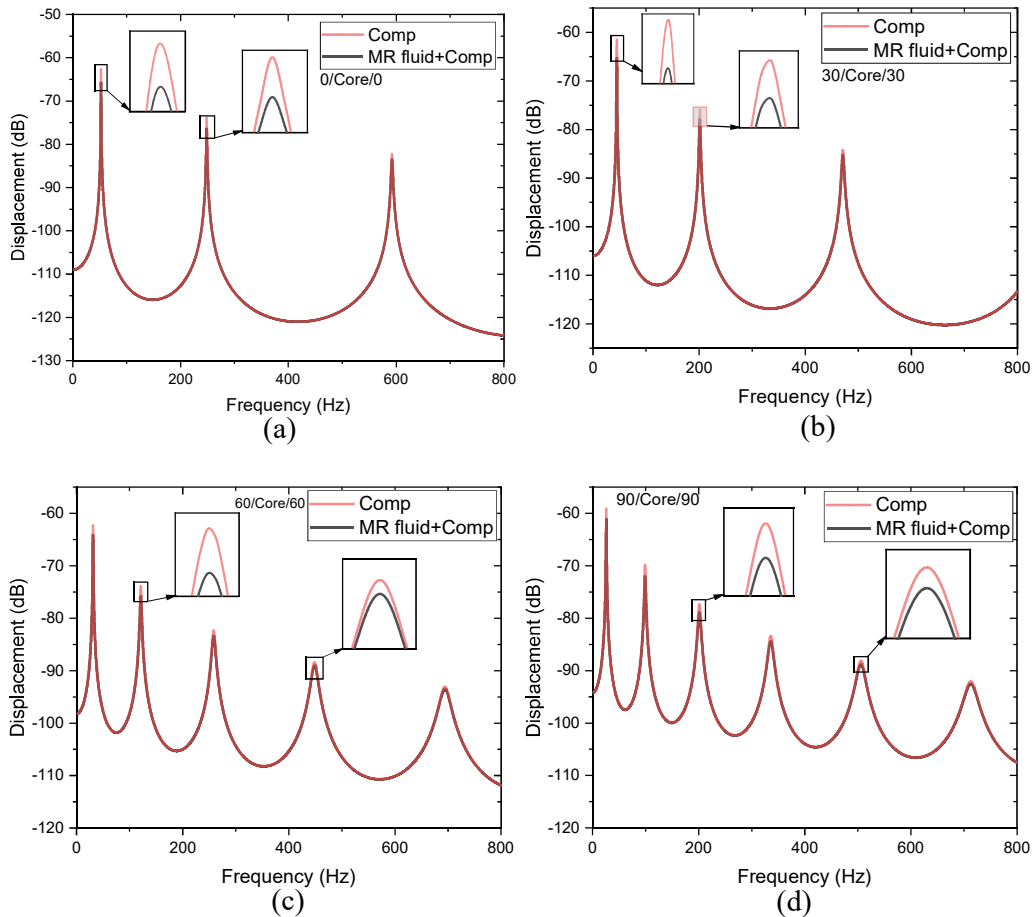


Figure 5.3 Influence of combined damping on vibration amplitude at different laminate angles of face layer (a)  $0^0$  (b)  $30^0$  (c)  $60^0$  and (d)  $90^0$  degrees

The frequency response study is executed to get the response of the sandwich beam structure under the applied harmonic load with respect to the frequency. The frequency response study is necessary for any structure to understand the dynamic behavior in terms of vibration amplitude at any particular frequency. For the clamped-clamped boundary condition, an amplitude of 2N harmonic load is applied exactly in the middle

of the sandwich beam. Frequency sweep is conducted in the range of 1 to 800Hz with a resolution of 0.5Hz. This resolution ensures to get the smooth data of frequency response without a big jump between the two consecutive points. The effectiveness of the combined damping on the peak amplitude of vibration compared to the damping due to only composite facings is presented in terms of forced vibration response. Figure 5.3 shows the frequency response comparison at  $0^\circ$ ,  $30^\circ$ ,  $60^\circ$ , and  $90^\circ$  degree laminate angles of the composite face layer. At all laminate angles, it is evident that the combined damping of composite facings and MR fluid has shown a significant reduction in the amplitude of vibration. MR fluid acts as a viscoelastic material and it provides a good amount of additional damping for the structural applications. The combined damping avoids the catastrophic failure of the structural components from high amplitudes of vibration due to external excitation.

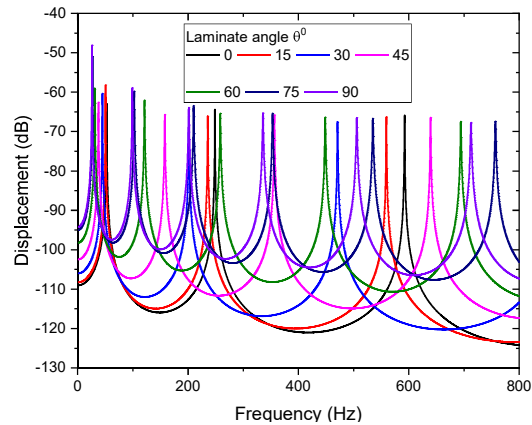


Figure 5.4 The forced vibration response of the sandwich beam at different laminate angles

Figure 5.4 illustrated the frequency response of the sandwich beam for different laminate angles. There is a shift in the frequency curve with the laminate angle observed. This is due to variation in stiffness of the composite facings with the laminate angle. The comparison study of the loss factor with the laminate angle of the composite facings is shown in figure 5.5.

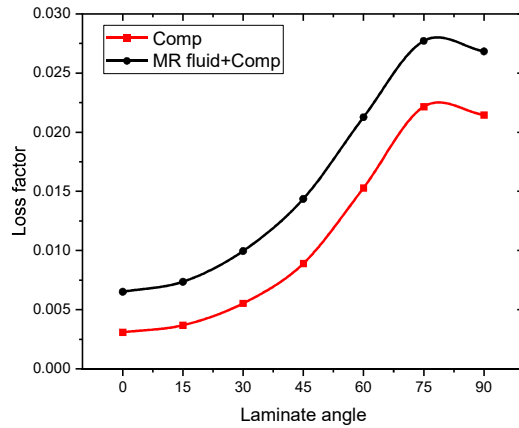


Figure 5.5 The combined damping effect on loss factor value with respect to the laminate angle

The comparison study shows that the combined damping produces higher loss factor values at all the laminate angles. Additional damping due to MR fluid along with composite damping will be more useful in structural applications to mitigate the higher vibration amplitudes. The additional damping added to the sandwich beam due to MR fluid can be observed from the figure 5.5 and it is effective in reducing the vibration amplitudes.

### 5.3 INFLUENCE OF MAGNETIC FIELD

The main feature of the MR fluid is to transform its rheological properties upon application of a magnetic field. This type of behavior of the MR fluid makes it to be used in structural applications to mitigate the amplitude of vibration and to provide an additional amount of stiffness.

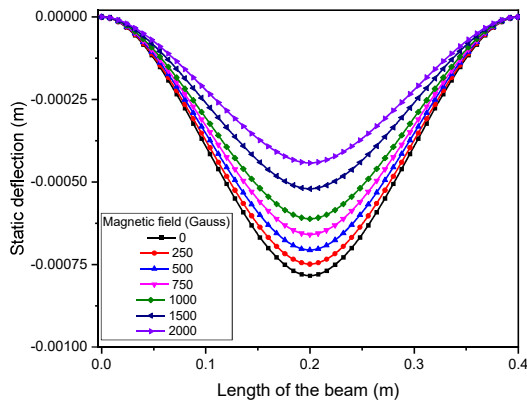


Figure 5.6 Effect of magnetic field on static deflection

In this section, the static, free, and forced vibration response under magnetic fields of 0G, 250G, 500G, 750G, 1000G, 1500G, and 2000G are discussed. Figure 5.6 illustrates the static deflection of the sandwich beam for different values of the magnetic field. The static deflection is less at higher magnetic fields compared to the lower magnetic fields. This is owing to the change in stiffness behavior of MR fluid with the applied magnetic field.

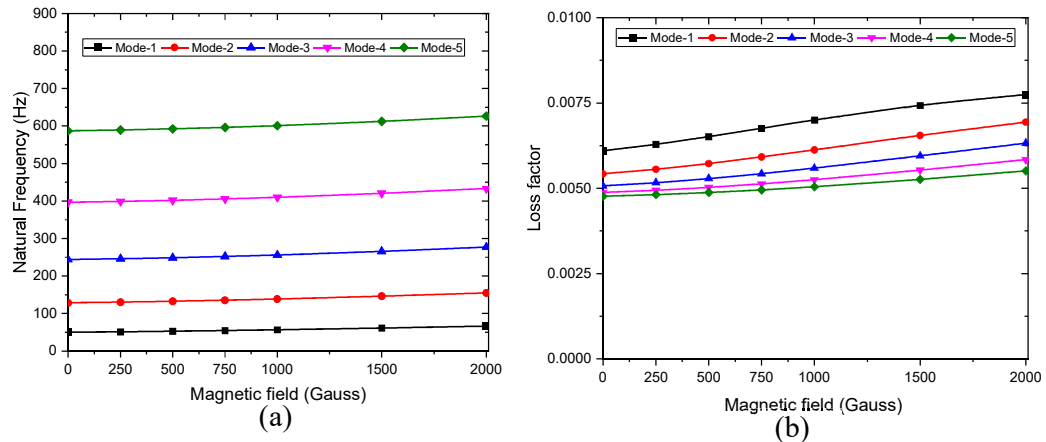


Figure 5.7 Variation in (a) natural frequency and (b) loss factor with the applied magnetic field

Higher magnetic fields make the MR fluid to transform its liquid form into a semi-solid state as the iron particles orient in the direction perpendicular to the applied field. Further, figure 5.7 (a) and (b) illustrate the influence of the magnetic field on natural frequency and loss factor for all the five fundamental modes, respectively. The natural frequency is increased for all the five modes as the magnetic field attains higher values. This is because of the change in MR fluid's stiffness when it is exposed to magnetic field. On the other hand, the loss factor has also attained higher values for all the modes as the magnetic field increased from 0G to 2000G. This type of behavior is highly recommended for structural applications to prevent the higher amplitude of the vibration. Figure 5.8 (a), (b), (c), and (d) shows the comparison study of frequency response under the influence of magnetic fields 0G, 500G, 1000G, and 2000G, respectively. For this study, a constant core thickness of 1 mm and a laminate angle of 30 degrees are considered.

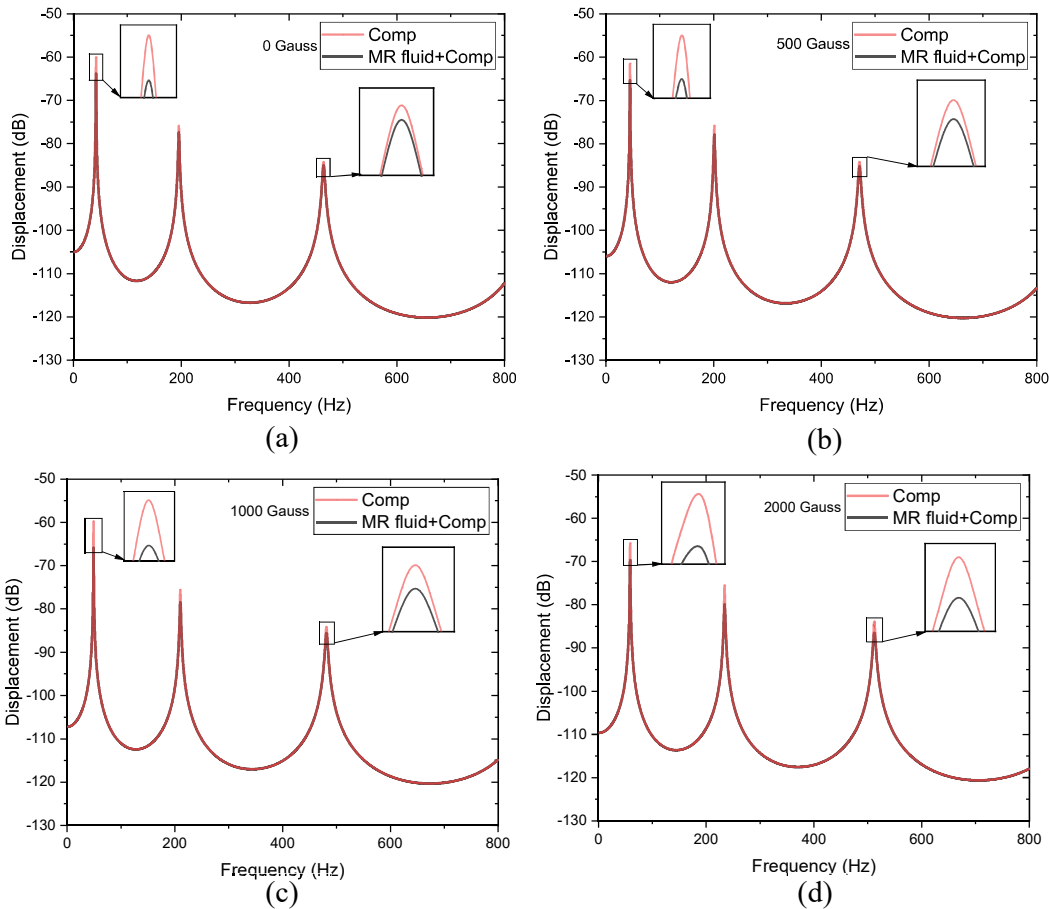


Figure 5.8 Influence of combined damping on vibration amplitude at different magnetic fields (a) 0G (b) 500G (c) 1000G and (d) 2000G for the sandwich beam laminate angle 30/Core/30 configuration

The combined damping has shown a greater reduction in the amplitude of vibration compared to only composite damping at all the magnetic field values. The reduction in amplitude of vibration is more at higher magnetic field values.

Figure 5.9 presents the forced vibration response of a composite sandwich beam in the frequency domain to demonstrate the influence of the magnetic field on vibration amplitude. There is a right shift in the frequency curve and a reduction in vibration amplitude observed as the magnetic field increases from 0G to 2000G. In practical applications, the shift in the frequency of the structural component avoids the resonance due to external excitation.

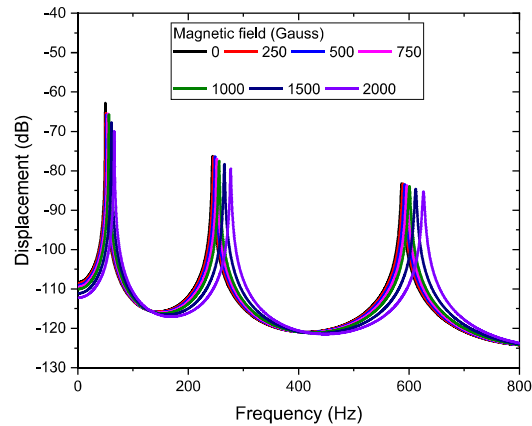


Figure 5.9 The forced vibration response of the sandwich beam at different magnetic fields

#### 5.4 INFLUENCE OF THICKNESS RATIO

In this section, the effect of the thickness ratio (core to face layer) on the sandwich beam's static, free, and forced vibration response are presented. For this, five different thicknesses of 0.5, 1, 2, 4, and 6 are considered.

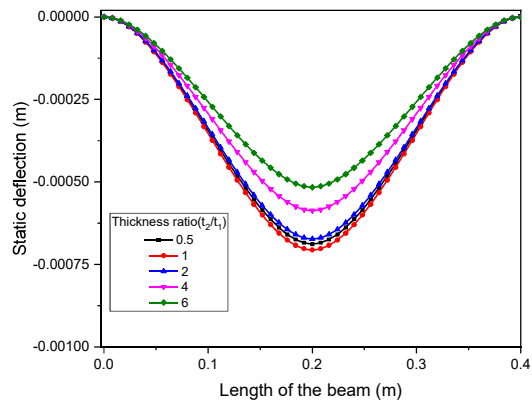


Figure 5.10 Effect of thickness ratio on static deflection

For this section, the magnetic field of 500G and laminate angle of zero ( $0^0$ ) degrees are kept constant. Figure 5.10 illustrates the influence of thickness ratio on the static deflection of the composite MR sandwich beam. There is minimal deflection for the higher thickness ratios is observed. Higher thickness ratios prevent larger deflections under the static transverse load. Further, the influence of thickness ratio on natural frequency and loss factor is also presented. Figure 5.11 (a) and (b) illustrate the variation in natural frequency and loss factor with thickness ratio, respectively. The

natural frequency is decreasing with the thickness ratio for all the five fundamental modes (Arvin et al., 2010; Rajamohan et al., 2010b). The decrease in natural frequency at higher modes is more rapid than at lower modes. This may be due to the change in mass of the sandwich beam is more compared to the change in stiffness as the thickness ratio increases. Figure 5.11 (b) shows that the loss factor value is increased with the thickness ratio for all the five fundamental modes. Lower modes have shown more loss factor values compared to the higher modes for all the thickness ratios.

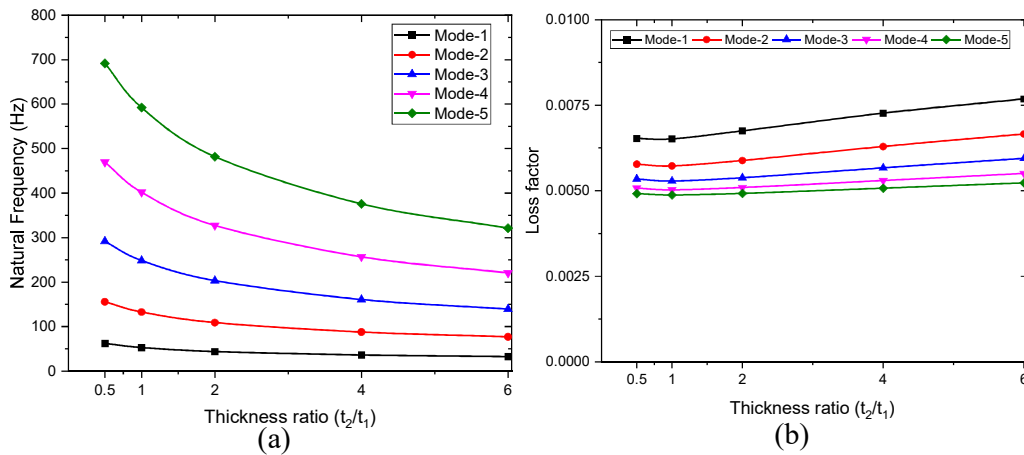


Figure 5.11 Variation in (a) natural frequency and (b) loss factor with the thickness ratio

Further, the forced vibration response of the sandwich beam at different thickness ratios of 0.5, 2, 4, and 6 have shown in figure 5.12 (a), (b), (c), and (d), respectively. The combined damping significantly reduced the peak amplitude of vibration at all the thickness ratios. Figure 5.13 illustrates the frequency response curve of the sandwich beam for different thickness ratios. There is a left shift in the frequency response curve observed as the thickness ratio increases. This is due to the relative change in the mass of the composite sandwich beam is more compared to the relative change in the stiffness vales as the thickness ratio increases.



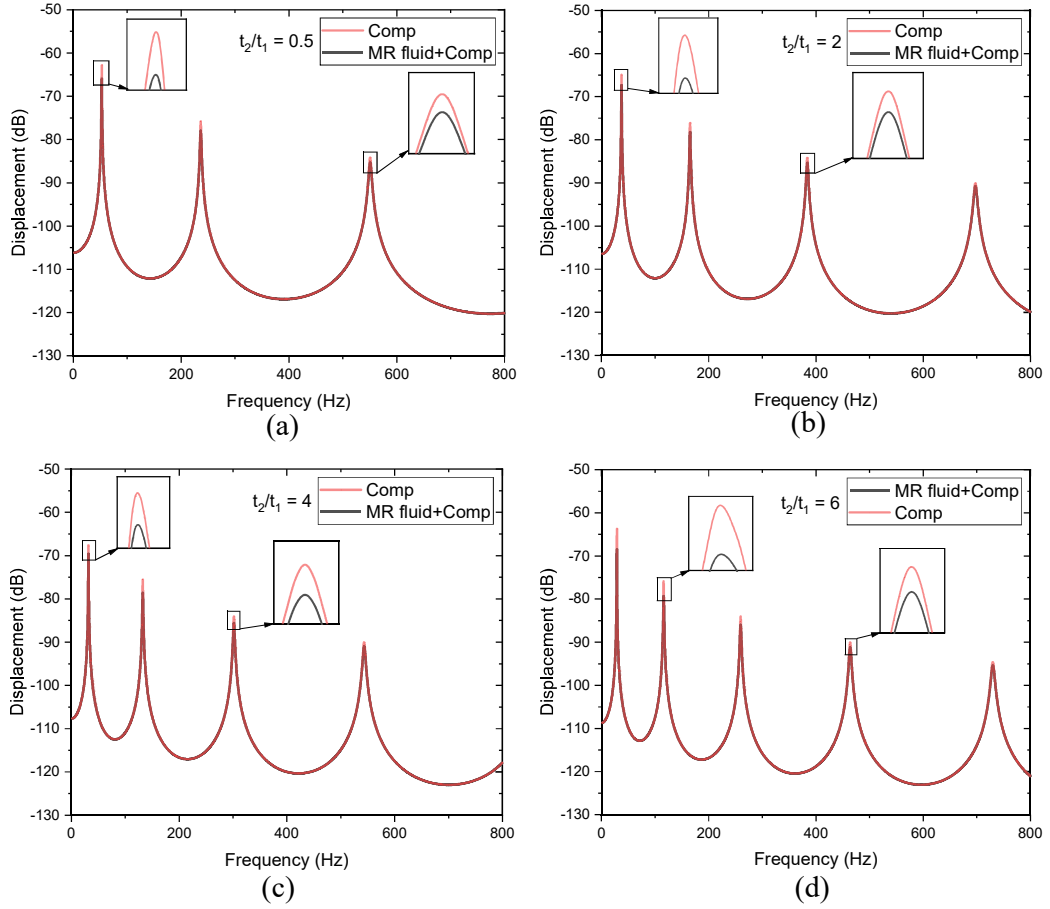


Figure 5.12 Influence of combined damping on vibration amplitude response at different thickness ratios (a) 0.5 (b) 2 (c) 4 and (d) 6

Further, the percentage of deviation in natural frequency and loss factor for the applied magnetic field is calculated as follows

$$\text{Natural frequency deviation (NFD) percentage(\%)} = \frac{f_{MF} - f_0}{f_0} \times 100 \quad (5.1)$$

$$\text{Loss factor deviation (LFD) percentage(\%)} = \frac{\eta_{MF} - \eta_0}{\eta_0} \times 100 \quad (5.2)$$

$f_{MF}$  and  $f_0$  in the Eq. 5.1 are natural frequencies at the applied magnetic field and at without magnetic field, respectively. Similarly,  $\eta_{MF}$  and  $\eta_0$  in the Eq. 5.2 are loss factor values at the applied magnetic field and at without magnetic field, respectively.

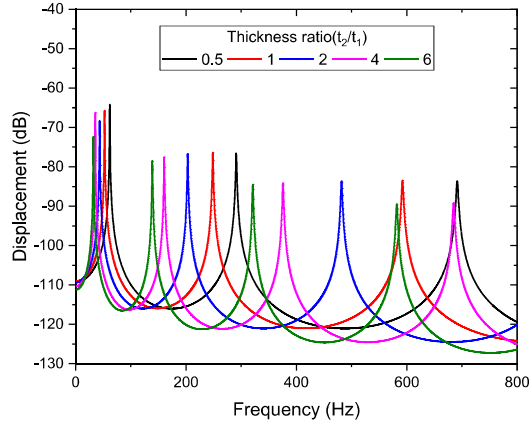


Figure 5.13 The forced vibration response of the sandwich beam at thickness ratios

The percentage (%) of deviation in natural frequency and loss factor for the MR sandwich beam are illustrated in figure 5.14 (a) and (b), respectively. The percentage (%) of deviation in natural frequency is increased for all the modes as the applied magnetic field goes from 0G to 2000G. The deviation in natural frequency for the first fundamental mode is 2.29%, 5.28%, 8.86%, 12.95%, 22.22% and 32.39% at the magnetic fields of 250G, 500G, 750G, 1000G, 1500G and 2000G, respectively. First fundamental mode shown more deviation in natural frequency with the applied magnetic field. Even, the percentage of deviation in loss factor is also increased for all the modes as the magnetic field increases. The deviation in loss factor for the first fundamental mode is 3.10%, 6.83%, 10.82%, 14.79%, 21.83% and 28.07% at the magnetic field of 250G, 500G, 750G, 1000G, 1500G and 2000G, respectively. Further, the percentage (%) of reduction in static deflection of the sandwich beam is calculated as follows

$$\text{The percentage (\%)} \text{ of reduction in static deflection} = \frac{q_0 - q_{MF}}{q_0} \times 100 \quad (5.3)$$

$q_{MF}$  and  $q_0$  in Eq. 5.3 are the static deflections at the applied magnetic field and at without magnetic field, respectively. Figure 5.15 shows the percentage (%) of reduction in static deflection of the sandwich beam as the applied magnetic field goes from 0G to 2000G. The radial plot is used to show this. The percentage of reduction in static deflection is increased with the applied magnetic field and a maximum reduction of 77.21% is observed at the magnetic field of 2000G.

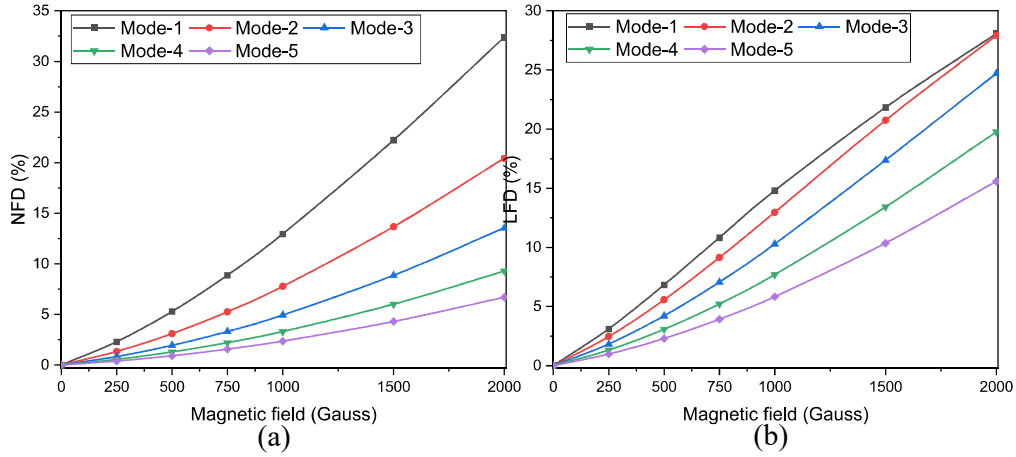


Figure 5.14 The percentage (%) of deviation in (a) natural frequency and (b) loss factor with the applied magnetic field

Further, the free vibration response of the sandwich beam with different configurations of MR fluid pocket under CF, CC, SS, CS and SF boundary condition are discussed. The constraints utilized for the boundary conditions are tabulated in table 3.1.

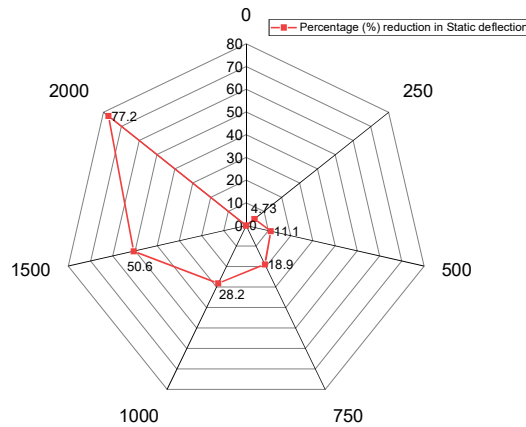


Figure 5.15 The percentage (%) of reduction in static deflection of the sandwich beam with the applied magnetic field

### 5.5 INFLUENCE OF BOUNDARY CONDITION

The influence of magnetic field on the free vibration response of the MR composite sandwich beam for CF, CC, SS, CS and SF boundary conditions are presented in this section. The variation in natural frequency and loss factor for the five fundamental modes at 0G, 500G, 1000G, 1500G and 2000G are discussed. The different

configurations of the MR fluid pocket are tabulated in the table 5.2. The C4 configuration (fully filled) is considered to study the influence of magnetic field on free vibration response of the composite sandwich beam for this particular section. The variation in natural frequency and loss factor with the applied magnetic field for different boundary conditions are tabulated in the table 5.3 and 5.4.

Table 5.2 Length and location of the MR fluid pocket and silicone rubber for different configurations of sandwich beam

Configuration type		MR fluid pocket length (mm)	MR fluid location (mm)	Silicone rubber location (mm)
I	C1	100 (1/4 <sup>th</sup> length)	0-100	100-400
	C2	200 (1/2 <sup>th</sup> length)	0-200	200-400
	C3	300 (3/4 <sup>th</sup> length)	0-300	300-400
	C4	400 (full length)	0-400	--
II	C5	100 (1/4 <sup>th</sup> length)	100-200	0-100 & 200-400
	C6	200 (1/2 <sup>th</sup> length)	100-300	0-100 & 300-400
	C7	300 (3/4 <sup>th</sup> length)	100-400	0-100
III	C8	100 (1/4 <sup>th</sup> length)	200-300	0-200 & 300-400
	C9	200 (1/2 <sup>th</sup> length)	200-400	0-200
IV	C10	100 (1/4 <sup>th</sup> length)	300-400	0-300

Figure 5.16 (a, b, c, d and e) shows the variation in natural frequency corresponding to the respective mode number for various boundary conditions. For all the boundary conditions considered, the value of natural frequency is increased as the magnetic field value goes from 0G to 2000G. This variation is owing to the change in shear modulus of the MR fluid with the magnetic field. This leads to the change in the overall stiffness of the sandwich beam. The percentage of deviation in the first fundamental natural frequency at 1000G are 17.31%, 16.87%, 32.27%, 24.14% and 27.01% for CF, CC, SS, CS and SF boundary conditions respectively.

Table 5.3 Natural frequency of C4 (fully filled) configuration at different magnetic field value for CF, CC, SS, CS and SF boundary conditions

Config.	Magnetic field (G)	Boundary condition	Natural frequency (Hz)				
			Mode-1	Mode-2	Mode-3	Mode-4	Mode-5
C4	0	CF	12.22	48.46	111.55	200.90	319.79
		CC	41.97	104.84	195.72	315.35	464.27
		SS	27.18	74.69	150.23	254.59	388.35
		CS	33.60	88.76	171.97	283.99	425.35
		SF	10.00	39.64	95.58	177.37	288.59
	500	CF	13.24	52.32	118.15	208.38	327.76
		CC	44.93	109.52	201.47	321.68	470.98
		SS	30.93	80.25	156.89	261.77	395.82
		CS	37.03	93.88	178.17	290.73	432.42
		SF	11.29	43.60	102.49	185.28	297.00
	1000	CF	14.34	57.20	127.38	219.45	339.91
		CC	49.06	116.36	210.21	331.48	481.48
		SS	35.96	88.16	166.84	272.77	407.43
		CS	41.71	101.29	187.52	301.12	443.46
		SF	12.70	48.64	112.04	196.88	309.72
	1500	CF	15.28	62.40	138.10	233.19	355.49
		CC	53.83	124.72	221.36	344.30	495.41
		SS	41.60	97.58	179.29	286.98	422.73
		CS	47.02	110.22	199.33	314.6	458.07
		SF	13.94	54.12	123.05	211.14	325.93
2000	CF	16.04	67.57	149.47	248.72	373.72	
	CC	58.84	134.01	234.31	359.63	512.36	
	SS	47.41	107.84	193.48	303.74	441.16	
	CS	52.53	120.05	212.93	330.68	475.75	
	SF	14.95	59.65	134.68	227.13	344.77	

Table 5.4 Loss factor of C4 (fully filled) configuration at different magnetic field value for CF, CC, SS, CS and SF boundary conditions

Config. type	Magnetic field (G)	Boundary condition	Loss factor ( $\eta$ )				
			Mode-1	Mode-2	Mode-3	Mode-4	Mode-5
C4	0	CF	0.00499	0.00458	0.00403	0.00344	0.00289
		CC	0.0044	0.00471	0.00499	0.00517	0.00523
		SS	0.0031	0.00375	0.00444	0.00499	0.00536
		CS	0.0019	0.00247	0.00319	0.00391	0.00454
		SF	0.00126	0.00169	0.00229	0.00296	0.0036
	500	CF	0.00369	0.00229	0.00148	0.00101	7.2E-4
		CC	0.00442	0.00293	0.00199	0.00138	0.001
		SS	0.00515	0.00369	0.00266	0.00192	0.00142
		CS	0.00568	0.00441	0.00339	0.00254	0.00193
		SF	0.00596	0.00499	0.00406	0.00318	0.00249
	1000	CF	0.00739	0.00387	0.00226	0.00142	9.6E-4
		CC	0.00797	0.00468	0.00293	0.00191	0.00133
		SS	0.0084	0.00556	0.00379	0.0026	0.00185
		CS	0.00858	0.00628	0.00463	0.00335	0.00248
		SF	0.00853	0.00681	0.00535	0.00409	0.00313
	1500	CF	0.00541	0.00298	0.00183	0.00119	8.3E-4
		CC	0.00615	0.00372	0.00241	0.00162	0.00115
		SS	0.0068	0.00456	0.00318	0.00223	0.00162
		CS	0.00718	0.0053	0.00397	0.00292	0.00219
		SF	0.00731	0.00588	0.00468	0.00361	0.00279
2000	CF	0.0076	0.00551	0.00382	0.00229	0.00147	
	CC	0.00686	0.00582	0.0045	0.00293	0.00197	
	SS	0.00594	0.00612	0.0052	0.00371	0.00263	
	CS	0.00499	0.00633	0.00573	0.00446	0.00334	
	SF	0.00414	0.00641	0.00608	0.0051	0.00402	

Though there is an increase in the natural frequency for all the boundary conditions with the magnetic field, the SS condition provides more percentage of deviation in natural frequency at the applied magnetic field.

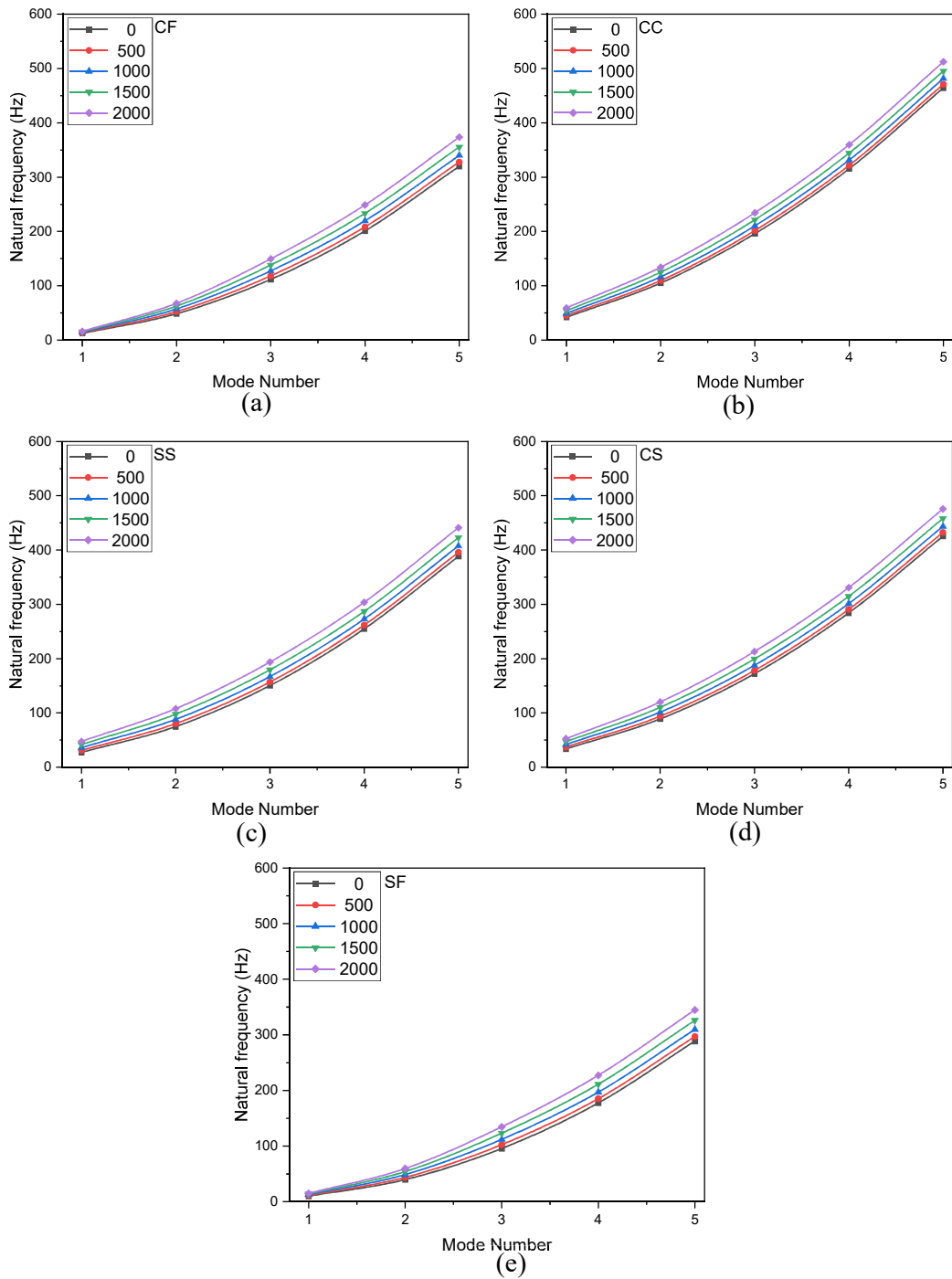


Figure 5.16 Variation in Natural frequency under (a) CF (b) CC (c) SS (d) CS and (e) SF boundary conditions at different magnetic fields

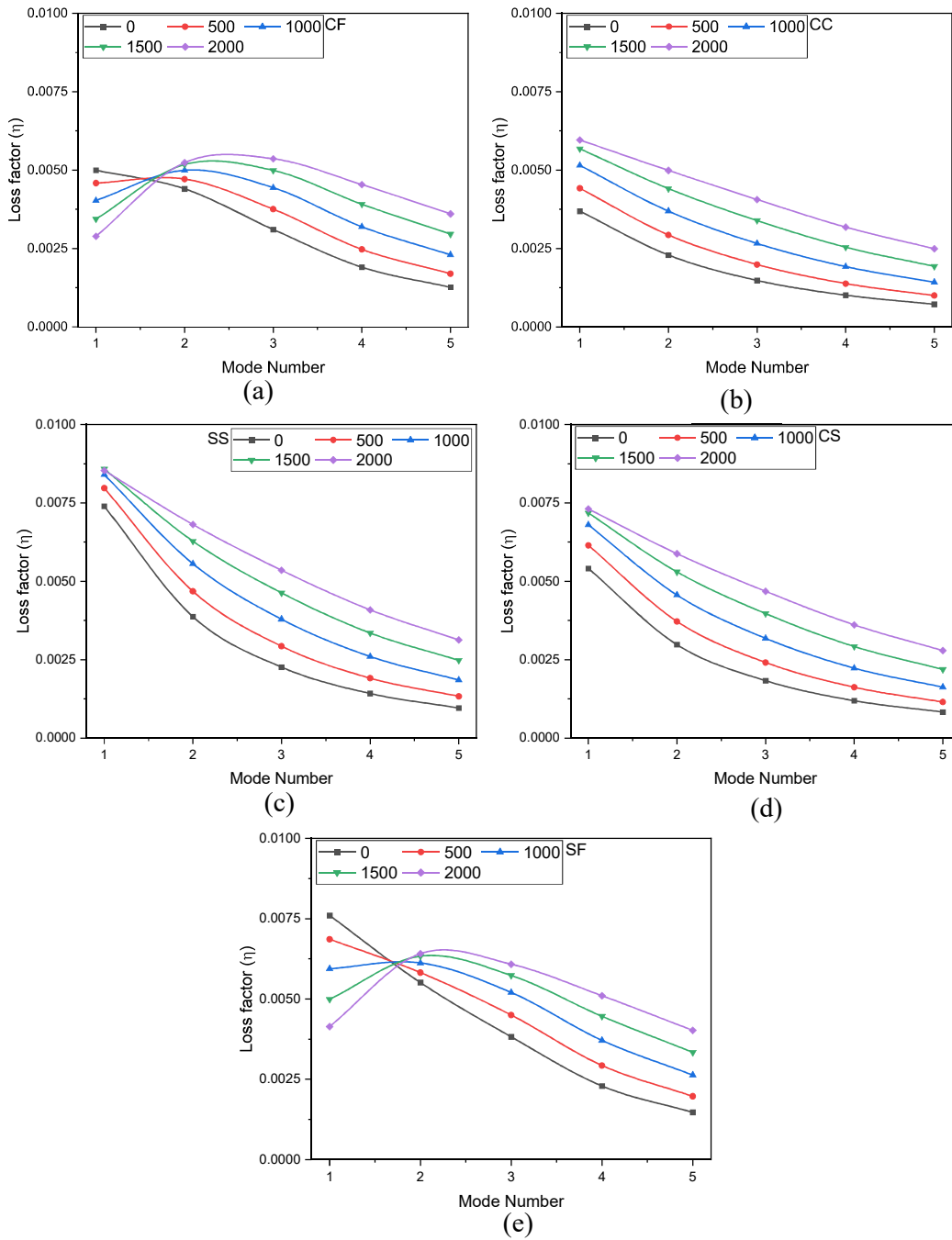


Figure 5.17 Variation in loss factor under (a) CF (b) CC (c) SS (d) CS and (e) SF boundary conditions at different magnetic fields

Figure 5.17 (a, b, c, d, and e) illustrate the variation in loss factor corresponding to five fundamental modes at various boundary conditions. The CF and SF boundary conditions display less loss factor values due to the minimum effect of the magnetic field induced on them. The loss factor decreases as the magnetic field increases at the



first mode (Rajamohan et al., 2010b) as shown in figure 5.17 (a) and (e). The above-mentioned trend is observed at the first mode may be due to the relative change in loss modulus is less compared to the change in storage modulus for the CF and SF boundary conditions. The loss factor is generally described as ratio of energy dissipated per cycle to the total stored energy in the system. At higher modes, the relative change in the loss modulus is slightly greater compared to the change in storage modulus. This leads to more loss factor values at high modes, whereas, for CC, SS and CS boundary conditions, loss factor is increased for all the modes as the magnetic field value is increasing as illustrated in figure 5.17 (b), (c) and (d). The SS condition gives more loss factor value at first fundamental mode among all the boundary conditions considered.

### 5.6 INFLUENCE OF MR FLUID POCKET CONFIGURATION

In this section, the dynamic response of sandwich beam is evaluated under the influence of different MR fluid pocket configurations. Four different MR fluid pocket configurations are considered to study the influence of length and location of MR fluid pocket. The representation of configurations type I, II, III and IV are illustrated in figure 5.18, 5.19, 5.20 and 5.21 respectively. The length and location of the MR fluid pocket and silicone rubber for the different configurations of the sandwich beam are tabulated in the table 5.2. Further, the influence of configuration type on natural frequency and loss factor are presented in the following sections. The magnetic field of 500G is taken for all the results presented.

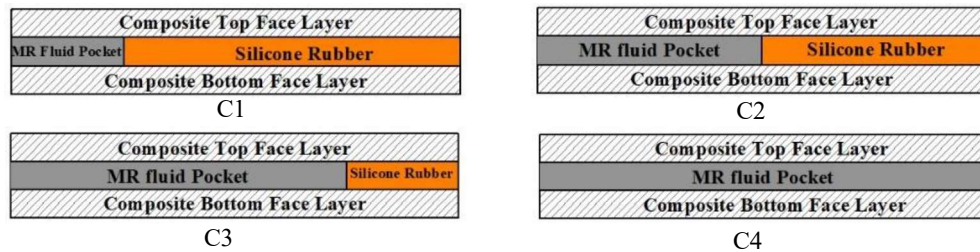


Figure 5.18 Configuration Type - I

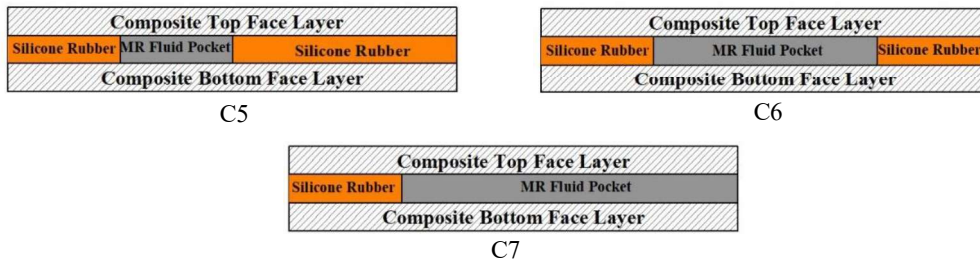


Figure 5.19 Configuration Type - II

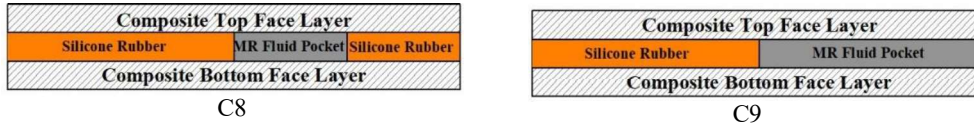


Figure 5.20 Configuration Type - III

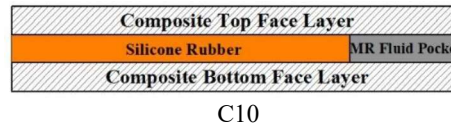


Figure 5.21 Configuration Type - IV

### 5.6.1 Configuration type-I

Type-I has four configurations C1, C2, C3 and C4 as shown in figure 5.18. The variation in natural frequency for the configuration type-I at different boundary conditions is illustrated in Figure 5.22 (a, b, c, d and e). The length of the MR fluid pocket has a realistic influence on higher modes. Though, there is a variation in natural frequency at lower modes but the change is very less. This trend is followed for all the boundary conditions considered. The variation in natural frequency at first mode is little higher for the CC boundary condition compared to the other boundary conditions.

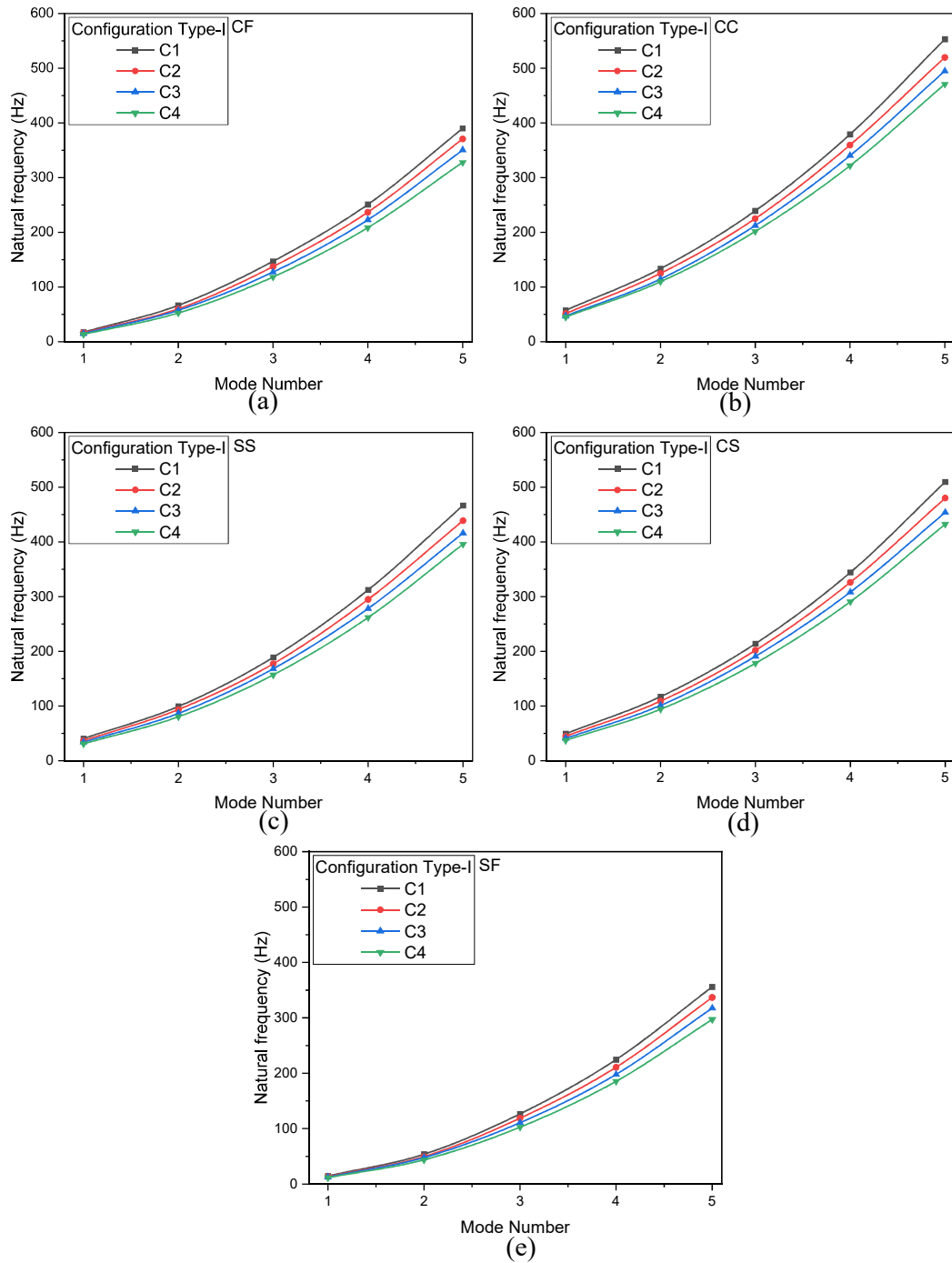


Figure 5.22 Variation in Natural frequency under (a) CF (b) CC (c) SS (d) CS and (e) SF boundary conditions for type-I configuration

The present study shows a decrease in natural frequency with the increase in length of the MR fluid pocket for all the boundary conditions. This might be due to the variation

in value of mass of the sandwich beam is relatively more dominant compared to the variation in value of stiffness as the length of the MR fluid pocket increases.

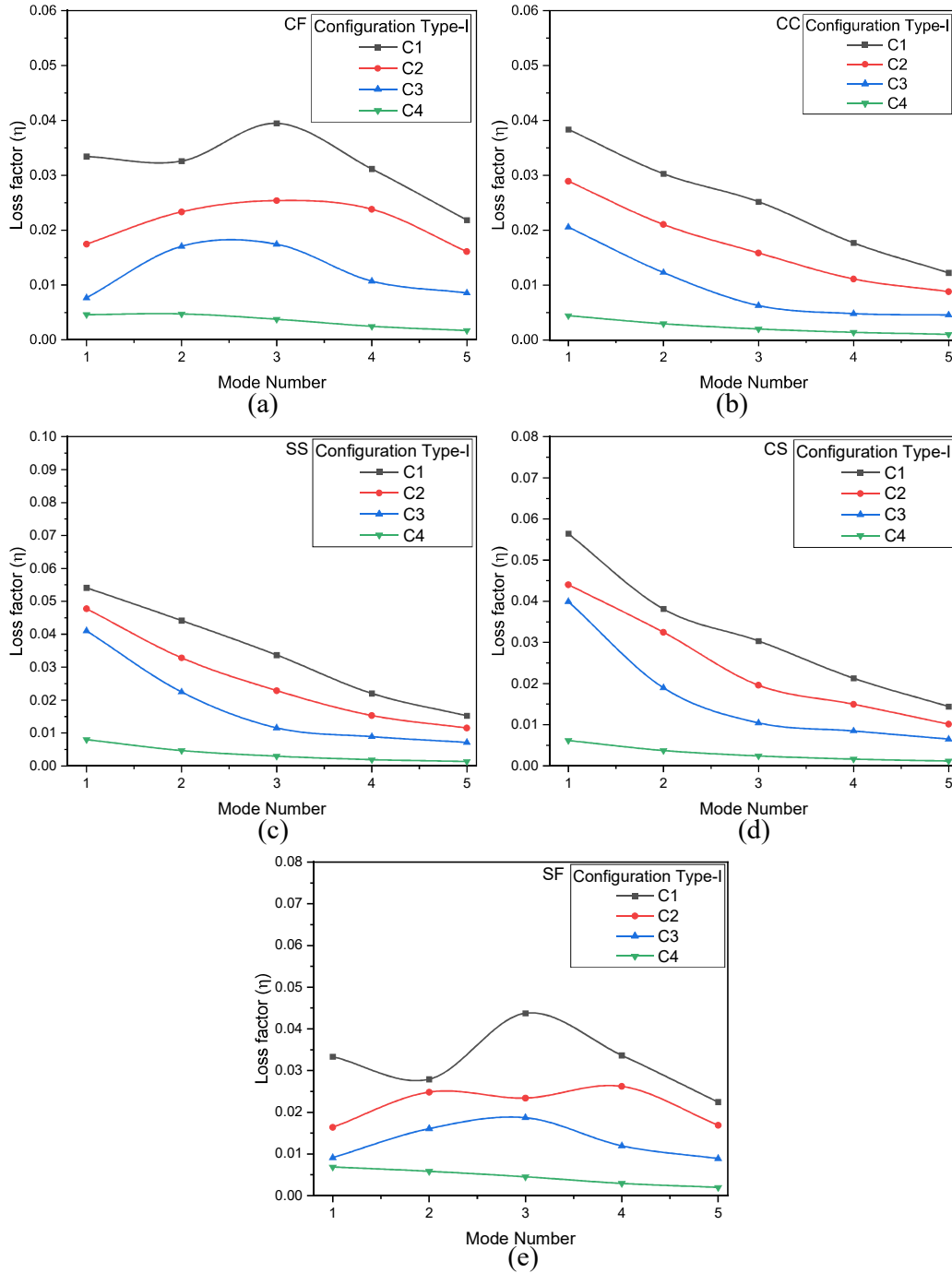


Figure 5.23 Variation in Loss factor under (a) CF (b) CC (c) SS (d) CS and (e) SF boundary conditions for type-I configuration

Further, figure 5.23 (a, b, c, d and e) illustrate the influence of configuration type-I on loss factor for different boundary conditions. The variation in loss factor for the configuration C1 is not linear and this configuration yields more loss factor values compared to the configuration C2, C3 and C4. The configuration type-I has shown a remarkable influence on loss factor at all the boundary conditions. This type of configurations will be more useful for the structural applications where amplitude of the particular mode is needed to be suppressed.

### 5.6.2 Configuration type-II

The configuration type-I dealt with the influence of length of the MR fluid pocket on the natural frequency and loss factor. Type-II also deals with the length of the MR fluid pocket but pocket starts from the length of 100 mm from the left side of the sandwich beam as shown in figure 5.19. The influence of type-II configuration on natural frequency for different boundary conditions is illustrated in figure 5.24 (a, b, c, d and e). The natural frequency shows the similar trend as of type-I configuration as the length of the MR fluid pocket increases. This might be due to the variation in mass of the sandwich beam is relatively more dominant compared to the variation in stiffness as the length of the MR fluid pocket increases. Further, figure 5.25 (a, b, c, d and e) shows the influence of type-II configuration on loss factor for various boundary conditions. The loss factor is more at lower modes for CC, SS and CS boundary conditions. The variation in loss factor is not linear for CF and SF boundary conditions and 2<sup>nd</sup> mode provides more loss factor value compared to the other modes. This non-linearity might be due to more shear dissipation of vibrational energy at particular modes. The configuration C5 produces more loss factor values among the type-II configurations at all the boundary conditions.

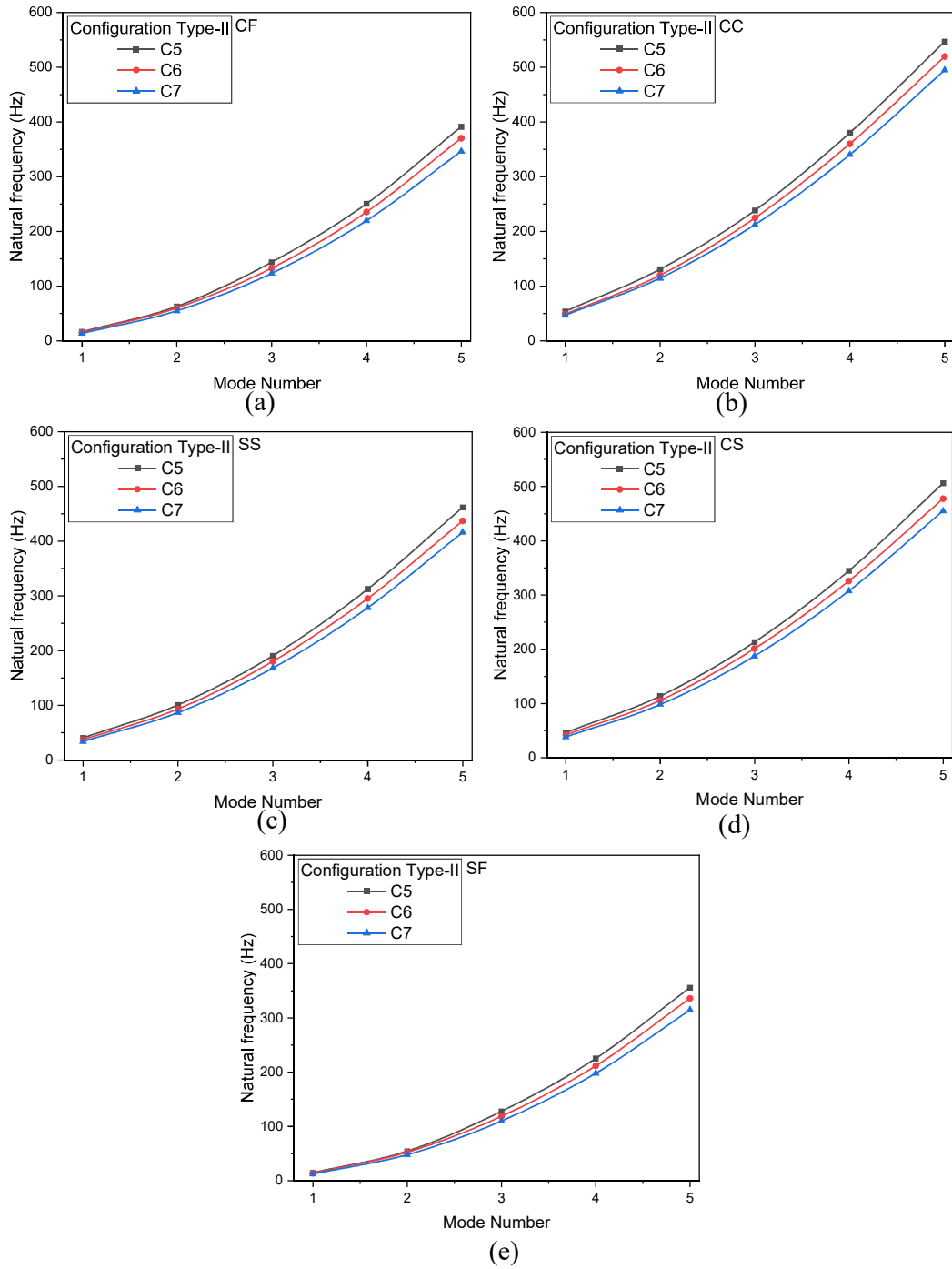


Figure 5.24 Variation in Natural frequency under (a) CF (b) CC (c) SS (d) CS and (e) SF boundary conditions for type-II configuration

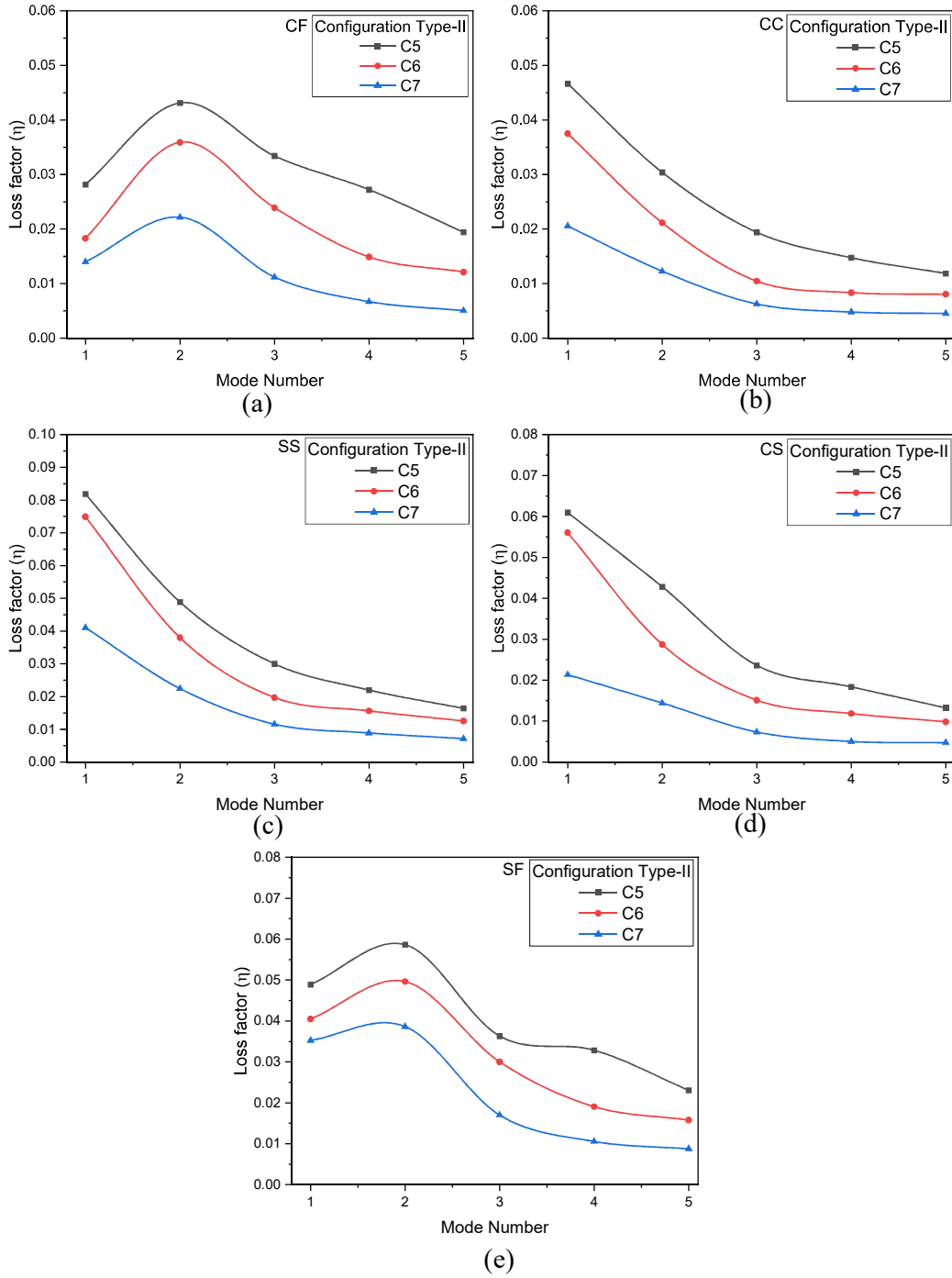


Figure 5.25 Variation in Loss factor under (a) CF (b) CC (c) SS (d) CS and (e) SF boundary conditions for type-II configuration

### 5.6.3 Configuration type-III

Type-III consists of two configurations C8 and C9 as shown in figure 5.20. The natural frequency is more for the C8 configuration compared to the C9 configuration for all the boundary conditions as shown in figure 5.26 (a, b, c, d and e). Though, there is a variation in natural frequency at lower modes but the change is very less. This trend is followed for all the boundary conditions considered. Further, the loss factor of C8 and C9 configuration is more at lower modes for the CC, SS and CS boundary conditions as shown in figure 5.27 (b, c and d). The variation in loss factor is not linear for the CF and SF boundary condition as shown in figure 5.27 (a and e). There is a significant impact of C8 configuration on the 2<sup>nd</sup> mode loss factor for CF boundary condition.

### 5.6.4 Configuration type-IV

Type-IV consists of only one configuration C10. The MR fluid pocket is considered near the tip of the sandwich beam as shown in figure 5.21. The length of the MR fluid pocket is 100 mm. The influence of C10 configuration at a magnetic field of 500G on natural frequency and loss factor is illustrated in figure 5.28 (a) and (b) respectively for various boundary conditions. The activation of MR fluid pocket near the tip region has a significant influence on the SF boundary condition. The maximum loss factor is obtained at all the modes for the SF boundary condition as illustrated in figure 5.28 (b).



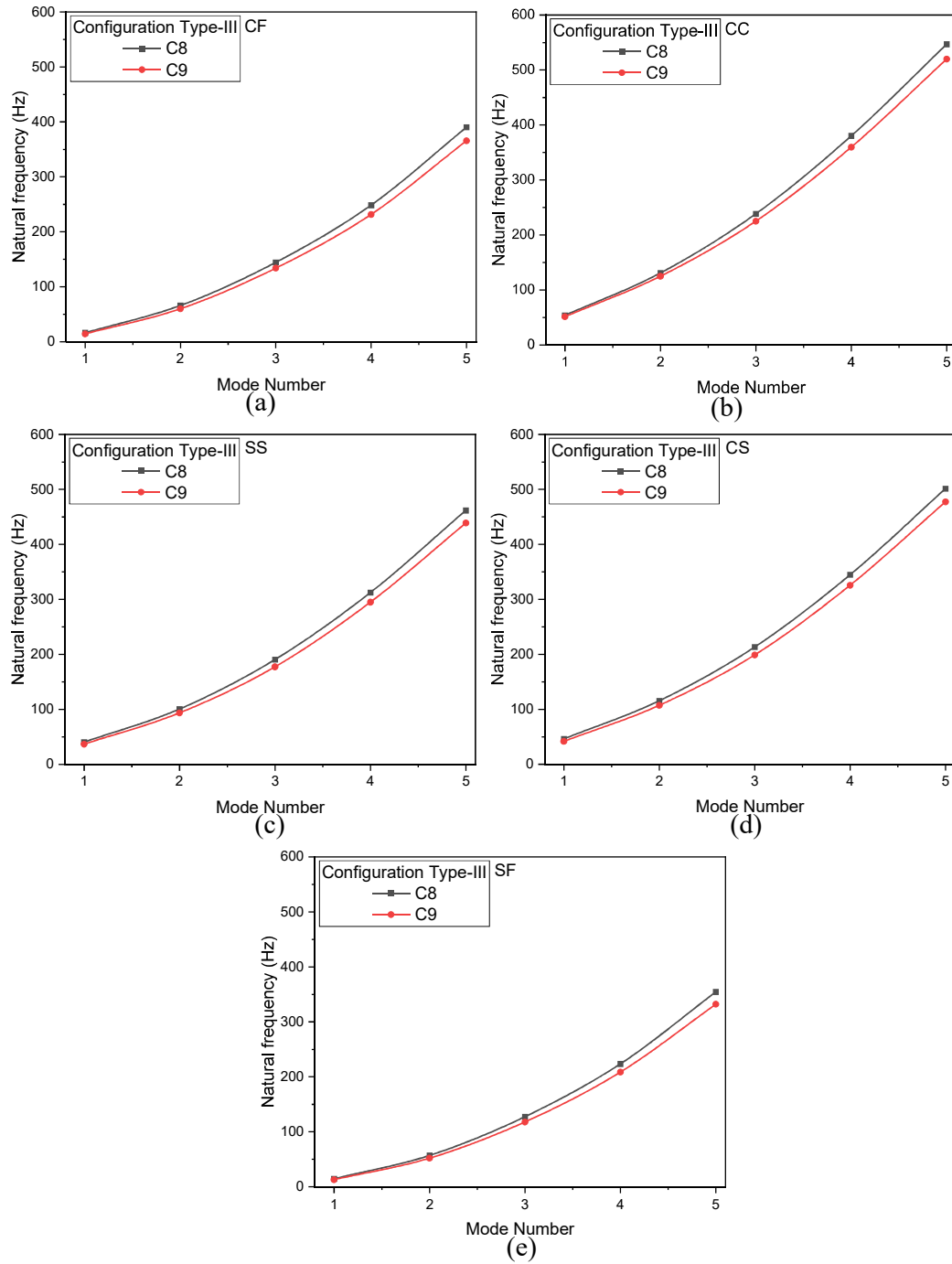


Figure 5.26 Variation in Natural frequency under (a) CF (b) CC (c) SS (d) CS and (e) SF boundary conditions for type-III configuration

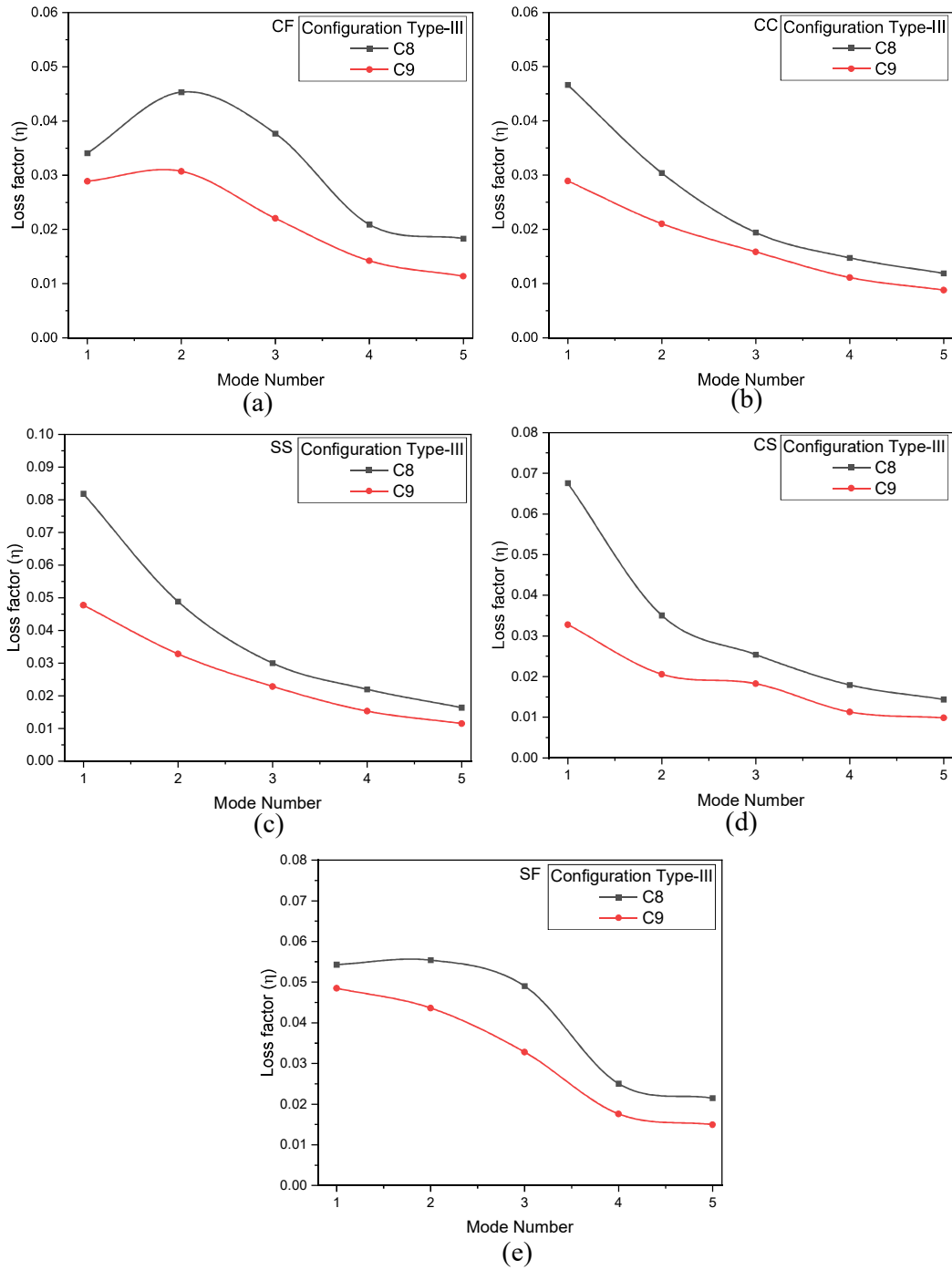


Figure 5.27 Variation in Loss factor under (a) CF (b) CC (c) SS (d) CS and (e) SF boundary conditions for type-III configuration

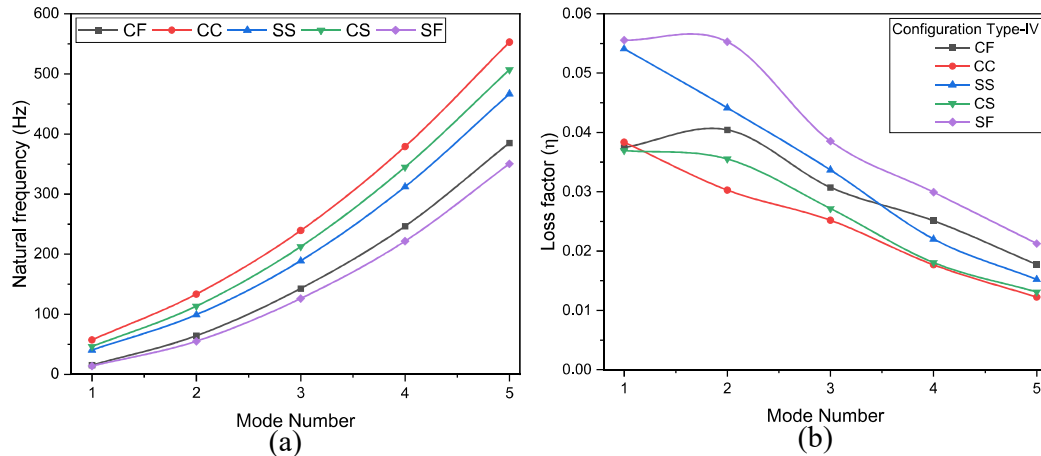


Figure 5.28 Variation in (a) Natural frequency and (b) Loss factor under different boundary conditions for type-IV configuration

### 5.7 INFLUENCE OF LOCATION OF MR FLUID POCKET

In the previous section, the influence of type of configuration on free vibration response of the MR composite sandwich beam is discussed. The length of the activated MR fluid pocket has a reasonable and considerable impact on the natural frequency and loss factor as discussed in the previous section. The comparison study on influence of MR fluid pocket location is discussed in this section. For this, four configurations C1 (type-I), C5 (type-II), C8 (type-III) and C10 (type-IV) are considered. For all these configurations, MR fluid pocket length is of 100 mm but the location is different. The influence of location on natural frequency for the different boundary conditions are illustrated in figure 5.29. Irrespective of the boundary condition, C1 configuration produces higher values of natural frequency. Though, the length of the MR fluid pocket is same for all the configurations considered in this section, the relative change in stiffness for C1 configuration is higher compared to the others. This leads to the change in the overall stiffness of the composite sandwich beam. For the sandwich beams with symmetric boundary condition on both the sides and symmetric location of MR fluid pocket produces similar results. The same can be observed for both the natural frequency and loss factor as shown in figure 5.29 and 5.30 for the CC and SS boundary conditions, respectively. For the CF boundary condition, configuration C10 produces higher loss factor values at the 1<sup>st</sup> mode and configuration C8 at the 2<sup>nd</sup> mode. The C1 configuration has a significant effect on higher modes as shown in figure 5.30 (b). For CC and SS boundary condition, C5 and C8 configurations are more effective at 1<sup>st</sup> and

2<sup>nd</sup> modes whereas C1 and C10 configurations provides more loss factor values at higher modes. The configuration C8 is able to suppress the more amplitude of vibration at 1<sup>st</sup> mode and C5 at 2<sup>nd</sup> mode for the CS and SF boundary conditions.

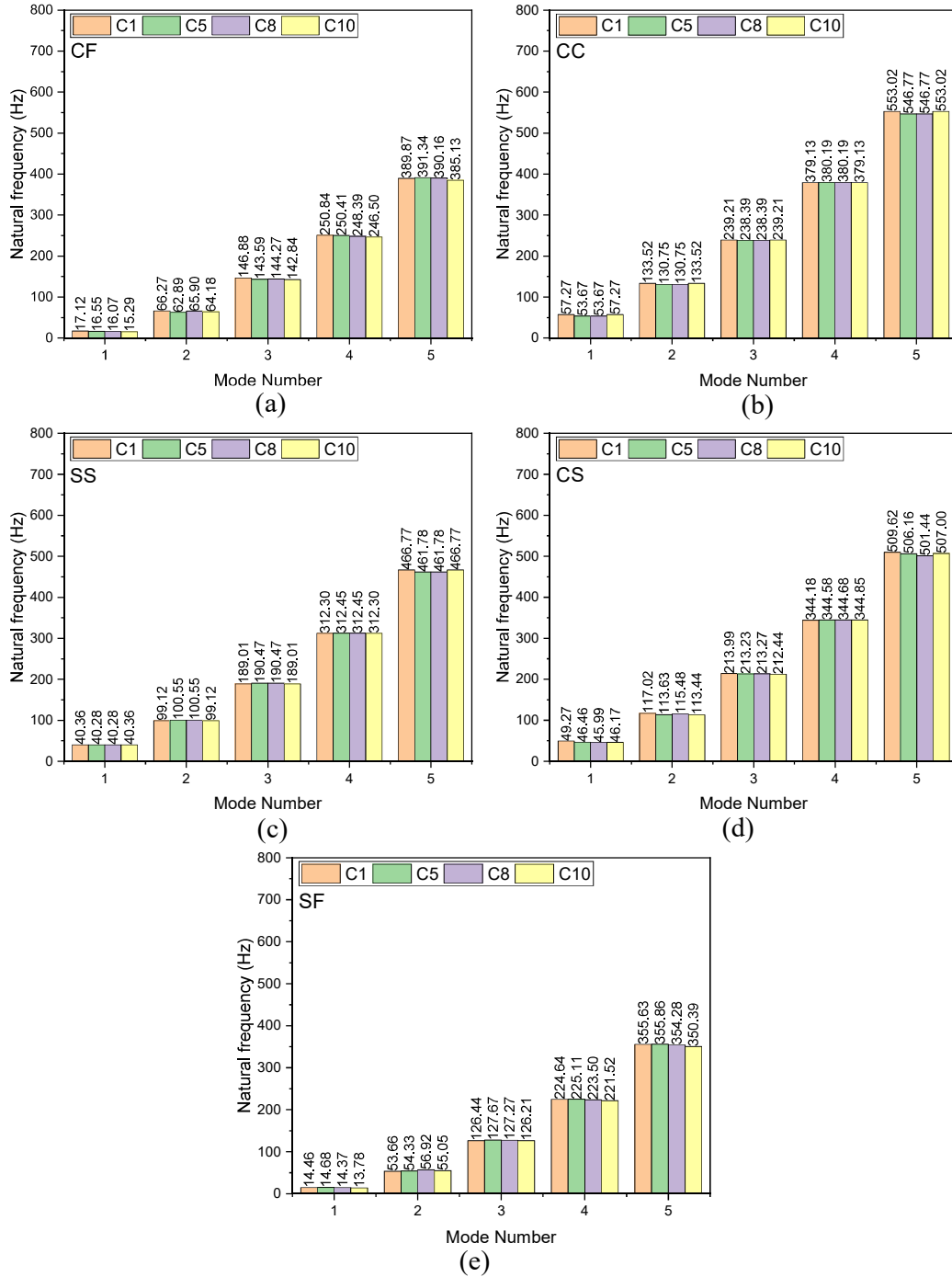


Figure 5.29 Influence of location of MR fluid pocket type on the natural frequency for (a) CF, (b) CC, (c) SS, (d) CS and (e) SF boundary conditions

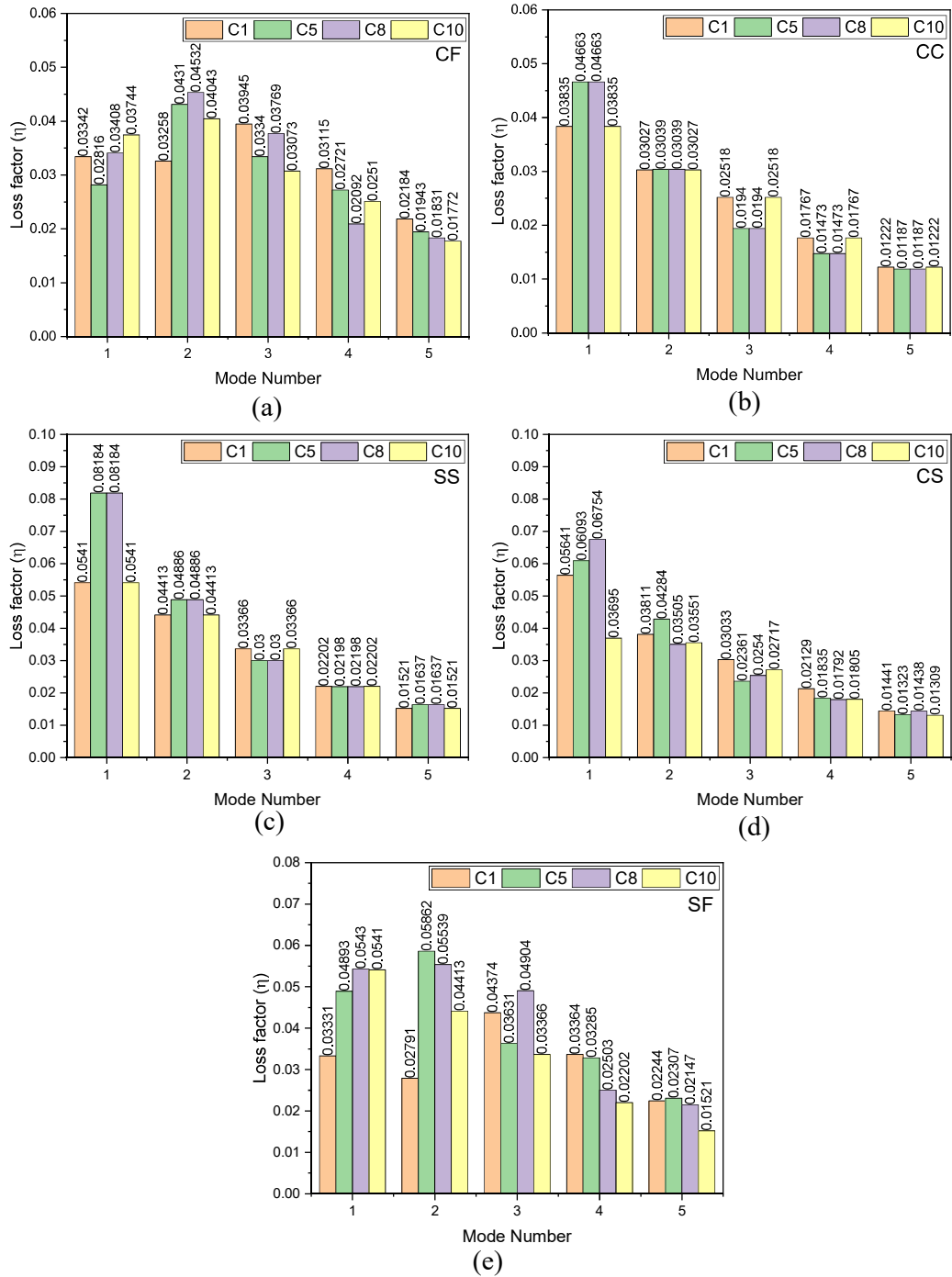


Figure 5.30 Influence of location of MR fluid pocket type on loss factor for (a) CF, (b) CC, (c) SS, (d) CS and (e) CF boundary conditions

From the results presented, it is learned that the length and location of the MR fluid pocket has a substantial effect on both the natural frequency and loss factor and also concluded that the effect of configuration depends on the type of boundary condition.

In addition, the frequency response study is also conducted to get the dynamic response of the sandwich beam structure under the applied harmonic load. The frequency response is necessary for any structure to understand the dynamic behavior in terms of vibration amplitude at any particular frequency. For the CF and SF boundary condition, harmonic force is applied at the free end of the top face layer. For the CC, SS and CS boundary conditions, force is applied in the middle of the top face layer (at exactly half-length). For all the boundary conditions, harmonic force of 2N is applied. The frequency sweep is done in the range of 1 to 800Hz with the resolution of 0.5Hz. This resolution ensures to get the smooth data of frequency response without a big jump between the two consecutive points. The influence of configuration of MR fluid pocket on the frequency response of the composite sandwich beam for the SS boundary condition is presented as shown in figure 5.31. The configuration of MR fluid pocket has a considerable impact on vibration amplitude and this type of behavior is more important phenomenon for the structural applications to suppress vibration amplitude at certain modes. The variation in peak amplitude of vibration for the different configurations can be witnessed from the figure 5.31.

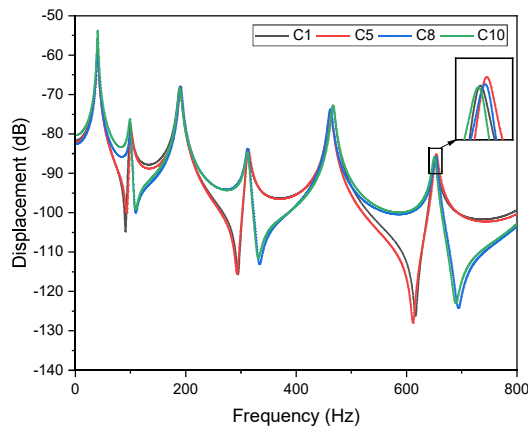


Figure 5.31 The influence of location of MR fluid pocket on the forced vibration response of the MR composite sandwich beam

Although there have been a few experimental studies on the dynamic behavior of the MR fluid sandwich beams with different face layers were conducted (Acharya et al., 2021; Allien et al., 2020), a comprehensive investigation on the dynamic response of in-house prepared MR fluids in sandwich structures in the pre-yield region of the MR fluid is still lacking. In this chapter, two different MR fluid samples are prepared to study the rheological properties in the pre-yield region. Further, the influence of magnetic field and the volume percentage of iron particles on the rheological properties of in-house prepared MR fluids are reported and also the dynamic behaviour of the MR sandwich beam is explored.

## 5.8 PREPARATION AND CHARACTERIZATION OF AN IN-HOUSE MAGNETORHEOLOGICAL FLUID

### 5.8.1 Materials and equipment used for the preparation of MR fluid samples

The MR fluid contains iron powder particles suspended in the carrier fluid medium. In this work, iron particles used are CI particles, and silicone oil is used as the carrier fluid. The CI particles, low in magnesium and manganese compounds with a purity of 99.5%, are purchased from Sigma Aldrich with a density of 7.86 g/cm<sup>3</sup>. The viscosity of the silicone oil is 340 Cst (at 25<sup>0</sup>C), and the density is 0.970 g/cm<sup>3</sup> (at 25<sup>0</sup>C) which is supplied by Merck Life Science Private Limited. Additionally, a small amount of white lithium grease is used as a surfactant (surface modifier or additive) to avoid the sedimentation of the iron particles. White lithium grease, which is a paste-like substance, is bought from Permatex. This surfactant will accumulate around the iron particles to make them float in the carrier fluid (Kciuk, M.; Turczyn, 2012). Two types of MR fluid samples are prepared with different compositions of CI particles, as given in table 5.5.

Table 5.5 MR fluid samples composition

SI.No.	Volume percentage (Vol%)		Additive (Vol%)
	CI particles	Silicone Oil	White lithium grease
S-I	30	70	0.5
S-II	24	76	0.5

### 5.8.2 MR fluid preparation procedure

The MR fluid samples are prepared at room temperature. The S-I and S-II MR fluid samples are prepared with the different compositions as shown in table 5.5. The volume fraction calculations are used to prepare the MR fluid samples. The desired volume fractions are converted into weight fractions using the density property of the iron particles and silicone oil. The weight fractions of the materials are easy to measure using the weighing machine. The weight fraction proportions for both the samples are measured using high precision weighing machine tool. For S-I MR fluid sample, 44.8 grams of silicone oil is taken in the container. Then, the container which contains the carrier fluid is kept under a Mechanical stirrer. The REMI RQ-5 Plus mechanical type stirrer is used for the stirring of MR fluid. The stirrer shaft or rotator of the mechanical stirrer is arranged in such a way that it should not touch the base of the container. Initially, 0.5% of white lithium grease is added to the carrier fluid while stirring. The speed maintained for this stirring process is 600 rpm and this process is continued for 2 hours for the uniform mixing of an additive in the carrier fluid. Then, 155.2 grams of CI particles are added in small amounts while the fluid is stirring at 800 rpm. This stirring process is continued for at least 12 hours without interruption for uniform mixing of CI particles in the carrier fluid. For S-II MR fluid sample, 56.24 grams of silicone oil, 0.5% of white lithium grease, and 143.76 grams of CI particles are taken. A similar procedure is followed for the preparation of the S-II MR fluid sample. The mixing process of silicone oil and white lithium grease without adding CI particles turns the silicone oil into white color. The whitish color indicates the uniform mixing of white lithium grease in the carrier fluid. After this mixing process, the fluid is turned into black color because of the added CI particles. The diagram of the mechanical stirrer and MR fluid sample preparation process using the mechanical stirrer are shown in figure 5.32 (a) and (b), respectively.



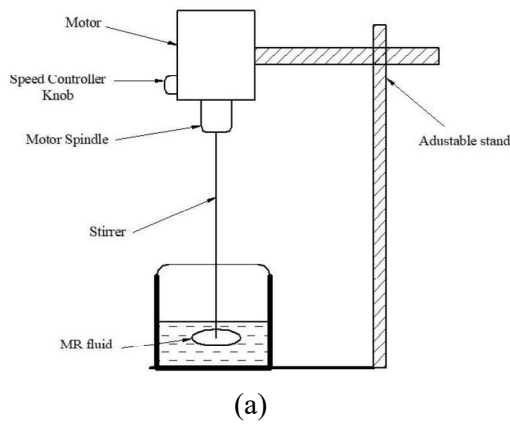


Figure 5.32 (a) Line diagram of the stirrer (b) MR fluid preparation using a mechanical stirrer

### 5.8.3 The microstructure of CI particles

The Scanning electron microscopy (SEM) and particle size distribution analyser tests are conducted on carbonyl iron particles to confirm the surface morphology and particle size. Figure 5.33 shows the density distribution (%) and cumulative value (%) histogram with respect to particle size diameter.

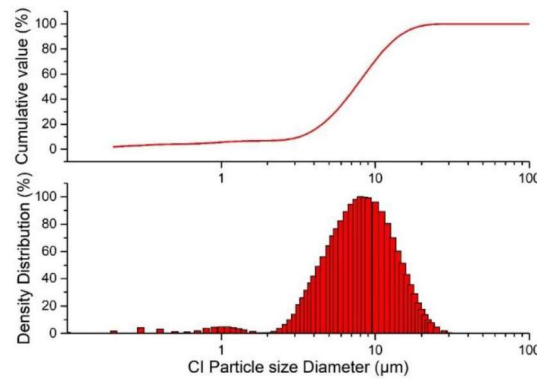


Figure 5.33 Particle size distribution curve of the CI particles

From the SEM analysis, it is observed that iron particles are spherical and also observed that the average iron particle size is around 4 to 9  $\mu\text{m}$  as the supplier provided in the product catalogue. Further, figure 5.34 (a) shows the iron particle shape that is viewed at 4000x and figure 5.34 (b) shows the SEM analysis image that is viewed at 25000x.

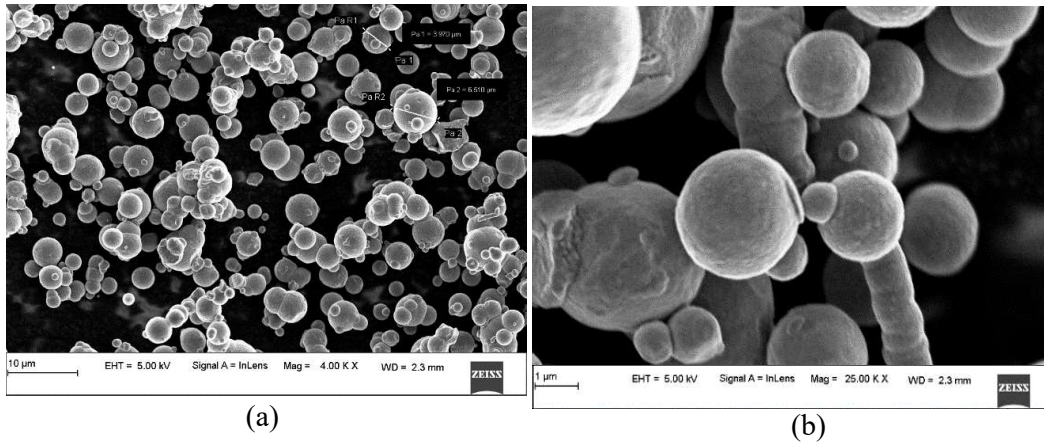


Figure 5.34 CI particles microstructure magnified view at (a) 4000x and (b) 25000x.

Vibratory sample magnetometer (VSM) test is conducted on 10 mg of sample at room temperature. Figure 5.35 illustrates the curve of magnetic field vs magnetic moment that is obtained in VSM testing. The test is performed from +15,000 Gauss to -15,000 Gauss with increment of 500 Gauss. The saturation magnetization of the iron particle is 208.4 emu/g. The coercivity and retentivity of the IC particles are 6.86 Gauss and 0.417 emu/g respectively.

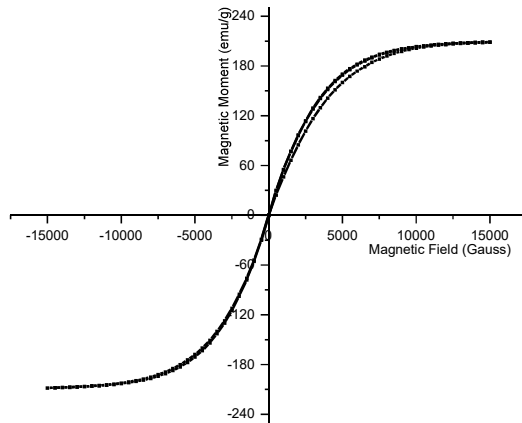


Figure 5.35 Magnetization curve of CI particles using VSM Testing

#### 5.8.4 Rheological experimental setup

The rheological characterization of the prepared MR fluid samples is performed using a Modular compact rheometer (MCR 702 Anton Paar make), as shown in figure 5.36.

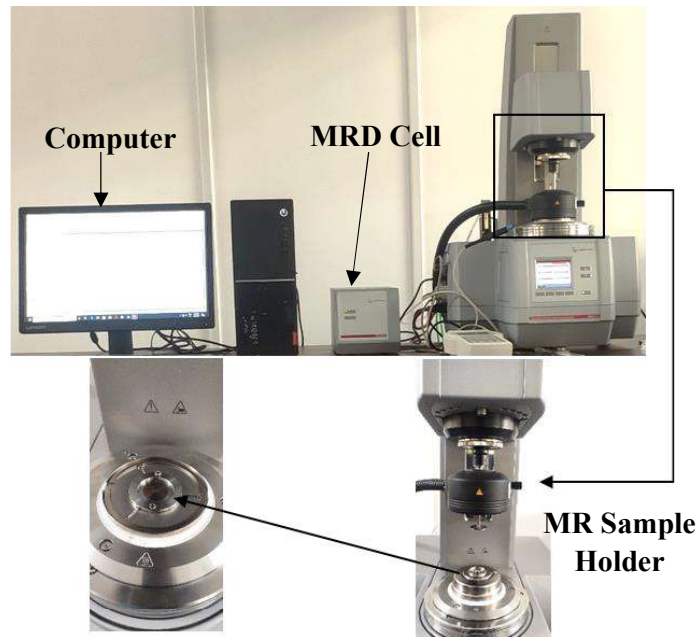


Figure 5.36 Rheometry setup

The measuring system includes mainly Magneto-rheology Device (MRD) cell for providing an external magnetic field, data processing sensors that are connected to the rheometer for measuring, and RheoCompass™ software to acquire the data from the sensors of the rheometer. For rheometry testing, a flat plate type configuration is used. A measuring gap of 0.5 mm is used for all the rheometer tests. For every test, approximately 0.4 ml of the fluid sample is filled in the gap of two parallel plates configuration.

### 5.8.5 Rheological results of MR fluid

The current sweep (0 to 5A) at a constant shear rate of 1/s is performed to find the relation between the applied current and the developed magnetic field. For every MR fluid, there exists a relationship between the applied current and the magnetic field produced. For MRF-132LD, the linear relation exists between the current and magnetic field (Li et al., 1999). This direct relationship may not be well fitted for all the fluids. Based on the results obtained, figure 5.37 (a) shows the linear relation between applied current and the magnetic flux developed for the prepared MR fluid. Further, the variation in viscosity with the current is illustrated in figure 5.37 (b). The viscosity of MR fluid is increased rapidly up to 2A of current. After that, the change in the viscosity curve is minimal and almost constant. This indicates that there will not be much

improvement in the fluid's viscosity, even if the current is increased further. The MR fluid exhibits linear viscoelasticity when the developed shear strain for the fluid is within the region of yield strain amplitude. Further, the oscillatory shear strain amplitude test is performed at 2A of current to determine the yield strain.

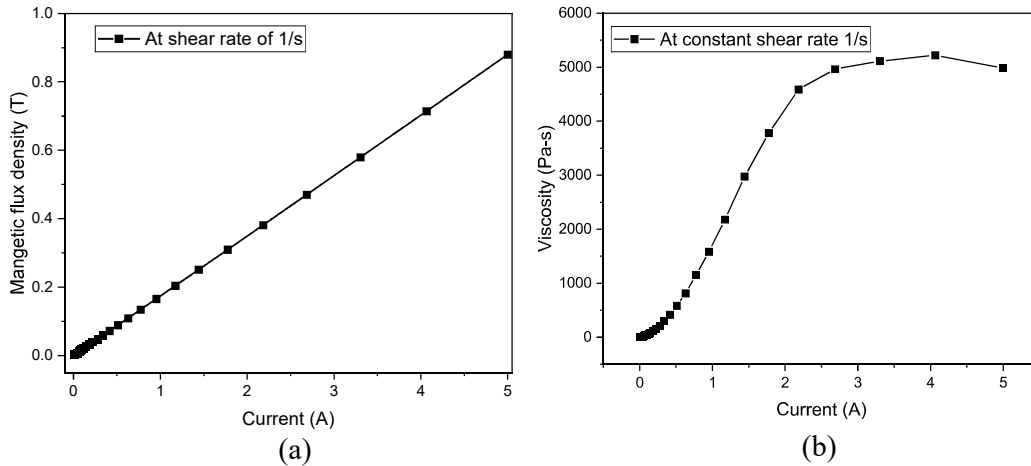


Figure 5.37 Variation in (a) Magnetic flux density, and (b) Viscosity with the applied current

The amplitude sweep is applied logarithmically up to 1% shear strain amplitude. The yield strain of 0.371% is determined for the prepared MR fluid sample, as shown in figure 5.38. The obtained yield strain for the prepared MR sample is in good agreement with the yield strain obtained in the research work (Li et al., 1999; Weiss et al., 1994).

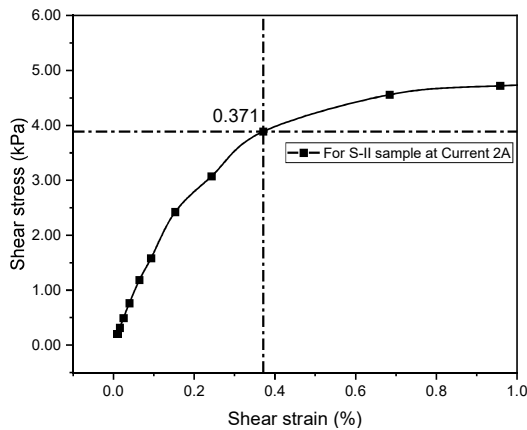


Figure 5.38 Shear stress-strain curve to find the yield strain

For all the further experiments, maximum shear strain amplitude ( $\gamma_0 = 0.04\%$ ) is applied to ensure the obtained results are well within the pre-yield region.

### 5.8.6 Frequency-dependent rheological properties

The frequency sweep is conducted at a constant shear strain amplitude ( $\gamma_0 = 0.04\%$ ). The frequency sweep is applied logarithmically from 1 to 100 Hz. Figures 5.39 (a) and (b) illustrate the variation of storage modulus and loss factor with the driving frequency at different magnetic fields. The storage modulus increases, and the loss factor value decreases as the applied magnetic field increases. At lower magnetic fields, all the CI particles in the MR fluid sample may not align properly, and there is a more chance of fluid nature in the MR fluid sample. This causes high loss factor values at low magnetic fields. At higher magnetic fields, the iron particles in the fluid arrange appropriately in a particular direction, and the fluid becomes semi-solid. This arrangement will restrict the iron particle movement in the MR sample. This might decrease the loss factor value at a particular driving frequency with the applied field.

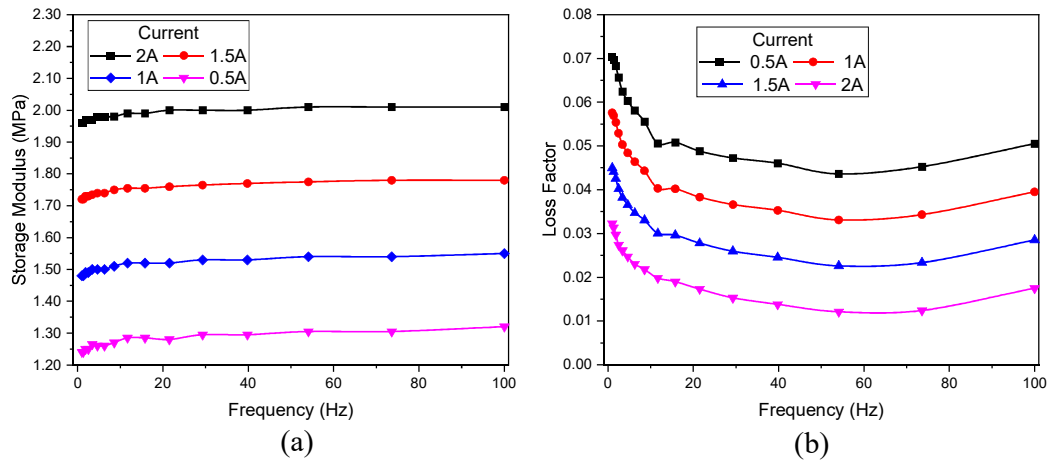


Figure 5.39 Frequency dependency of (a) Storage Modulus and (b) loss factor at different currents

### 5.8.7 Amplitude Strain dependent rheological properties

An amplitude strain sweep test is conducted at a constant angular frequency of 10 rad/sec. The amplitude sweep is applied logarithmically from 1 to 10% strain amplitude. Figure 5.40 (a) and (b) show the variation in storage modulus and loss factor with strain amplitude, respectively. The storage modulus of the MR sample is

decreased, and the loss factor is increased as the strain amplitude goes from 1 to 10% of shear strain. The amplitude strain-dependent properties like storage modulus and loss factor obtained in this research work are in good agreement with the research work (Li et al. (1999)).

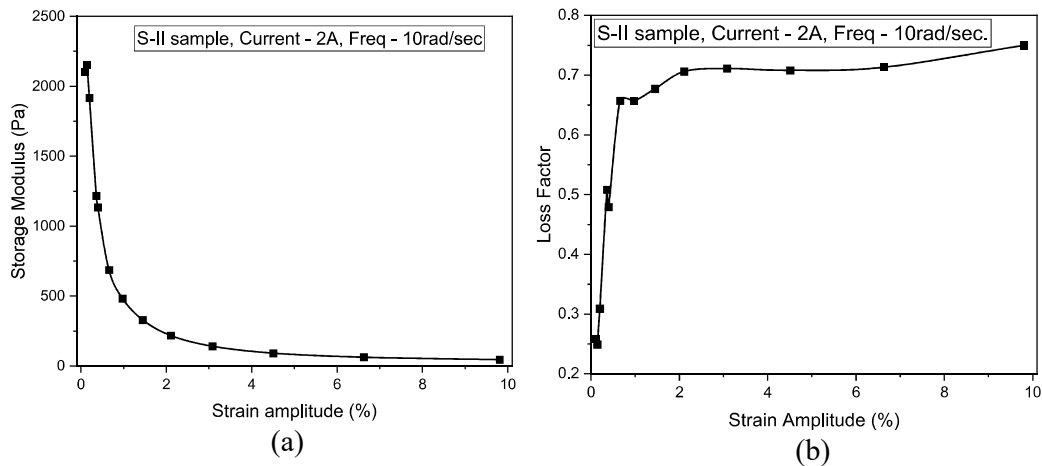


Figure 5.40 Strain amplitude dependency of (a) Storage modulus, (b) Loss factor at 2A current

### 5.8.8 Magnetic field dependent rheological properties

The magnetic field dependent storage modulus and loss factor at different driving frequencies 10 Hz, 20 Hz, 40 Hz, 70 Hz, and 100 Hz at a constant 0.04% of the amplitude of strain are plotted as shown in figures 5.41 (a) and (b), respectively. All the results presented in this section are taken from the frequency sweep test. The storage modulus at any driving frequency is increased with the applied magnetic field value. The iron particles in the MR fluid start to arrange in a chain-like structure with the applied magnetic field value. The MR fluid changes its rheological properties due to changes in the arrangement of iron particles in the MR fluid. At 100 Hz of frequency, the storage modulus value is higher than the 10 Hz driving frequency at the same applied field value. The storage modulus value is increased with the driving frequency at any particular magnetic field. However, the loss factor value is decreased with the applied field value at any driving frequency, as shown in figure 5.41 (b). The loss factor value at any particular magnetic field is initially decreasing then starts increasing as the driving frequency increases.

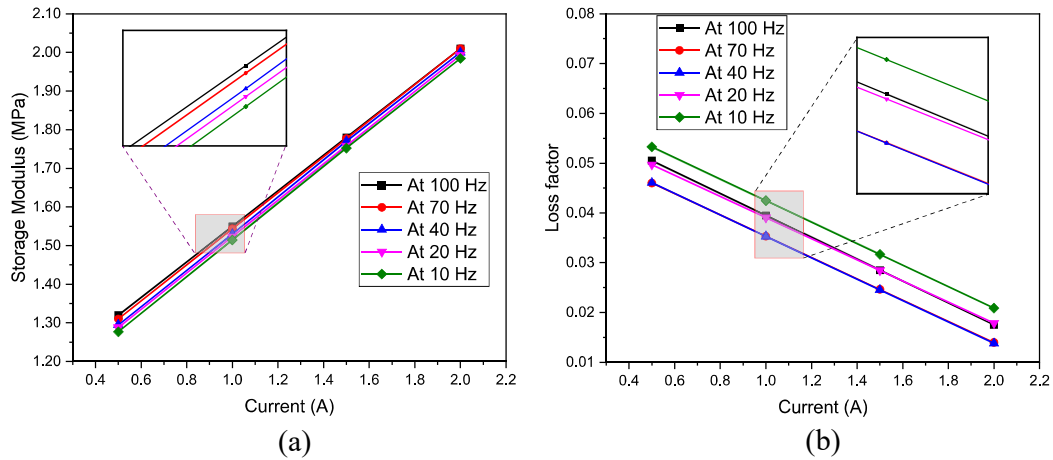


Figure 5.41 Magnetic field dependency of (a) Storage modulus (b) Loss factor at different driving frequencies

### 5.8.9 Volume fraction dependent rheological properties

The MR fluid rheological properties dependency on the volume percentage of CI particles is presented in this section. The storage modulus and loss factor for the S-I and S-II samples are shown in figures 5.42 (a) and (b), respectively.

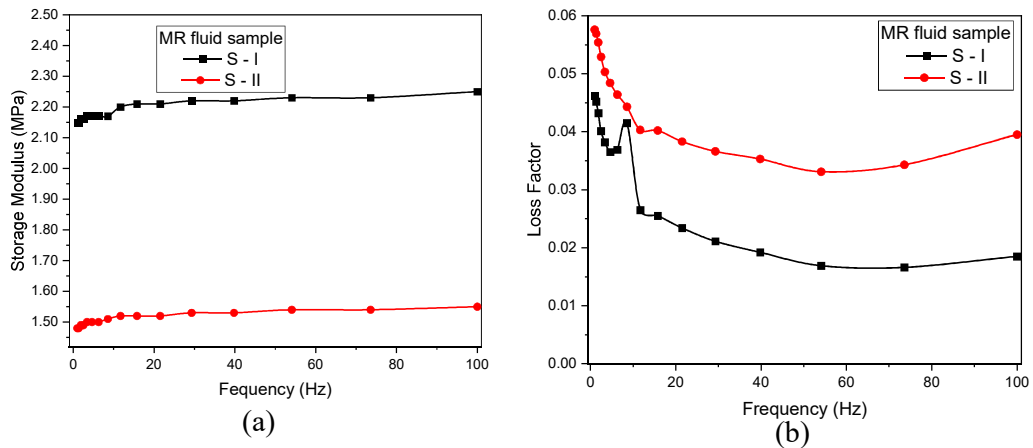


Figure 5.42 Volume fraction dependency of (a) Storage modulus, (b) Loss factor for S-I and S-II samples with frequency

The storage modulus of S-I sample is more compared to the S-II MR fluid sample. For the applied magnetic field value, the MR effect is more for the higher vol% of CI particles MR fluid sample. However, the loss factor value of S-I is less than the S-II MR fluid sample. From the results obtained in this work, it is confirmed that iron particle concentration in the MR fluid strongly influences the rheological properties.

## 5.9 ESTIMATION OF STORAGE MODULUS AND LOSS FACTOR EQUATIONS FROM RHEOLOGICAL STUDIES

The storage modulus and loss factor are formulated in terms of magnetic field based on the experimental results. The linear regression model is used for the estimation of equations in terms of magnetic field.

The complex shear modulus of the MR fluid is given as

$$G^*(B) = G'(B) + iG''(B) \quad (5.4)$$

Where, the real part  $G'(B)$  is the storage modulus and the imaginary part  $G''(B)$  is the loss modulus of the MR fluid, Here B is in Tesla.

The equations are formulated in the pre-yield linear region of the in-house prepared MR fluid. The estimated storage modulus and loss factor equations for the prepared fluid are shown in table 5.6.

Table 5.6 Storage modulus and loss factor equations of MR fluid samples		
Property	S-II MR fluid sample	S-I MR fluid sample
Storage Modulus (Pa)	$1.0986 \times 10^6 + 2.40817 \times 10^6 (B)$	$1.60168 \times 10^6 + 3.3731 \times 10^6 (B)$
Loss factor	$0.06149 - 0.11019(B)$	$0.05766 - 0.13321(B)$

## 5.10 INFLUENCE OF VOLUME FRACTION OF MR FLUID ON THE DYNAMIC RESPONSE OF THE SANDWICH BEAM

The influence of CI particle volume percentage on the vibrational response of the sandwich beam is performed at a constant magnetic field density of 500G. For this constant face layers thickness of 1mm and MR fluid core thickness of 1mm is maintained. The natural frequency of the MR fluid sample S-I and S-II are illustrated in figure 5.43 (a) and (b), respectively. For both the fluid samples, there is an increment in the natural frequency of the sandwich beam with the applied magnetic field.



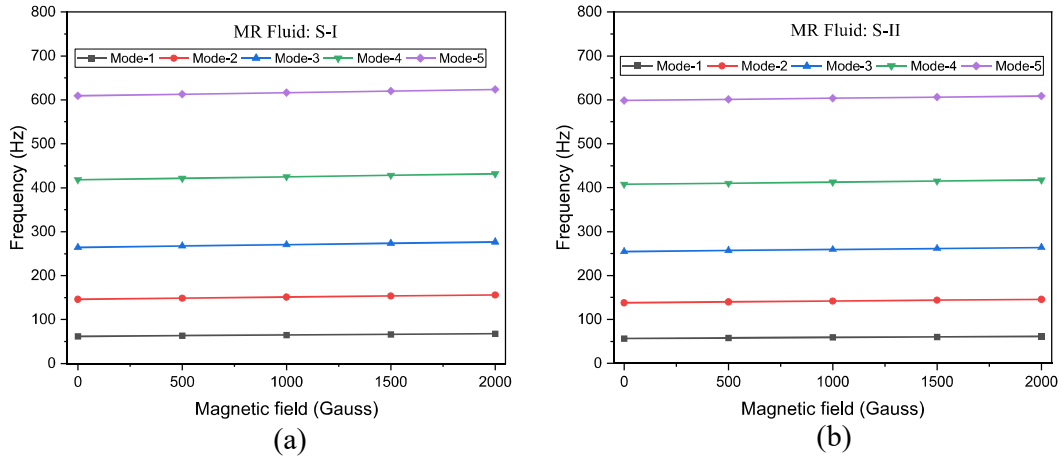


Figure 5.43 Variation in natural frequency for (a) S-I sample (b) S-II sample with respect to the magnetic field (c) Natural frequency (d) Frequency response for S-I and S-II samples

The comparison study of natural frequencies for both fluid samples are shown in figure 5.44 (a). As the percentage of CI particles in the MR fluid sample increases, there is a significant right shift in the frequency response curve along with the reduction in vibration amplitude for the MR fluid sandwich beam observed. It indicates that as the volume percentage of CI particles increases, there is an increment in the stiffness as well as the damping of the sandwich beam, as shown in Figures 5.44 (b). The increase in stiffness influences the natural frequency of the MR fluid sandwich beam.

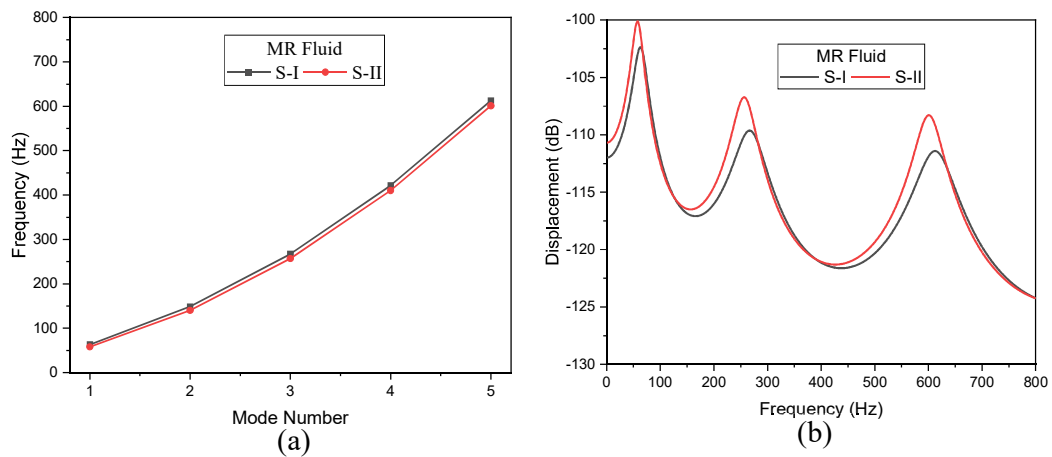


Figure 5.44 Variation in (a) Natural frequency (b) Frequency response of the sandwich beam for S-I and S-II samples

## 5.11 SUMMARY

In this chapter, the effect of combined damping due to composite facings and MR fluid on the static and dynamic response of composite sandwich beam is discussed. The presented study helps to understand the influence of various parameters on the static and dynamic response of the MR fluid sandwich beam applications. The static, free, and forced vibration analyses of composite sandwich beam are conducted. A detailed study is conducted to evaluate the impact of composite laminate angle, magnetic field, and thickness ratio on static deflection, natural frequency, loss factor, and frequency response. The influence of magnetic field on the percentage of deviation in natural frequency, loss factor, and static deflection is also discussed. In addition, Four MR fluid pocket configuration types are considered. The configuration types include 1/4th, 1/2th, 3/4th and the full length of the MR fluid pockets at different locations of sandwich beam. In addition, a detailed study of the influence of each MR fluid pocket configuration type on the natural frequency, loss factor and frequency response are presented for the CF, CC, SS, CS and SF boundary conditions.

Further, two different compositions of MR fluid samples with 24 and 30 percent (%) volume fractions of CI particles are prepared. The influence of oscillating driving frequency, strain amplitude, magnetic field, and the percentage of CI particle on the rheological properties of the MR fluid samples are discussed. In addition, the properties of MR fluid samples are used in the numerical formulation to explore the influence of the iron particles volume percentage in the MR fluid on the dynamic response of the MR sandwich beam.

## CHAPTER – 6

# ACTIVE VIBRATION CONTROL OF COMPOSITE SANDWICH BEAM

### 6.1 INTRODUCTION

Active control techniques have been using for the structural applications to reduce the effects of vibrations, noise, and other dynamic disturbances on the structure. Though, literature suggests there is some studies on the dynamic response of the sandwich beams with viscoelastic and MR fluid for the structural applications. The combination of these techniques with active control further improves the structural stability. A very few literatures available on the combined effect of these techniques. This chapter explored combined effect of active and passive vibration control as well as active with semi-active vibration control of composite sandwich beam.

### 6.2 MODELLING AND ANALYSIS OF SANDWICH BEAMS USING PID CONTROLLER

Figure 6.1 shows the methodology followed for the present study. It is started with the modelling of the composite sandwich beam with the viscoelastic material and MR fluid as the core layer.

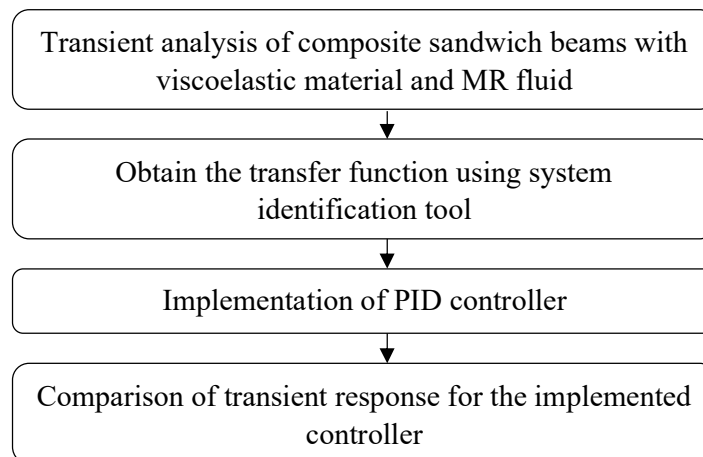


Figure 6.1 Procedure to implement the PID control on sandwich beam

Transient structural study is conducted in the ANSYS workbench module to obtain the time domain response of the composite sandwich beam. Then, the transfer function is taken using system identification tool which is available in the MATLAB platform. The PID controller is implemented using transfer function to obtain the time response with the tuned controller parameters.

ANSYS composite Pre-post (ACP) module is used for the modelling of the composite sandwich beams. The composite layers of sandwich beam are modelled in a layer-wise. The ACP module provides more flexibility in designing the layer-wise composite sandwich beams. The bond between the composite face layers and core material is assumed to be perfect. Figure 6.2 illustrates the created sandwich beam modelled with a length of 300 mm and a width of 25 mm dimensions.

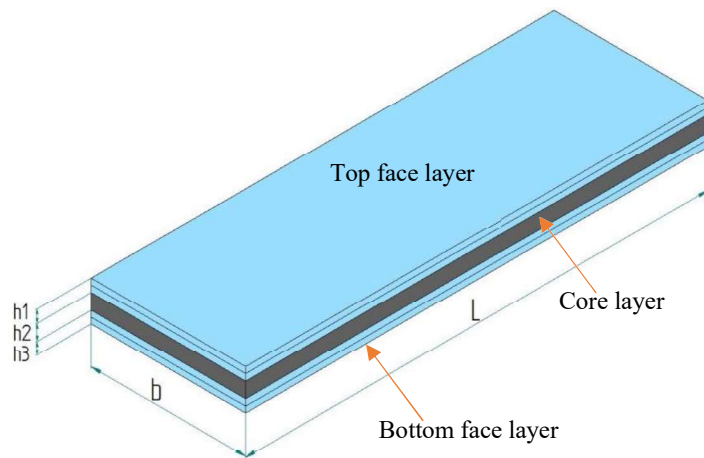


Figure 6.2 Composite sandwich beam with the core material

System Identification toolbox is a MATLAB tool that provides tools for estimating the mathematical models of dynamic systems from the measured data. The system identification toolbox can be used for an accurate model of complex systems using a variety of data-driven methods such as time-domain and frequency-domain techniques. This tool is utilised to get the transfer function of sandwich beam from the transient response. The system identification technique determines the mathematical model of a dynamic system based on the input-output response of a system. It is concerned with obtaining system parameters from the observed responses of a system. The obtained transient input-output response data is needed to feed to the system identification tool to interpret the mathematical model of the system. This tool will check the data matching

percentage between the original response and that of the model created by this application. In the present work, time data obtained from the transient response of the composite sandwich beam is used to get the mathematical model of the system as shown the procedure in figure 6.3.

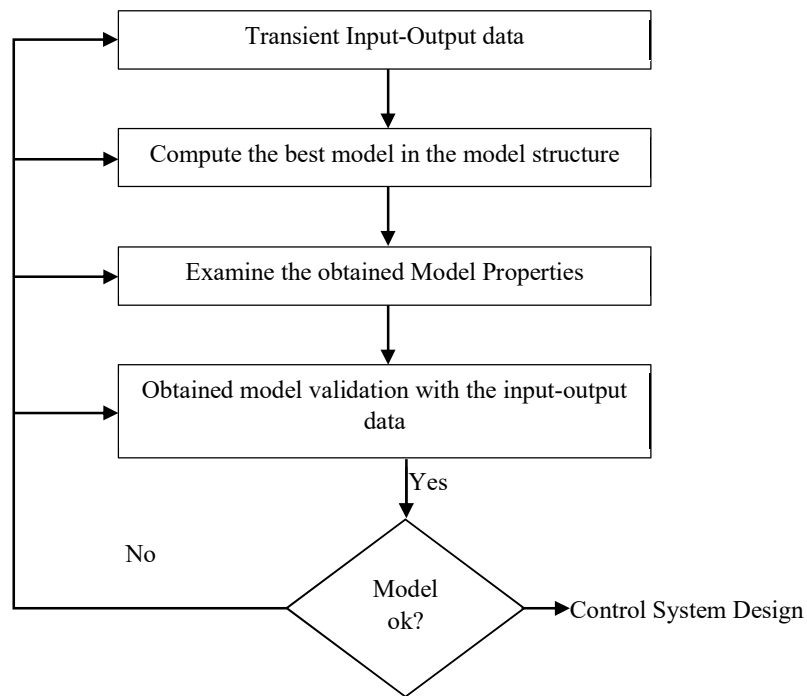


Figure 6.3 System identification procedure flowchart to get the transfer function

Simulink is a powerful simulation and modeling tool that allows you to create models of dynamic systems using block diagrams. The simulink platform is used to implement the PID controller as shown in figure 6.4. The PID controller is a feedback control mechanism used in industrial control systems to regulate and control the behavior of a process or system. The PID controller continuously measures the error between the desired setpoint and the actual output of the system and uses three control parameters, proportional, integral, and derivative, to calculate the output that will minimize the error and bring the system to its setpoint.

The proportional term of the PID controller generates a control output that is proportional to the error between the setpoint and the actual process output. The integral term calculates the cumulative error over time and adjusts the control output accordingly, which helps to eliminate steady-state error. The derivative term calculates

the rate of change of the error and generates an output that counteracts any sudden changes in the process output, helping to stabilize the system. The three parameters of the PID controller,  $K_p$ ,  $K_i$ , and  $K_d$ , are adjusted to optimize the controller's performance for a specific process or system. The selection of these parameters can significantly affect the controller's response to changes in the system or process.

The PID controller output  $u(t)$  is the summation of the proportional gain term ( $K_p$ ), integral gain term ( $K_i$ ) and derivative gain term ( $K_d$ ) and the controller output  $u(t)$  is given as,

$$u(t) = K_p e(t) + K_i \int_0^t e(t) dt + K_d \frac{d}{dt} e(t) \quad (6.1)$$

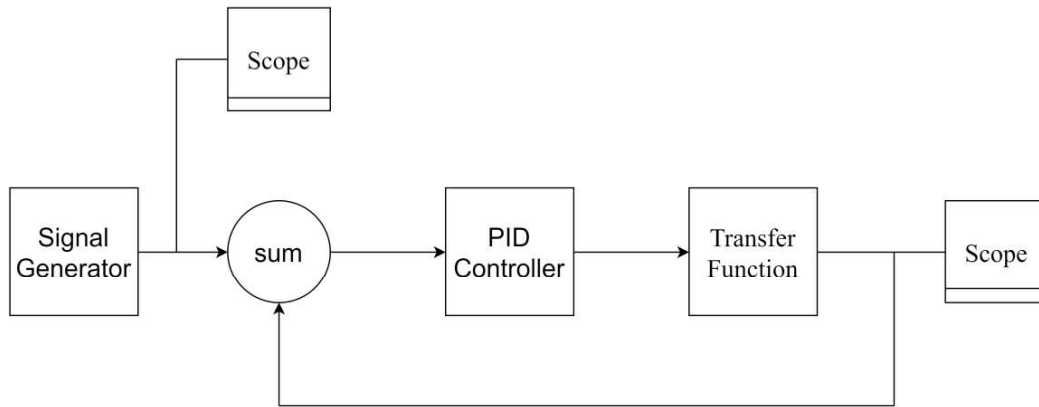


Figure 6.4 PID Controller Block Diagram

The blocks used for the PID controller are signal generator, sum (where different signals can be combined), PID controller block, Transfer function and scope. The signal generator is used to generate the different type of signals. For the present study, Impulse and sine signals are used as an input for the PID controller as shown in figure 6.5. The PID controller block consists of gains for the proportional, Integral and Derivative controller. We need to supply gain values in the PID controller block based on the tuning technique. The transfer function block defines the mathematical model that is supplied in terms of numerator and denominator. We need to supply the coefficients of the numerator and denominator to define the transfer function.

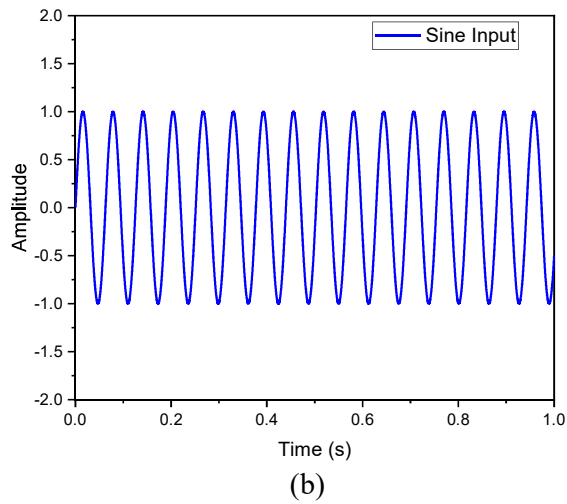
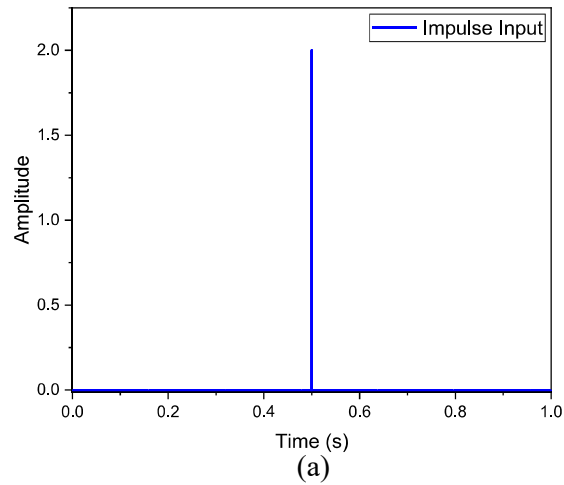


Figure 6.5 Input signals (a) Impulse and (b) Sine signal

### 6.2.1 Combined effect of Passive and Active vibration control on sandwich beam response

The transient analysis is conducted on the viscoelastic sandwich beam using ANSYS transient module. The transient response of the system is fed to the system identification tool in MATALAB. The transfer function obtained for the viscoelastic sandwich beam from the system identification tool is shown in Eq. 6.2.

$$\text{Transfer Function (TF)} = \frac{-3.076e04s^3 - 5.518e05s^2 - 4.214e08s - 6.344e09}{s^5 + 41.93s^4 + 2.594e04s^3 + 1.008e06s^2 + 1.675e08s + 6.001e09} \quad (6.2)$$

Further, for the obtained transfer function, PID controller is developed in Simulink platform. The gains for the PID controller are obtained by trial-and-error method. The gains supplied for the PID controller are  $K_p = -0.8$ ,  $K_i = -0.001$ ,  $K_d = 0$ .

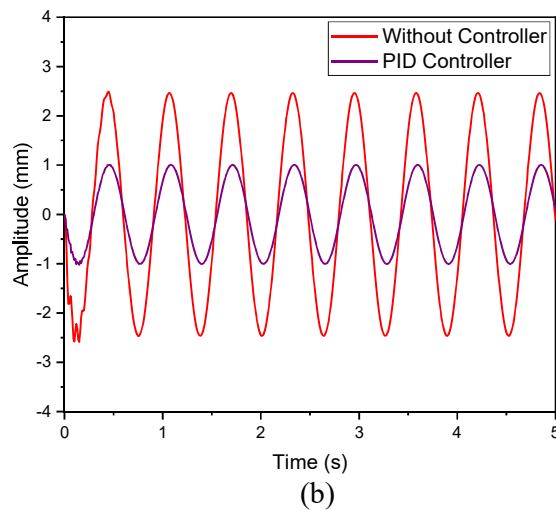
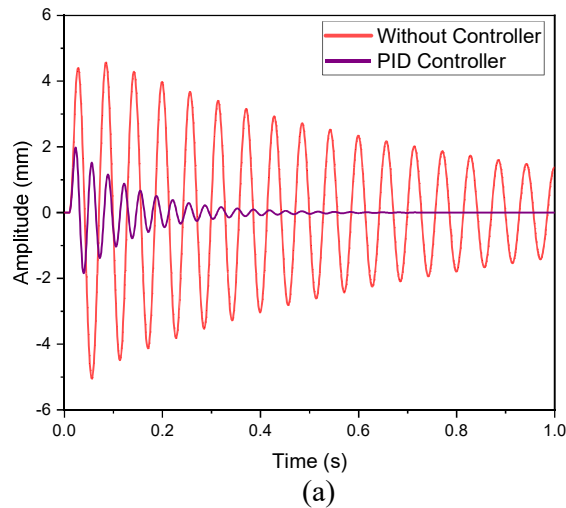


Figure 6.6 Combined effect of active and passive control on (a) Free vibration and (b) Forced vibration response

For the given gains, the amplitude and settling time of the viscoelastic sandwich beam are improved as shown in figure 6.6 (a) and (b), respectively. The active control techniques along with viscoelastic sandwich beams improve the structural stability by mitigating the vibration amplitude.



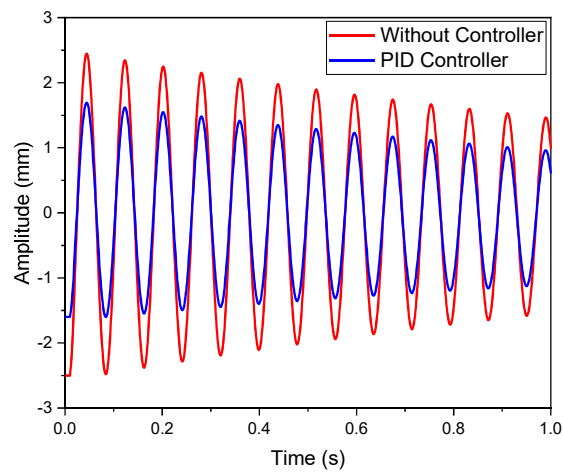
### 6.2.2 Combined effect of Semi-active and Active vibration control on sandwich beam response

The transient analysis is conducted on the MR fluid sandwich beam using ANSYS transient module. The obtained the transient response is fed to the system identification tool in MATALAB. The transfer function obtained for the MR fluid sandwich beam from the system identification tool is shown in Eq. 6.3.

$$TF = \frac{-106.5s^2 - 2.493e04s - 2.605e06}{s^3 + 1.056s^2 + 6362s + 1.278e-09} \quad (6.3)$$

Further, for the obtained transfer function, PID controller is developed in Simulink platform. The gains for the PID controller are obtained by trial-and-error method. The gains supplied for the PID controller are  $K_p = -0.0002$ ,  $K_i = 0.01$ ,  $K_d = 0$ .

For the given gains, the amplitude and settling time of the MR fluid sandwich beam are improved as shown in figure 6.7 (a) and (b), respectively. The active control techniques along with MR fluid sandwich beams improve the structural stability by mitigating the vibration amplitude. The combination effect of active and semi-active control techniques leads to design of optimal design for the structural applications. These techniques improve the structural life for sandwich structural applications.



(a)

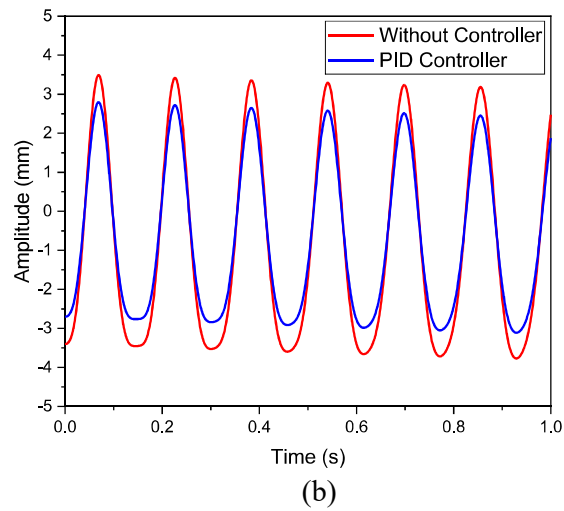


Figure 6.7 Combined effect of active and Semi-active control on (a) Free vibration and (b) Forced vibration response

### 6.3 SUMMARY

This chapter discusses the active vibration control of sandwich beam with the combination of passive and semi-active control technique. The PID controller is implemented to compare the transient response of the viscoelastic and MR fluid sandwich beam with the controller and without the controller.

## CHAPTER – 7

### SUMMARY AND CONCLUSIONS

#### 7.1 SUMMARY

In the present study, the passive, semi-active and active vibration control methods are implemented to investigate the influence of different parameters and boundary conditions on the dynamic response of the composite sandwich beam. The FE formulations are developed for the composite sandwich beam. The FE formulation developed by considering a Euler-Bernoulli's method for the sandwich beam element and the Lagrange's approach is utilized to obtain the EOM. Further, the developed FE formulations solution is validated with the available literature by taking different case studies.

The influence of viscoelastic material and boundary conditions on natural frequency, loss factor and frequency response are investigated as a part of the initial study. Further, the influence of axial gradation configurations of the viscoelastic materials on the dynamic response is reported. In addition, a comparison study of all the four configurations at different boundary conditions is discussed.

The effect of combined damping due to composite facings and MR fluid on the static and dynamic response of composite sandwich beam is discussed. The present study helps to understand the influence of various parameters on the static and dynamic response of the sandwich beam applications. The static, free, and forced vibration analyses of composite sandwich beam are extracted. A detailed study is conducted to evaluate the impact of composite laminate angle, magnetic field, and thickness ratio on static deflection, natural frequency, loss factor, and frequency response of a composite sandwich beam. The influence of magnetic field on the percentage of deviation in natural frequency, loss factor, and static deflection is also discussed. Further, Four MR fluid pocket configuration types are considered. In addition, two different compositions of MR fluid samples with 24 and 30 percent (%) volume fractions of CI particles are prepared. The influence of oscillating driving frequency, strain amplitude, magnetic field, and the percentage of CI particle on the rheological properties of the MR fluid

samples are discussed. In addition, the properties of MR fluid samples are used in the numerical formulation to explore the influence of the Iron particles percentage in the MR fluid on the dynamic response of the MR sandwich beam.

Further, the study is extended to investigate the active vibration control of sandwich beam with the combination of passive and semi-active is presented. The PID controller is implemented to compare the transient response of the sandwich beam with controller and without controller.

## **7.2 CONCLUSIONS**

The salient conclusions from the present research work are summarized into three categories as follows,

### **7.2.1 Passive vibration control of sandwich beam with viscoelastic material**

- VEM-1 material is able to produce higher loss factor values compared to the VEM-2 material for all the boundary conditions considered, and the loss factor value at the first fundamental mode is more for the CS boundary condition.
- The loss factor of the VEM-1 is increased by 72.98%, 71.16%, 71.77%, and 71.32% when compared to the VEM-2 at the first fundamental mode for the CF, CS, SS, and CC boundary conditions, respectively.
- For CF condition, axial gradation of VEM configuration-I is more effective at the first three fundamental modes compared to the other configurations.
- For SS condition, axial gradation of VEM Configuration-I produced high loss factor values at the first fundamental mode whereas for higher modes, configuration-III is more effective.
- For CS condition, axial gradation of VEM configuration-II provided the higher loss factor values at the lower modes whereas configuration-IV has given good damping values at higher modes.
- Among all the viscoelastic material axial gradation configurations considered, CC boundary condition has the least effect on the variation in natural frequency and loss factor. This may be due to very less variation in the relative change in stiffness and mass value of the sandwich beam.
- The axial gradation configuration of viscoelastic material has a considerable impact on loss factor and frequency response for all the boundary conditions

and this technique can be implemented to the structural applications to control higher vibration amplitudes at particular modes for a given boundary condition.

### **7.2.2 Semi-active vibration control of sandwich beam with MR fluid**

- The central static deflection of the sandwich beam is more for the composite facings at higher laminate angles than at the lower laminate angles. This is due to a decrease in the overall stiffness of the sandwich beam at the higher laminate angles.
- A maximum of 77.21% reduction in static deflection is observed for the clamped-clamped boundary condition at a magnetic field of 2000G. The decrease in static deflection is due to the change in the shear modulus of the MR fluid at the applied magnetic field.
- The decrease in the natural frequency of the sandwich beam is more rapid at higher modes compared to the lower modes and there is a left shift in the frequency response curve is noticed as the thickness ratio increases. The shift in the frequency response curve isolates the sandwich beam from the resonance due to external excitation.
- The combined damping effect of composite facings and MR fluid core has shown a considerable reduction in vibration amplitude and there is a good improvement in the loss factor value. The combined damping effect plays a crucial role in reducing the high amplitudes of vibration for structural applications.
- The influence of configuration on sandwich beam response depends on the type of boundary condition used and the configuration type aid in suppressing the higher amplitudes of vibration for the structural applications where selected modes are severe to the structure.
- The configuration C5 and C8 (both 1/4th MR fluid pocket length) produces more loss factor values for the SS boundary condition at first fundamental mode among all the configurations considered.
- Activation of MR fluid pocket at the tip region (C10 configuration) of the sandwich beam is best suited for the SF boundary condition among all the configurations considered.

- The sandwich beams with symmetric boundary condition on both the sides and symmetric location of MR fluid pocket produces similar results.
- The CI particle volume fraction percentage in the MR fluid has shown a strong influence on the rheological properties. The storage modulus is more for the higher volume percentage of CI particles MR fluid.
- The higher CI particles MR fluid sample improved the natural frequency of the sandwich beam and also showed a significant reduction in the vibration amplitude.

### **7.2.3 Combined effect of passive, semi-active and active vibration control for the sandwich beam**

- The implemented PID controller has shown a significant reduction in the settling time of the sandwich beam for both the viscoelastic and MR fluid sandwich beams.
- There is considerable reduction in amplitude of vibration also observed for the both the viscoelastic and MR fluid sandwich beams.
- The active control techniques further improve the stability of the structural components by reducing the amplitude of vibration and these techniques can be employed with the combination of passive and semi-active control methods for the better performance of sandwich structures under the dynamic environments.

## **7.3 SCOPE OF FUTURE WORK**

The present work focused on the theoretical studies on the dynamic response of the sandwich beam with the viscoelastic elastic core material, MR fluid core material and implementation of active control techniques along with passive and semi-active control method.

- The numerical and experimental studies can be extended to the sandwich plates and shell structures by taking different viscoelastic core material and face layer materials for better understanding of the dynamic response of the sandwich structures.
- The numerical and experimental studies on the fully filled and partially filled MR fluid sandwich plates and shell structures can be investigated to study the

influence of the length of the location of the MR fluid pocket on the dynamic response of the sandwich structure.

- The optimization study can be conducted to determine optimal location of the MR fluid pocket and number of MR fluid pocket required to reduce the maximum amplitude of vibration.
- Though, the implemented PID controller is effective in reducing the vibration amplitude of the sandwich structures, there is a lot of scope to explore the newly evolved active controller techniques to improve the damping performance and settling stability of mechanical structures.





## APPENDIX-I

### 1. FESEM (Field emission scanning electron Microscope) (Make: Carl Zeiss-sigma)



**Specification:** Electron Source: Schottky Thermal Field Emitter, Resolution\* at 30 kV (STEM): 1.0 nm, Resolution\* at 15 kV: 1.0 nm, Resolution\* at 1 kV: 1.6 nm, Resolution\* at 30 kV (VP Mode) :2.0 nm, Maximum Scan Speed :50 ns/pixel, Accelerating Voltage :0.02 – 30 kV Magnification: 10× – 1,000,000×, Probe Current: 3 pA - 20 nA (100 nA (optional), Image Frame store 32 k × 24 k pixels.

### 2. CILAS 1064 Particle size analyser



Specification: Particle size range: 0.04 to 500  $\mu\text{m}$ , Number of lasers: 2, Laser source: Fibre and collimated laser diodes, Wavelength: 635 and 830 nm, Power :3/7 mW, Beam diameter: 2 and 20 mm, Repeatability:  $\pm 0.5 \%$ , Reproducibility:  $< 2 \%$ .

### 3. Lakeshore:7407- Vibration sample Magnetometer (VSM)



**Specification:** Make and Model: Lakeshore, USA, Model 7407, Max. Magnetic field: 2.5 T, Dynamic moment range:  $1 \times 10^{-6} \text{emu} - 10^3 \text{emu}$ .

Vibrating Sample magnetometer feasible measurements

- M Versus H at Room Temperature.
- M Versus T at constant H (Selected Field) M Versus H at constant Temperature (Low Temperature range 20-300K and High Temperature range 300 -1270K)

#### 4. Weighing balance



**Specification:** Maximum capacity: 1 Kg, Accuracy: 0.1g, Power: 230V AC, 50Hz

#### 5. Mechanical stirrer (Make: Remitek)

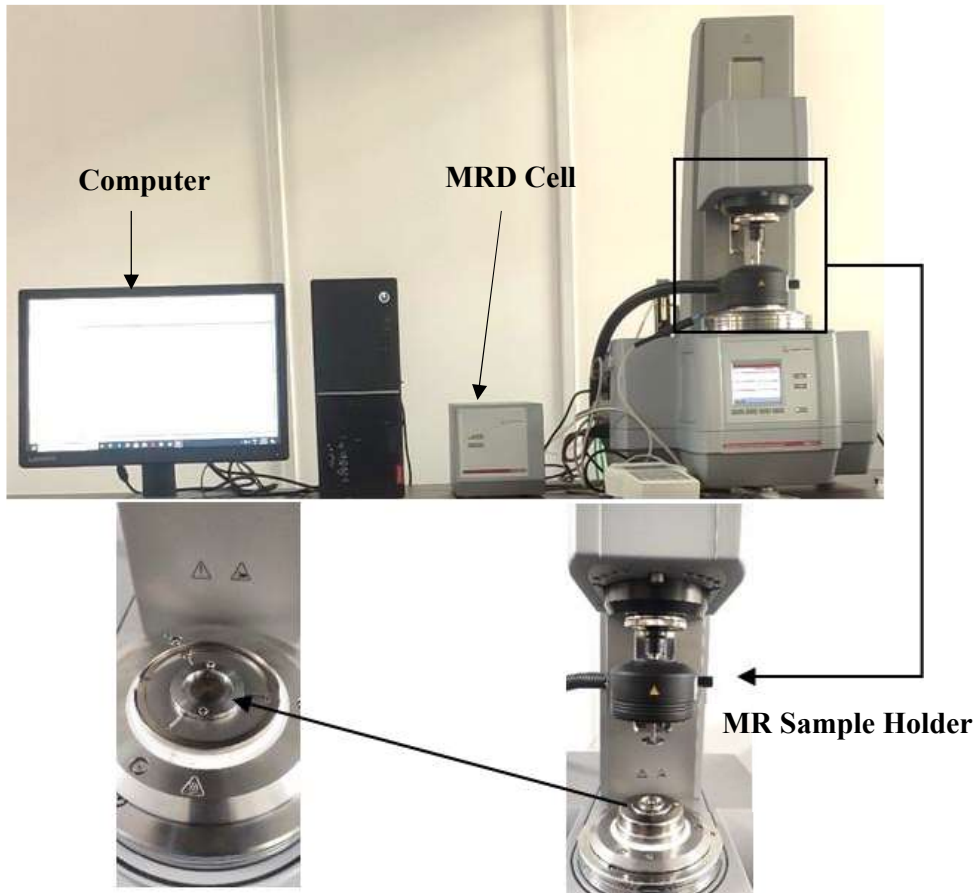


**Parameter Specification:** Max. Capacity: 5litres, Speed range: 50-1500 rpm, Power: 10W Voltage: 220-240V, frequency: 50 Hz

#### 6. Rheometer MCR702(Make: Anton-Paar, Austria)

**Specification:** Minimum torque, rotation: 1nNm, Maximum torque, rotation: 230mNm  
Minimum torque, oscillation: 0.5nNm, Maximum angular frequency: 628 rad/s,  
Normal force: 0.005 to 50 N, Maximum temperature:160°C to 1000°C, Pressure: up to

1000bar Rheometer Software: RheoCompass, MRD Cell: 1Tesla, Temperature range: -10 to 170°C (Peltier Heating/Cooling), Oil free Motor Power: 0.55 kW, Output (5 bar): 55 l/min max., Pressure: 8 bar, Tank Volume: 10, Weight: 59 kg Power Supply Magneto Cell 230V HCP 14-12500,12.5,1 mA.



**MATLAB Software**

Parameter	Specification
Name of the software	MATLAB/SIMULINK
Version	R2019b, R2022b
Licensed to	NITK
Company	MathWorks

## ANSYS

<b>Parameter</b>	<b>Specification</b>
Name of the software	ANSYS
Version	2020, 2022 R1 student Version
Licensed to	Student Version
Company	ANSYS



## REFERENCES

- Abdel-Wahab, A. A., Murmu, T., and Olabi, A.-G. (2018). “Applications of Magnetorheological (MR) Fluids in the Biomedical Field.” *Encycl. Smart Mater.*, Elsevier, 284–307.
- Acharya, S., Allien, V. J., N P, P., and Kumar, H. (2021). “Dynamic behavior of sandwich beams with different compositions of magnetorheological fluid core.” *Int. J. Smart Nano Mater.*, 12(1), 88–106.
- Afshin, M., Sadighi, M., and Shakeri, M. (2011). “Vibration and damping analysis of cylindrical sandwich panels containing a viscoelastic flexible core.” *J. Sandw. Struct. Mater.*, 13(3), 331–356.
- Ahmed, K. M. (1971). “Free vibration of curved sandwich beams by the method of finite elements.” *J. Sound Vib.*, 18(1), 61–74.
- Aldemir, U. (2003). “Optimal control of structures with semiactive-tuned mass dampers.” *J. Sound Vib.*, 266(4), 847–874.
- Allien, J. V., Kumar, H., and Desai, V. (2020). “Semi-active vibration control of MRF core PMC cantilever sandwich beams: Experimental study.” *Proc. Inst. Mech. Eng. Part L J. Mater. Des. Appl.*, 234(4), 574–585.
- Arikoglu, A., and Ozkol, I. (2010). “Vibration analysis of composite sandwich beams with viscoelastic core by using differential transform method.” *Compos. Struct.*, 92(12), 3031–3039.
- Arumugam, A. B., Rajamohan, V., Pandey, A., and Sudhagar, P. E. (2017). “Finite element vibration analysis of rotating laminated composite beam with varying cross-section using HSDT.” *Int. J. Interact. Des. Manuf.*, 11(3), 703–712.
- Arvin, H., Sadighi, M., and Ohadi, A. R. (2010). “A numerical study of free and forced vibration of composite sandwich beam with viscoelastic core.” *Compos. Struct.*, 92(4), 996–1008.
- Ashour, O., Rogers, C. A., and Kordonsky, W. (1996). “Magnetorheological Fluids:

Materials, Characterization, and Devices.” *J. Intell. Mater. Syst. Struct.*, 7(2), 123–130.

Ashtiani, M., Hashemabadi, S. H., and Ghaffari, A. (2015). “A review on the magnetorheological fluid preparation and stabilization.” *J. Magn. Magn. Mater.*, 374, 711–715.

Baber, T. T., Maddox, R. A., and Orozco, C. E. (1998). “A finite element model for harmonically excited viscoelastic sandwich beams.” *Comput. Struct.*, 66(1), 105–113.

Balamurugan, V., and Narayanan, S. (2002). “Finite element formulation and active vibration control study on beams using smart constrained layer damping (SCLD) treatment.” *J. Sound Vib.*, 249(2), 227–250.

Barbosa, F. S., and Farage, M. C. R. (2008). “A finite element model for sandwich viscoelastic beams: Experimental and numerical assessment.” *J. Sound Vib.*, 317(1–2), 91–111.

Berg, C. D., Evans, L. F., and Kermode, P. R. (1996). “Composite structure analysis of a hollow cantilever beam filled with electro-rheological fluid.” *J. Intell. Mater. Syst. Struct.*, 7(5), 494–502.

Bilasse, M., Daya, E. M., and Azrar, L. (2010). “Linear and nonlinear vibrations analysis of viscoelastic sandwich beams.” *J. Sound Vib.*, 329(23), 4950–4969.

Bolat, F. C., and Sivrioglu, S. (2020). “Bending vibration control of a MR fluid embedded smart beam exposed by the conjunction of wind-induced galloping effects.” *Smart Mater. Struct.*, 29(11), 115036.

Chakraborty, B. C., and Ratna, D. (2020). *Polymers for Vibration Damping Applications. Polym. Vib. Damping Appl.*, Elsevier.

Chiriac, H., and Stoian, G. (2010). “Influence of particle size distributions on magnetorheological fluid performances.” *J. Phys. Conf. Ser.*, 200(SECTION 7).

Choi, S. B., and Han, Y. M. (2005). “Hysteretic behavior of a magnetorheological fluid: Experimental identification.” *Acta Mech.*, 180(1–4), 37–47.

Choi, S. B., Seo, J. W., Kim, J. H., and Kim, K. S. (2001). “Electrorheological fluid-based plate for noise reduction in a cabin: Experimental results.” *J. Sound Vib.*, 239(1),



178–185.

Choi, Y., Sprecher, A. F., and Conrad, H. (1990). “Vibration Characteristics of a Composite Beam Containing an Electrorheological Fluid.” *J. Intell. Mater. Syst. Struct.*, 1(1), 91–104.

Choi, Y., Sprecher, A. F., and Conrad, H. (1992). “Response of Electrorheological Fluid-Filled Laminate Composites to Forced Vibration.” *J. Intell. Mater. Syst. Struct.*, 3(1), 17–29.

Daniel, C., Hemalatha, G., Sarala, L., Tensing, D., and Sundar Manoharan, S. (2019). “Seismic Mitigation of Building Frames using Magnetorheological Damper.” *Int. J. Eng. Trans. B Appl.*, 32(11), 1543–1547.

DiTaranto, R. A., and Blasingame, W. (1967). “Composite Damping of Vibrating Sandwich Beams.” *J. Eng. Ind.*, 89(4), 633–638.

Dyke, S. J., Spencer, B. F., Sain, M. K., and Carlson, J. D. (1998). “An experimental study of MR dampers for seismic protection.” *Smart Mater. Struct.*, 7(5), 693–703.

Elizabeth Premalatha, S., Chokkalingam, R., and Mahendran, M. (2012). “Magneto Mechanical Properties of Iron Based MR Fluids.” *Am. J. Polym. Sci.*, 2(4), 50–55.

Elliott, S. J. (2010). “Active noise and vibration control in vehicles.” *Veh. Noise Vib. Refinement*, 235–251.

Eshaghi, M., Rakheja, S., and Sedaghati, R. (2015). “An accurate technique for pre-yield characterization of MR fluids.” *Smart Mater. Struct.*, 24(6).

Eshaghi, M., Sedaghati, R., and Rakheja, S. (2017). “Vibration analysis and optimal design of multi-layer plates partially treated with the MR fluid.” *Mech. Syst. Signal Process.*, 82, 80–102.

Gamota, D. R., and Filisko, F. E. (1991). “High frequency dynamic mechanical study of an aluminosilicate electrorheological material.” *J. Rheol. (N. Y. N. Y.)*, 35(7), 1411–1425.

Gandhi, M. V., Thompson, B. S., and Choi, S. B. (1989). “A New Generation of Innovative Ultra-Advanced Intelligent Composite Materials Featuring Electro-

Rheological Fluids: An Experimental Investigation.” *J. Compos. Mater.*, 23(12), 1232–1255.

Gao, Y. S., Zhang, S. Q., Zhao, G. Z., and Schmidt, R. (2022). “Numerical modeling for cantilever sandwich smart structures with partially covered constrained viscoelastic layer.” *Compos. Struct.*, 281(March 2021), 114981.

Garg, A., Chalak, H. D., Li, L., Belarbi, M. O., Sahoo, R., and Mukhopadhyay, T. (2022). “Vibration and Buckling Analyses of Sandwich Plates Containing Functionally Graded Metal Foam Core.” *Acta Mech. Solida Sin.*

Genc, S. (2022). “Experimental Studies on Magnetorheological Fluids.” *Encycl. Smart Mater.*, Elsevier, 248–259.

Ghorbanpour Arani, A., and Soleymani, T. (2019a). “Size-dependent vibration analysis of a rotating MR sandwich beam with varying cross section in supersonic airflow.” *Int. J. Mech. Sci.*, 151(November 2018), 288–299.

Ghorbanpour Arani, A., and Soleymani, T. (2019b). “Size-dependent vibration analysis of an axially moving sandwich beam with MR core and axially FGM faces layers in yawed supersonic airflow.” *Eur. J. Mech. A/Solids*, 77(April), 103792.

Ghorbanpour Arani, A., and Soleymani, T. (2019c). “Size-dependent vibration analysis of a rotating MR sandwich beam with varying cross section in supersonic airflow.” *Int. J. Mech. Sci.*, 151(June 2018), 288–299.

Ghorbanpour Arani, A., and Soleymani, T. (2019d). “Size-dependent vibration analysis of a rotating MR sandwich beam with varying cross section in supersonic airflow.” *Int. J. Mech. Sci.*, 151, 288–299.

Gould, T. E., Jesunathadas, M., Nazarenko, S., and Piland, S. G. (2019). “Mouth Protection in Sports.” *Mater. Sport. Equip.*, Elsevier, 199–231.

Grewal, J. S., Sedaghati, R., and Esmailzadeh, E. (2013). “Vibration analysis and design optimization of sandwich beams with constrained viscoelastic core layer.” *J. Sandw. Struct. Mater.*, 15(2), 203–228.

Guo, Y. Q., Sun, C. L., Xu, Z. D., and Jing, X. (2018). “Preparation and tests of MR

- fluids with CI particles coated with MWNTS.” *Front. Mater.*, 5(August), 1–8.
- Gupta, A., and Panda, S. (2021). “Hybrid damping treatment of a layered beam using a particle-filled viscoelastic composite layer.” *Compos. Struct.*, 262(January), 113623.
- Gupta, A., Panda, S., and Reddy, R. S. (2020). “Improved damping in sandwich beams through the inclusion of dispersed graphite particles within the viscoelastic core.” *Compos. Struct.*, 247(April), 112424.
- Haiqing, G., and King, L. M. (1997). “Vibration Characteristics of Sandwich Beams Partially and Fully Treated with Electro-Rheological Fluid.” *J. Intell. Mater. Syst. Struct.*, 8(5), 401–413.
- Haiqing, G., King, L. M., and Cher, T. B. (1993). “Influence of a Locally Applied Electro-Rheological Fluid Layer on Vibration of a Simple Cantilever Beam.” *J. Intell. Mater. Syst. Struct.*, 4(3), 379–384.
- Hao, M., and Rao, M. D. (2005). “Vibration and damping analysis of a sandwich beam containing a viscoelastic constraining layer.” *J. Compos. Mater.*, 39(18), 1621–1643.
- Harland, N. R., Mace, B. R., and Jones, R. W. (2001). “Adaptive-passive control of vibration transmission in beams using electro/magnetorheological fluid filled inserts.” *IEEE Trans. Control Syst. Technol.*, 9(2), 209–220.
- HE, J. M., and HUANG, J. (2005). “MAGNETORHEOLOGICAL FLUIDS AND THEIR PROPERTIES.” *Int. J. Mod. Phys. B*, 19(01n03), 593–596.
- Heganna, S. S., and Joglekar, J. J. (2016). “Active Vibration Control of Smart Structure Using PZT Patches.” *Procedia Comput. Sci.*, 89, 710–715.
- Howson, W. P., and Zare, A. (2005). “Exact dynamic stiffness matrix for flexural vibration of three-layered sandwich beams.” *J. Sound Vib.*, 282(3–5), 753–767.
- Huang, Z., Qin, Z., and Chu, F. (2016a). “Damping mechanism of elastic-viscoelastic-elastic sandwich structures.” *Compos. Struct.*, 153(May), 96–107.
- Huang, Z., Qin, Z., and Chu, F. (2016b). “Damping mechanism of elastic–viscoelastic–elastic sandwich structures.” *Compos. Struct.*, 153, 96–107.

Iglesias, G. R., López-López, M. T., Durán, J. D. G., González-Caballero, F., and Delgado, A. V. (2012). “Dynamic characterization of extremely bidisperse magnetorheological fluids.” *J. Colloid Interface Sci.*, 377(1), 153–159.

Jack R., V., and Sierakowski, R. L. (2008). *The Behavior Of Structures Composed Of Composite Materials*. Springer, Dordrecht.

Jolly, M. R., Bender, J. W., and Carlson, J. D. (1999). “Properties and Applications of Commercial Magnetorheological Fluids.” *J. Intell. Mater. Syst. Struct.*, 10(1), 5–13.

Kamble, V. G., Kolekar, S., Panda, H. S., Ammourah, S., and Jagadeesha, T. (2021). “Magneto rheological fluid: Fabrication and characterization of its temperature-dependent properties.” *Mater. Today Proc.*, 45, 4813–4818.

Kciuk, M.; Turczyn, R. (2012). “Properties and applications of magnetorheological fluids.” *Frat. ed Integrita Strutt.*, 23(May 2014), 57–61.

Kerwin, E. M. (1959). “Damping of Flexural Waves by a Constrained Viscoelastic Layer.” *J. Acoust. Soc. Am.*, 31(7), 952–962.

Khalfi, B., and Ross, A. (2016). “Transient and harmonic response of a sandwich with partial constrained layer damping: A parametric study.” *Compos. Part B Eng.*, 91, 44–55.

Khot, S. M., Yelve, N. P., and Shaik, S. (2013). “Experimental study of active vibration control of a cantilever beam.” *Int. Conf. Emerg. Trends Eng. Technol. ICETET*, (December), 1–6.

Khot, S. M., Yelve, N. P., Tomar, R., and Desai, S. (2011). “Active vibration control of cantilever beam by using PID based output feedback controller.”

Khot, S. M., Yelve, N. P., Tomar, R., Desai, S., and Vittal, S. (2012). “Active vibration control of cantilever beam by using PID based output feedback controller.” *JVC/Journal Vib. Control*, 18(3), 366–372.

Kolekar, S., and Venkatesh, K. (2019). “Experimental Investigation of Damping Effect in Semi-active Magnetorheological Fluid Sandwich Beam Under Non-Homogeneous Magnetic Field.” *J. Vib. Eng. Technol.*, 7(2), 107–116.

- Kumar Kariganaur, A., Kumar, H., and Arun, M. (2022a). “Effect of Temperature on Sedimentation Stability and Flow characteristics of Magnetorheological Fluids with Damper as the Performance Analyser.” *J. Magn. Magn. Mater.*, 555(April), 169342.
- Kumar Kariganaur, A., Kumar, H., and Arun, M. (2022b). “Influence of temperature on magnetorheological fluid properties and damping performance.” *Smart Mater. Struct.*, 31(5), 055018.
- Kumar, S., Sehgal, R., Wani, M. F., and Sharma, M. D. (2021). “Stabilization and tribological properties of magnetorheological (MR) fluids: A review.” *J. Magn. Magn. Mater.*, 538, 168295.
- Kumbhar, B. K., Patil, S. R., and Sawant, S. M. (2015). “Synthesis and characterization of magneto-rheological (MR) fluids for MR brake application.” *Eng. Sci. Technol. an Int. J.*, 18(3), 432–438.
- Kung, S. W., and Singh, R. (1998). “Vibration analysis of beams with multiple constrained layer damping patches.” *J. Sound Vib.*, 212(5), 781–805.
- Kusagur, S. M., Arunkumar, G., and Manjunath, T. C. (2020). “Modelling of smart intelligent materials with PZT & PVDF sensors/actuators to control the active vibrations of flexible aluminum mechanical cantilever beams using proportional integral derivative (PID) techniques.” *Mater. Today Proc.*, 37(Part 2), 2075–2082.
- Lakes, R. (2009). *Viscoelastic Materials*. Cambridge University Press.
- Lam, M. J., Inman, D. J., and Saunders, W. R. (1997). “Vibration control through passive constrained layer damping and active control.” *Smart Struct. Mater. 1997 Passiv. Damping Isol.*, L. P. Davis, ed., 60–69.
- Lara-Prieto, V., Parkin, R., Jackson, M., Silberschmidt, V., and Kęsy, Z. (2010). “Vibration characteristics of MR cantilever sandwich beams: Experimental study.” *Smart Mater. Struct.*, 19(1).
- Lee, C. (1995). “Finite Element Formulation of a Sandwich Beam with Embedded Electro-Rheological Fluids.” *J. Intell. Mater. Syst. Struct.*, 6(5), 718–728.
- Lewandowski, R., Wielentejczyk, P., and Litewka, P. (2021). “Dynamic characteristics

of multi-layered, viscoelastic beams using the refined zig-zag theory.” *Compos. Struct.*, 259(October 2020).

Li, W. H., Chen, G., and Yeo, S. H. (1999). “Viscoelastic properties of MR fluids.” *Smart Mater. Struct.*, 8(4), 460–468.

Lifshitz, J. M., and Leibowitz, M. (1987). “Optimal sandwich beam design for maximum viscoelastic damping.” *Int. J. Solids Struct.*, 23(7), 1027–1034.

Lopez-Lopez, M. T., Duran, J. D. G., and Zubarev, A. Y. (2021). “Rheological Analysis of Magnetorheological Fluids.” *Encycl. Smart Mater.*, Elsevier, 237–247.

López-López, M. T., Kuzhir, P., Lacis, S., Bossis, G., González-Caballero, F., and Durán, J. D. G. (2006). “Magnetorheology for suspensions of solid particles dispersed in ferrofluids.” *J. Phys. Condens. Matter*, 18(38).

Mahmoudkhani, S., and Laghaie, K. S. (2022). “Flutter analysis of sandwich panel with the constrained viscoelastic layer considering the effects of the imperfection and the core thickness deformation.” *Thin-Walled Struct.*, 173, 108980.

Makris, N., Burton, S. A., and Taylor, D. P. (1996). “Electrorheological damper with annular ducts for seismic protection applications.” *Smart Mater. Struct.*, 5(5), 551–564.

Marur, S. R., and Kant, T. (1996). “Free vibration analysis of fiber reinforced composite beams using higher order theories and finite element modelling.” *J. Sound Vib.*, 194(3), 337–351.

Mazlan, S. A., Ekreem, N. B., and Olabi, A. G. (2007). “The performance of magnetorheological fluid in squeeze mode.” *Smart Mater. Struct.*, 16(5), 1678–1682.

Mead, D. J. (2013). “Governing Equations for Vibrating Constrained-Layer Damping Sandwich Authors’ Closure.” (December 1972), 2–3.

Mead, D. J., and Markus, S. (1969). “The forced vibration of a three-layer, damped sandwich beam with arbitrary boundary conditions.” *J. Sound Vib.*, 10(2), 163–175.

Mead, D. J., and Markus, S. (1970). “Loss factors and resonant frequencies of encastred damped sandwich beams.” *J. Sound Vib.*, 12(1), 99–112.

- Muddebihal, A. B., and Patil, S. F. (2020). "Preparation and Study of Characteristics of Iron Based MR Fluids." *Mater. Today Proc.*, 24, 1132–1137.
- Muhammad, A., Yao, X., and Deng, Z. (2006). "Review of magnetorheological (MR) fluids and its applications in vibration control." *J. Mar. Sci. Appl.*, 5(3), 17–29.
- Naji, J. (2017). "VIBRATION BEHAVIOR OF LAMINATED COMPOSITE BEAMS INTEGRATED WITH MAGNETORHEOLOGICAL FLUID LAYER." 33(4), 417–425.
- Naji, J., Zabihollah, A., and Behzad, M. (2016). "Layerwise theory in modeling of magnetorheological laminated beams and identification of magnetorheological fluid." *Mech. Res. Commun.*, 77, 50–59.
- Naji, J., Zabihollah, A., and Behzad, M. (2018). "Vibration characteristics of laminated composite beams with magnetorheological layer using layerwise theory." *Mech. Adv. Mater. Struct.*, 25(3), 202–211.
- Nezami, M., and Gholami, B. (2019). "Optimal locations of magnetorheological fluid pockets embedded in an elastically supported honeycomb sandwich beams for supersonic flutter suppression." *Eur. J. Mech. A/Solids*, 74(April 2018), 81–95.
- Nguyen, Q.-H., and Choi, S.-B. (2009). "Optimal design of MR shock absorber and application to vehicle suspension." *Smart Mater. Struct.*, 18(3), 035012.
- Oberst, H.; Becker, G. W.; Frankenfeld, K. (1952). "Über die Dämpfung der Biegeschwingungen dünner Bleche durch fest haftende Beläge." *Acustica*, 4, 181–194.
- Occhiuzzi, A., Spizzuoco, M., and Serino, G. (2003). "Experimental analysis of magnetorheological dampers for structural control." *Smart Mater. Struct.*, 12(5), 703–711.
- Oh, H.-U., and Onoda, J. (2002). "An experimental study of a semiactive magnetorheological fluid variable damper for vibration suppression of truss structures." *Smart Mater. Struct.*, 11(1), 156–162.
- Olabi, A. G., and Grunwald, A. (2007). "Design and application of magneto-rheological fluid." *Mater. Des.*, 28(10), 2658–2664.

Oyadiji, S. O. (1996). “Applications of Electro-Rheological Fluids for Constrained Layer Damping Treatment of Structures.” *J. Intell. Mater. Syst. Struct.*, 7(5), 541–549.

Patil, R., Joladarashi, S., and Kadoli, R. (2020). “Studies on free and forced vibration of functionally graded back plate with brake insulator of a disc brake system.” *Arch. Appl. Mech.*, 90(12), 2693–2714.

Pradeep, V., and Ganesan, N. (2006). “Vibration behavior of ACLD treated beams under thermal environment.” *J. Sound Vib.*, 292(3–5), 1036–1045.

Pradeep, V., Ganesan, N., and Bhaskar, K. (2007). “Vibration and thermal buckling of composite sandwich beams with viscoelastic core.” *Compos. Struct.*, 81(1), 60–69.

Qin, H., and Sun, Y. (2020). “Autonomous control of underwater offshore vehicles.” *Fundam. Des. Autom. Technol. Offshore Robot.*, Elsevier, 115–160.

Rabinow, J. (1948). “The Magnetic Fluid Clutch.” *Trans. Am. Inst. Electr. Eng.*, 67, 1308–1315.

Rahn, C. D., and Joshi, S. (1998). “Modeling and Control of an Electrorheological Sandwich Beam.” *J. Vib. Acoust.*, 120(1), 221–227.

Rajamohan, V., Rakheja, S., and Sedaghati, R. (2010a). “Vibration analysis of a partially treated multi-layer beam with magnetorheological fluid.” *J. Sound Vib.*, 329(17), 3451–3469.

Rajamohan, V., Sedaghati, R., and Rakheja, S. (2010b). “Vibration analysis of a multi-layer beam containing magnetorheological fluid.” *Smart Mater. Struct.*, 19(1).

Rajamohan, V., Sedaghati, R., and Rakheja, S. (2011). “Optimal vibration control of beams with total and partial MR-fluid treatments.” *Smart Mater. Struct.*, 20(11).

Ramkumar, G., Jesu Gnanaprakasam, A., Thirumarimurugan, M., Nandhakumar, M., Nithishmohan, M., Abinash, K., and Kishore, S. (2022). “Synthesis characterization and functional analysis of magneto rheological fluid – A critical review.” *Mater. Today Proc.*

Rao, D. K. (1978). “Frequency and Loss Factors of Sandwich Beams Under Various Boundary Conditions.” *J Mech Eng Sci*, 20(5), 271–282.



- Raville, M. E., Ueng, E. S., and Lei, M. M. (1960). "Natural frequencies of vibration of fixed-fixed sandwich beams." *J. Appl. Mech. Trans. ASME*, 28(3), 367–371.
- Reddy, R. S., Panda, S., and Gupta, A. (2021). "Nonlinear dynamics and active control of smart beams using shear/extensional mode piezoelectric actuators." *Int. J. Mech. Sci.*, 204(January), 106495.
- Rimašauskienė, R., Jūrėnas, V., Radziński, M., Rimašauskas, M., and Ostachowicz, W. (2019). "Experimental analysis of active–passive vibration control on thin-walled composite beam." *Compos. Struct.*, 223, 110975.
- Robert M., J. (1999). *Mechanics of Composite Materials*. CRC Press.
- Rokn-Abadi, M. R., Shahali, P., and Haddadpour, H. (2020a). "Effects of magnetoelastic loads on free vibration characteristics of the magnetorheological-based sandwich beam." *J. Intell. Mater. Syst. Struct.*, 31(7), 1015–1028.
- Rokn-Abadi, M., Yousefi, M., Haddadpour, H., and Sadeghmanesh, M. (2020b). "Dynamic stability analysis of a sandwich beam with magnetorheological elastomer core subjected to a follower force." *Acta Mech.*, 231(9), 3715–3727.
- S Genç.; PP Phulé. (2007). "Rheological properties of magnetorheological fluids." *Int. J. Mod. Phys. B*, 21(28–29), 4849–4857.
- Sakiyama, T., Matsuda, H., and Morita, C. (1996). "Free vibration analysis of sandwich beam with elastic or viscoelastic core by applying the discrete green function." *J. Sound Vib.*, 191(2), 189–206.
- Seid, S., Chandramohan, S., and Sujatha, S. (2019). "Design and evaluation of a magnetorheological damper based prosthetic knee." *Int. J. Eng. Trans. A Basics*, 32(1), 146–152.
- Selvaraj, R., and Ramamoorthy, M. (2020). "Experimental and finite element vibration analysis of CNT reinforced MR elastomer sandwich beam." *Mech. Based Des. Struct. Mach.*, 0(0), 1–13.
- Selvaraj, R., Subramani, M., More, G., and Ramamoorthy, M. (2021). "Dynamic responses of laminated composite sandwich beam with double-viscoelastic core

layers.” *Mater. Today Proc.*, 46, 7468–7472.

Shakouri, M., Permoon, M. R., Askarian, A., and Haddadpour, H. (2021). “Dynamic analysis of three-layer cylindrical shells with fractional viscoelastic core and functionally graded face layers.” *JVC/Journal Vib. Control*, 27(23–24), 2738–2753.

Sharnappa, Ganesan, N., and Sethuraman, R. (2007). “Dynamic modeling of active constrained layer damping of composite beam under thermal environment.” *J. Sound Vib.*, 305(4–5), 728–749.

Sivrioglu, S., and Bolat, F. C. (2020). “Switching linear quadratic Gaussian control of a flexible blade structure containing magnetorheological fluid.” *Trans. Inst. Meas. Control*, 42(3), 618–627.

Souza Eloy, F. de, Gomes, G. F., Ancelotti, A. C., Cunha, S. S. da, Bombard, A. J. F., and Junqueira, D. M. (2018). “Experimental dynamic analysis of composite sandwich beams with magnetorheological honeycomb core.” *Eng. Struct.*, 176(August), 231–242.

Souza Eloy, F. de, Gomes, G. F., Ancelotti, A. C., Cunha, S. S. da, Bombard, A. J. F., and Junqueira, D. M. (2019). “A numerical-experimental dynamic analysis of composite sandwich beam with magnetorheological elastomer honeycomb core.” *Compos. Struct.*, 209(August 2018), 242–257.

Stanway, R., Sproston, J. L., and El-Wahed, A. K. (1996). “Applications of electro-rheological fluids in vibration control: a survey.” *Smart Mater. Struct.*, 5(4), 464–482.

Sun, Q., Zhou, J. X., and Zhang, L. (2003). “An adaptive beam model and dynamic characteristics of magnetorheological materials.” *J. Sound Vib.*, 261(3), 465–481.

Sun, Z., Mei, Z., Li, Y., Gong, H., Wang, G., and Wang, Q. (2022). “Design of lightweight damping core for composite sandwich structure.” *Polym. Compos.*, 43(9), 6578–6588.

Tian, J., Guo, Q., and Shi, G. (2020). “Laminated piezoelectric beam element for dynamic analysis of piezolaminated smart beams and GA-based LQR active vibration control.” *Compos. Struct.*, 252, 112480.

- Toulson, R., and Wilmschurst, T. (2012). “An Introduction to Control Systems.” *Fast Eff. Embed. Syst. Des.*, Elsevier, 273–295.
- Trindade, M. A., Benjeddou, A., and Ohayon, R. (2000). “Modeling of Frequency-Dependent Viscoelastic Materials for Active-Passive Vibration Damping.” *J. Vib. Acoust.*, 122(2), 169.
- Tzou, H. S., Lee, H. J., and Arnold, S. M. (2004). “Smart materials, precision sensors/actuators, smart structures, and structronic systems.” *Mech. Adv. Mater. Struct.*, 11(4–5), 367–393.
- Vishwakarma, P. N., Mishra, P., and Sharma, S. K. (2022). “Characterization of a magnetorheological fluid damper a review.” *Mater. Today Proc.*, 56, 2988–2994.
- Weiss, K. D., Carlson, J. D., and Nixon, D. A. (1994). “Viscoelastic properties of magneto- and electro-rheological fluids.” *J. Intell. Mater. Syst. Struct.*, 5(6), 772–775.
- Welsh, W. A. (2018). “Helicopter Vibration Reduction.” *Morphing Wing Technol.*, Elsevier, 865–892.
- Yalcintas, M., and Coulter, J. P. (1995a). “Electrorheological Material Based Adaptive Beams Subjected to Various Boundary Conditions.” *J. Intell. Mater. Syst. Struct.*, 6(5), 700–717.
- Yalcintas, M., and Coulter, J. P. (1995b). “An Adaptive Beam Model with Electrorheological Material Based Applications.” *J. Intell. Mater. Syst. Struct.*, 6(4), 498–507.
- Yalcintas, M., and Coulter, J. P. (1998). “Electrorheological material based non-homogeneous adaptive beams.” *Smart Mater. Struct.*, 7(1), 128–143.
- Yalcintas, M., Coulter, J. P., and Don, D. L. (1995). “Structural modeling and optimal control of electrorheological material based adaptive beams.” *Smart Mater. Struct.*, 4(3), 207–214.
- Yalcintas, M., and Dai, H. (1999). “Magnetorheological and electrorheological materials in adaptive structures and their performance comparison.” *Smart Mater. Struct.*, 8(5), 560–573.

Yalcintas, M., and Dai, H. (2004). "Vibration suppression capabilities of magnetorheological materials based adaptive structures." *Smart Mater. Struct.*, 13(1), 1–11.

Yeh, Z. F., and Shih, Y. S. (2006). "Dynamic characteristics and dynamic instability of magnetorheological material-based adaptive beams." *J. Compos. Mater.*, 40(15), 1333–1359.

Zabihollah, A., Najji, J., and Zareie, S. (2020). "Impact Analysis of MR-Laminated Composite Structures." *Emerg. Trends Mechatronics*, 1–14.

Zhang, J., He, L., Wang, E., and Gao, R. (2008). "A LQR controller design for active vibration control of flexible structures." *Proc. - 2008 Pacific-Asia Work. Comput. Intell. Ind. Appl. PACIIA 2008*, 1, 127–132.

Zhang, J., and Roschke, P. N. (1999). "Active control of a tall structure excited by wind." *J. Wind Eng. Ind. Aerodyn.*, 83(1–3), 209–223.

Zhang, S. Q., Gao, Y. S., Zhao, G. Z., Pu, H. Y., Wang, M., Ding, J. H., and Sun, Y. (2021). "Numerical modeling for viscoelastic sandwich smart structures bonded with piezoelectric materials." *Compos. Struct.*, 278(August 2020).

Zhao, T., Li, K., and Ma, H. (2022a). "Study on dynamic characteristics of a rotating cylindrical shell with uncertain parameters." *Anal. Math. Phys.*, 12(4), 1–28.

Zhao, T. Y., Cui, Y. S., Pan, H. G., Yuan, H. Q., and Yang, J. (2021a). "Free vibration analysis of a functionally graded graphene nanoplatelet reinforced disk-shaft assembly with whirl motion." *Int. J. Mech. Sci.*, 197(February), 106335.

Zhao, T. Y., Cui, Y. S., Wang, Y. Q., and Pan, H. G. (2021b). "Vibration characteristics of graphene nanoplatelet reinforced disk-shaft rotor with eccentric mass." *Mech. Adv. Mater. Struct.*, 0(0), 1–21.

Zhao, T. Y., Jiang, L. P., Pan, H. G., Yang, J., and Kitipornchai, S. (2021c). "Coupled free vibration of a functionally graded pre-twisted blade-shaft system reinforced with graphene nanoplatelets." *Compos. Struct.*, 262(October 2020), 113362.

Zhao, T. Y., Jiang, L. P., Yu, Y. X., and Wang, Y. Q. (2022b). "Study on theoretical

modeling and mechanical performance of a spinning porous graphene nanoplatelet reinforced beam attached with double blades.” *Mech. Adv. Mater. Struct.*, 0(0), 1–12.

Zhao, T. Y., Ma, Y., Zhang, H. Y., Pan, H. G., and Cai, Y. (2021d). “Free vibration analysis of a rotating graphene nanoplatelet reinforced pre-twist blade-disk assembly with a setting angle.” *Appl. Math. Model.*, 93, 578–596.

Zhao, T. Y., Yan, K., Li, H. W., and Wang, X. (2022c). “Study on theoretical modeling and vibration performance of an assembled cylindrical shell-plate structure with whirl motion.” *Appl. Math. Model.*, 110, 618–632.

Zhou, X. Q., Yu, D. Y., Shao, X. Y., Zhang, S. Q., and Wang, S. (2016). “Research and applications of viscoelastic vibration damping materials: A review.” *Compos. Struct.*, 136, 460–480.

Zhu, W., Dong, X., Huang, H., and Qi, M. (2019). “Iron nanoparticles-based magnetorheological fluids: A balance between MR effect and sedimentation stability.” *J. Magn. Magn. Mater.*, 491, 165556.



## LIST OF PUBLICATIONS

### INTERNATIONAL JOURNALS

1. Suryarao Nagiredla, Sharnappa Joladarashi, Hemantha Kumar, “Combined Damping Effect of the Composite Material and Magneto-rheological Fluid on Static and Dynamic Behavior of the Sandwich Beam”, *Journal of Vibration Engineering Technologies (I.F: 2.333, SCIE)*, <https://doi.org/10.1007/s42417-022-00716-4>.
2. Suryarao Nagiredla, Sharnappa Joladarashi, Hemantha Kumar, “Influence of Magneto-rheological Fluid Pocket Configuration on the Dynamic Response of the Composite Sandwich Beam”, *Mechanics Based Design of Structures and Machines (I.F: 4.364, SCIE)*, <https://doi.org/10.1080/15397734.2022.2138914>
3. Suryarao Nagiredla, Sharnappa Joladarashi, Hemantha Kumar, “Characterization of an In-house Prepared MR Fluid and Vibrational Behaviour of Composite Sandwich Beam with MR Fluid Core”, *Scientia Iranica (I.F: 1.416, SCIE)*, <https://doi.org/10.24200/sci.2022.58527.5777>.
4. Suryarao Nagiredla, Sharnappa Joladarashi, Hemantha Kumar, “Rheological Properties of the In-house Prepared Magneto-rheological Fluid in the Pre-yield Region”, *International Journal of Engineering (ESCI, Scopus)*, <https://doi.org/10.5829/ije.2022.35.11b.19>.
5. Suryarao Nagiredla, Sharnappa Joladarashi, Hemantha Kumar, “Influence of Material and Geometrical Properties on Static and Dynamic Behavior of MR Fluid Sandwich Beam: Finite Element Approach”, *Iranian Journal of Science and Technology (I.F: 1.560, SCIE)*, <https://doi.org/10.1007/s40997-023-00603-7>.
6. Suryarao Nagiredla, Sharnappa Joladarashi, Hemantha Kumar, “Modelling and Predicting the Dynamic Response of An Axially Graded Viscoelastic Core Sandwich Beam”, *Defence Technology (I.F: 4.035, SCIE)*, DOI: <https://doi.org/10.1016/j.dt.2023.05.003>
7. Suryarao Nagiredla, Vivek R.S., Sharnappa Joladarashi, Hemantha Kumar, “Active vibration control of glass-epoxy composite beam using system identification technique”, *Periodica Polytechnica Mechanical Engineering (Scopus, Communicated)*.

## **INTERNATIONAL CONFERENCES**

1. Suryarao Nagiredla, Sharnappa Joladarashi, Hemantha Kumar (2020, July). “Experimental investigation of frequency and damping characteristics of magneto-rheological fluid core sandwich beams”, AIP Conference Proceedings, AIP Publishing LLC, <https://doi.org/10.1063/5.0003836>
2. Suryarao Nagiredla, Sharnappa Joladarashi, Hemantha Kumar (2022), “Passive and active vibration control of hybrid composite sandwich beam”, 3rd International Conference on Recent Advancements in Mechanical Engineering, ICRAME 2022, Department of Mechanical Engineering National Institute of Technology Silchar, Assam, India.



## CURRICULUM VITAE

1. Name: **NAGIREDLA SURYARAO**
  2. Date of Birth: 13/05/1993
  3. Permanent Address: Sahapuram Village, Laveru, Srikakulam,  
Andhra Pradesh, India – 575025.
  4. Mobile Number: 9553944950
  5. Email ID: [suryarao914@gmail.com](mailto:suryarao914@gmail.com)
  6. Education Qualification: Ph.D.
- 
- 2014 **Bachelor of Technology**
- Institution: RGUKT IIIT NUZVID  
Nuzvid, Krishna District, Andhra Pradesh,  
India.
- Specialization: Mechanical Engineering
- 2017 **Master of Technology**
- Institution: Acharya Nagarjuna University  
Mangalagiri, Guntur, Andhra Pradesh, India.
- Specialization: Machine Design
- 2023 **Doctor of Philosophy**
- Institution: National Institute of Technology Karnataka,  
Surathkal, Karnataka, India.
- Registration Date: 11/01/2018
- Thesis Submission Date: 08/05/2023
- Viva-Voice Date: 11/08/2023